MENDELOVA UNIVERZITA V BRNĚ
AGRONOMICKÁ FAKULTA

DISERTAČNÍ PRÁCE

BRNO 2016 **Ing. JIŘÍ KUDR**

Mendelova univerzita v Brně
Agronomická fakulta
Ústav chemie a biochemie

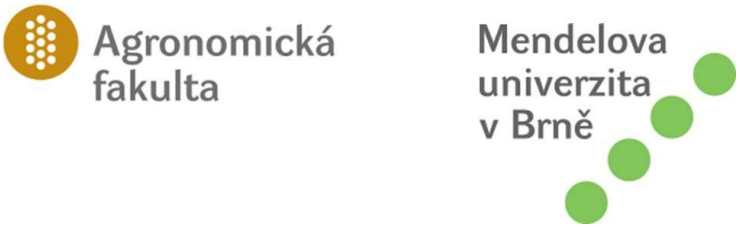

Vývoj elektrochemických metod využívajících nanotechnologie pro environmentální mobilní detekční systémy

Disertační práce
Studijní obor: 4106V017 Zemědělská chemie

Vedoucí práce:
RNDr. Ondřej Zítka, Ph.D.

Školitel specialista:
doc. RNDr. Pavel Kopel, Ph.D.

Vypracoval:
Ing. Jiří Kudr

Brno 2016

PROHLÁŠENÍ

Prohlašuji, že disertační práce na téma „Vývoj elektrochemických metod využívajících nanotechnologie pro environmentální mobilní detekční systémy“ je samostatným autorským dílem podle Autorského zákona. Nositelem majetkového autorského práva je pracoviště a univerzita.

Výsledky práce shrnuté v této závěrečné práci byly financovány z veřejných prostředků z Evropských fondů a státního rozpočtu České republiky.

Disertační práce a výsledky v ní prezentované jsou dílem vypracovaným v Laboratoři metalomiky a nanotechnologií působící na půdě Agronomické fakulty Mendelovy univerzity v Brně a mohou být použity k dalšímu prezentování případně ke komerčním účelům jen se souhlasem vedoucího disertační práce a děkana. V opačném případě se jedná o porušení zákona.

dne …….

podpis…….

Tato práce vznikla v rámci CEITEC - Středoevropského technologického institutu s pomocí výzkumné infrastruktury financované projektem CZ.1.05/1.1.00/02.0068 z Evropského fondu regionálního rozvoje.

EVROPSKÁ UNIE
EVROPSKÝ FOND PRO REGIONÁLNÍ ROZVOJ
INVESTICE DO VAŠÍ BUDOUCNOSTI

Poděkování

Na prvním místě bych chtěl poděkovat prof. Ing. Renému Kizekovi, DrSc. a prof. RNDr. Vojtěchu Adamovi, Ph.D. za příležitost být součástí jejich týmů, za cenné rady, připomínky a čas, který věnovali mně a mojí práci.

Děkuji RNDr. Ondřeji Zítkovi, Ph.D. a doc. RNDr. Pavlu Kopelovi, Ph.D. za odborné vedení mé práce.

Děkuji prof. RNDr. Bořivoji Klejdusovi, Ph.D. za otevření dveří na pole vědy.

Dále bych chtěl poděkovat všem spoluautorům za pomoc při experimentální práci, konzultaci výsledků a přípravě publikací, které jsou podkladem této práce.

Chtěl bych poděkovat kolegům z Ústavu chemie a biochemie Mendelovy univerzity v Brně za vytvoření příjemného pracovního prostředí a za přátelství, kterých si velice cením.

V neposlední řadě bych rád poděkoval své rodině a přátelům za zázemí, lásku a podporu.

Největší dík patří mé přítelkyni za to, že je…

Anotace

Znečišťování životního prostředí v 21. století znepokojujícím způsobem akcelerovalo. Kontinuální monitoring hladiny polutantů je nutnou součástí efektivní ochrany životního prostředí. Pro tyto účely vznikla potřeba analyzovat velká množství vzorků v krátkém čase. Odpovědí na tuto potřebu byl průnik automatizace do analytické chemie. Velkou popularitu si získaly především na průtoku založené techniky, které výrazně snižují potřebu manuální manipulace se vzorky a tím snižují i časovou náročnost analýz. Fluidní zařízení umožnují implementaci řady detektorů. Elektrochemické detektory se díky vysoké citlivosti, dostatečné selektivitě a schopnosti miniaturizace staly oblíbenou součástí fluidních a automatizovaných zařízení. Předložená práce se primárně zabývá metodami detekce kontaminace těžkými kovy a bakteriemi. Za tímto účelem byly vytvářeny elektrochemické automatizované systémy a systémy využívající nanotechnologie.

Klíčová slova: automatizace, elektroda, těžké kovy, senzor, voltametrie, znečištění

Annotation

During the 21st century pollution of environment was steadily increasing. Continuous monitoring of pollutants levels represents important part of effective environment protection. Demands for fast analysis of a large amount of samples caused introduction of automation to analytical chemistry. Techniques based on flow analysis attracted big attention. They are able to decrease need for manual treatment of samples and as a result decrease analysis duration. The advantage of flow-based analytical devices is also compatibility with several detection systems. Among others, electrochemical detectors are very attractive due to their high sensitivity, good selectivity and possibility of miniaturization. The presented thesis focuses on methods for detection of heavy metal and bacterial contamination. In order to it, electrochemical automatized methods and methods which utilized nanotechnology were developed.

Keywords: automation, electrode, heavy metals, pollution, sensor, voltammetry

OBSAH

1 ÚVOD

Znečištění životního prostředí je v současné době celosvětovým problémem. Ačkoli je možno mezi polutanty zahrnout jevy jako světlo či zvuk, nejzávažnějším problém zůstává kontaminace prostředí toxickými látkami. Podle WHO jen v roce 2012 vedlo znečištění životní prostředí k 12,6 miliónům úmrtí, což představuje 23 % z celkového ročního úhrnu *(WHO, 2012)*. Vzhledem k rostoucí industrializaci a urbanizaci znečišťování životního prostředí v průběhu 21. století výrazně akcelerovalo. Ochrana životního prostředí se stala veřejným zájmem upraveným legislativně jak na národní, tak mezinárodní úrovni. Jedinou možností, jak tyto legislativní požadavky plnit, je provádět kontinuální monitoring vybraných polutantů nejen v půdě, vodě a ovzduší, ale zejména v odpadech uvolňovaných do prostředí.

Potřeba provádět efektivně analýzy velkých množství vzorků se odrazila v průniku automatizace do analytické chemie. Jako odpověď na tyto požadavky byly vyvíjeny průtokové (fluidní) analytické metody a automatizovaná analytická zařízení. V polovině sedmdesátých let byla vyvinuta metoda průtokové injekční analýzy (flow injection analysis, FIA), jejímž hlavním atributem je dávkování měřeného kapalného vzorku to nesegmentovaného nosného proudu reagencií. Díky levné instrumentaci, jednoduché obsluze a kompatibilitě s téměř všemi běžnými detektory se FIA ocitla v centru zájmu vědecké komunity. FIA přinesla ve velké míře automatizaci do rutinních analytických měření a inspirovala celou řadu pozdějších, na průtoku založených technik.

Elektroanalytické metody jsou založeny na sledování elektrických veličin jako proud, potenciál nebo náboj v závislosti na chemických parametrech vzorku. Tyto univerzální metody dosahují dostatečné citlivosti a selektivity a stejně jako průtokové metody jsou vhodné k miniaturizaci. Desítky let vývoje na křemíku založených mikroelektronických zařízení, během nichž dosáhly postupy jejich výroby značné preciznosti, byly zúročeny při konstrukcích jak mikrofluidních zařízení, tak při samotné implementaci elektrochemických detektorů do nich.

Vývoj fluidních a jiných automatizovaných zařízení s elektrochemickou detekcí je důležitý nejen z důvodu rozvoje samotné analytické metody, ale především z důvodu jejich aplikace v environmentálních analýzách.

2 CÍLE PRÁCE

- Sumarizovat informace o fluidních zařízeních s elektrochemickou detekcí
- Vytvořit elektrochemickou metodu využívající nanotechnologie pro detekci anorganického znečištění
- Vytvořit elektrochemickou metodu pro detekci bakteriálního znečištění
- Implementovat některou z těchto metod do průtokového zařízení

3 LITERÁRNÍ PŘEHLED

3.1 Fluidní techniky

V současné době je v analytické chemii velká pozornost věnována automatizovaným zařízením. Jedním z nejslibnějších jsou na průtoku založené systémy, které se vyznačují vysokou efektivitou analýz při zachování opakovatelnosti měření. Dalším trendem současnosti v environmentálních analýzách je miniaturizace nejen detektorů, ale celých analytických zařízení. Cílem je vyhnout se odběru a transportu vzorků do laboratoře, kde jsou analýzy prováděny pomocí bench-top zařízení, ale umožnit jejich analýzu přímo v místě odběru (tzn. *in situ*).

3.1.1 Segmentová průtoková analýza

Počátky průtokových technik sahají do 40. let 20. století, kdy začal vznikat obor dnes nazývaný procesní analytická chemie. Jeho účelem bylo monitorovat chemickou výrobu a na základě získaných informací (elektrická vodivost, pH, absorbance aj.) v reálném čase tyto procesy řídit. Jinou oblastí využití průtokových technik a díky publikační činnosti a patentům lépe zdokumentovanou, byly laboratorní analýzy. V této oblasti se využívalo průtoku k manipulaci se vzorkem, k jeho přípravě a přenosu na detektor. Americký biochemik Leonard T. Skeggs ml., s cílem zvýšit efektivitu práce klinických laboratoří v nemocnicích, vyvinul v 50. letech metodu nazvanou segmentová průtoková analýza (segmented flow analysis, SFA) *(Skeggs, 1957)*. Při ní je vzorek vstřikován do toku reagencie rozděleného (segmentovaného) vzduchovými bublinami, tzn. směs reagencie a vzorků je rozdělena na segmenty (Obr. 1). Segmentace je udržována až po detektor (běžně fotometr) kde jsou vzduchové bubliny odstraněny ventilační průtokovou celou a obnoven nesegmentovaný (kontinuální) proud. Ačkoliv princip kontinuálního měření v průtoku již byl znám, tato metoda vzhledem k segmentaci toku vzduchovými bublinami omezovala rozptyl vzorku a přinesla výrazný pokrok v analytické klinické instrumentaci. SFA dominovala na poli klinických analýz přes dvě dekády a i v současnosti je hojně užívaná v laboratořích k environmentálním a průmyslovým analýzám *(Valcárcel a kol., 1988; Hollaarm a kol., 2008; Dafner, 2015)*. Z praktického hlediska je tato metoda složitě miniaturizovatelná kvůli přítomnosti vzduchových bublin.

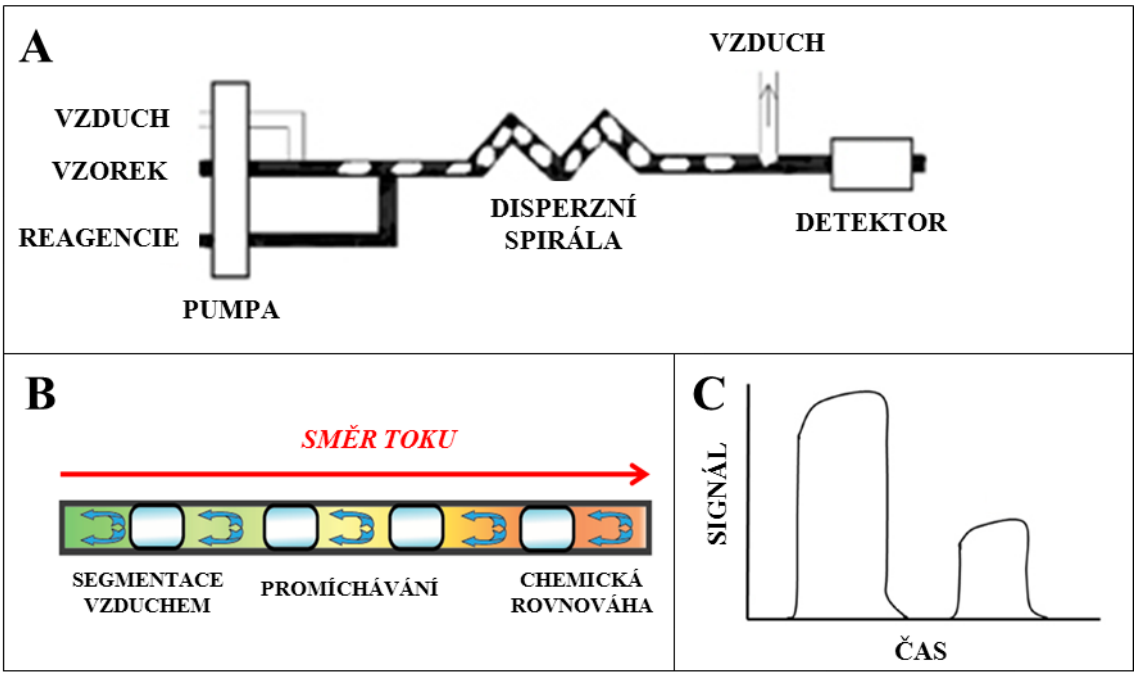

Obrázek 1. Schéma SFA systému (A), detail segmentovaného toku (B) a schéma signálu získaného analyzérem se segmentovaným průtokem (C). Převzato z: http://www.edu.utsunomiya-u.ac.jp/chem/v16n1/103Naser/Naser.html a http://www.flowinjectiontutorial.com/index.html

3.1.2 Průtoková injekční analýza

Odhodlání pokračovat ve vývoji laboratorních průtokových technik vyústilo v polovině 70. let v představením konceptu průtokové injekční analýzy (flow injection analysis, FIA). Tato metoda vyvinutá Růžičkou a Hansenem je založena na injektáži malého množství vzorku (typicky v řádech desítek µl) do nesegmentovaného proudu nosiče *(Ruzicka a kol., 1975)*. FIA nepředstavuje pouze metodu urychlující rutinní analýzy, ale byla novým konceptem práce se vzorkem navíc plně kompatibilním v přicházejícím věkem počítačových technologií. V případě FIA jsou zaznamenávány transientní signály v podobě ostrých píků, jejichž výška odpovídá koncentracím analytu. FIA se v nejjednodušší konfiguraci skládá z pumpy, která vytváří proud nosiče, injektážního portu, kterým je do proudu nosiče vpraveno definované množství vzorku, spirálou, ve které se vzorek rozptýlí (disperguje), reaguje se složkou/složkami nosiče a vytváří látky detekovatelné průtokovým detektorem (Obr. 2). Vhodně designovaný FIA systém umožňuje získání výsledků v řádech desítek sekund od injektáže včetně doby promytí detektoru pro následující vzorek. S cílem rozšířit potenciál FIA systémů je věnována pozornost vývoji zařízení umožňující současnou detekci více analytů bez využití klasických chromatografických nebo elektromigračních separačních metod.

V porovnání s kapalinovou chromatografií, kde je multikomponentní analýza umožněna na základě separace složek, v případě FIA je umožněna selektivní detekcí nebo specifickým zpracováním vzorku. Toho bývá dosaženo použitím větvených systémů s jedním detektorem nebo multi-detektorových systémů. Jinou možností je využití voltametrických detektorů (s velkou rychlostí polarizace), detektorů s diodovým polem (s různými vlnovými délkami měření) nebo detektorů atomových emisí ICP-OES.

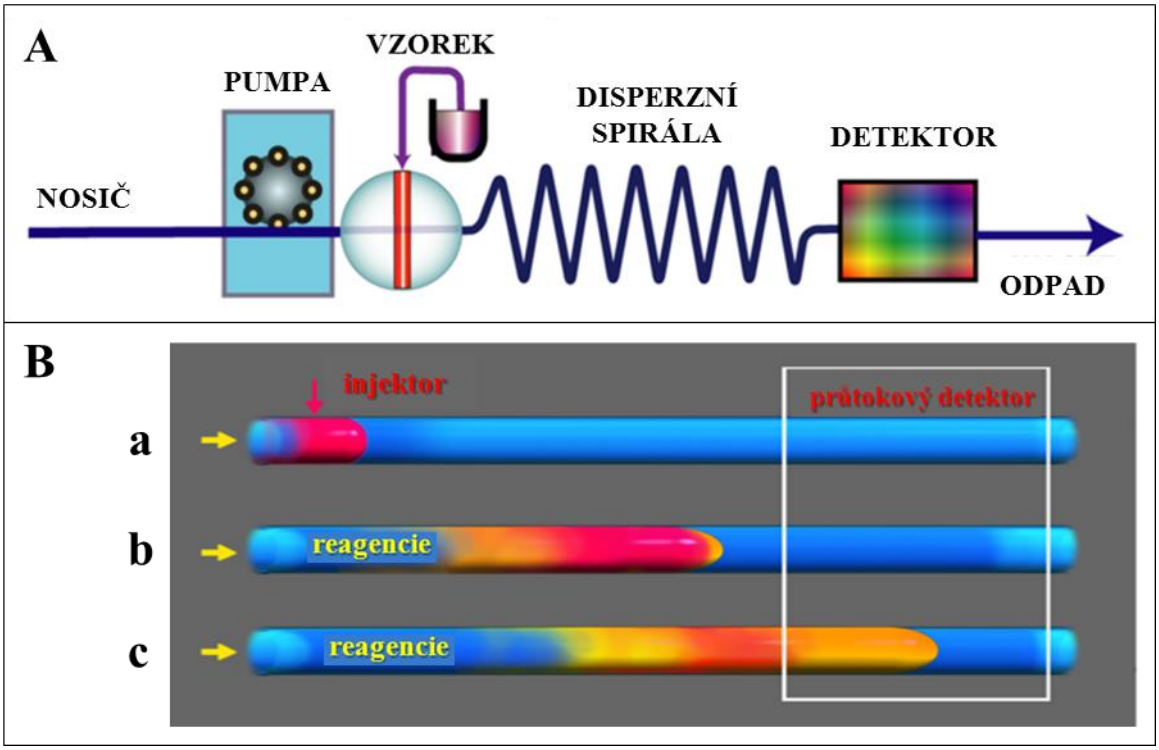

Obrázek 2. Schéma FIA systému (A). Proces disperze reagencie (modrá) do vzorku (červená) za vzniku detekovatelného produktu (žlutá) v různých fázích FIA analýzy (B). Převzato z: http://www.flowinjectiontutorial.com/index.html

3.1.3 Sekvenční injekční analýza

I přes velkou řadu výhod, které SFA a FIA přinesla, velká spotřeba reagencií, které je u nich potřeba neustále pumpovat aparaturou, přispěla k rozvoji dalších průtokových metod. Jednou z nich byla sekvenční průtoková analýza (sequential flow analysis, SIA), která je z důvodu mnoha společných znaků někdy považována za modifikaci FIA. Růžička a Marshall vyvinuli tuto metodu zejména pro potřeby procesní analytické chemie *(Ruzicka a kol., 1990)*. Je zde používán multipoziční ventil a obousměrná pumpa k precizní manipulaci se vzorkem – metoda se spoléhá na naprogramovanou změnu směru pohybu proudu nosiče spíše, než na jednosměrný kontinuální tok jako v případě SFA a FIA (obr. 3). Součástí SIA systémů jsou tedy počítače s příslušným

softwarem, které řídí samotný měřící cyklus (pohyby čerpadla) a uchovává o něm data. Během měřícího cyklu jsou vzorky a reagencie nasávány do disperzní spirály v zónách. Změnou směru pohybu proudu nosiče (tj. směru činnosti pumpy) dojde k dokonalému promísení zón a vzhledem ke změně pozice ventilu jsou zóny neseny k detektoru. Jak již bylo zmíněno, výhodou SIA je oproti FIA úspora reagencií, na druhou stranu frekvence dávkování vzorku je u SIA nižší. SIA je navíc poměrně náročná na preciznost synchronizace činnosti pumpy s ventilem. Nicméně všestrannost manipulace se vzorkem metody SIA se uplatnila i v kombinaci se separačními schopnostmi kapalinové chromatografie (sequential injection chromatography, SIC).

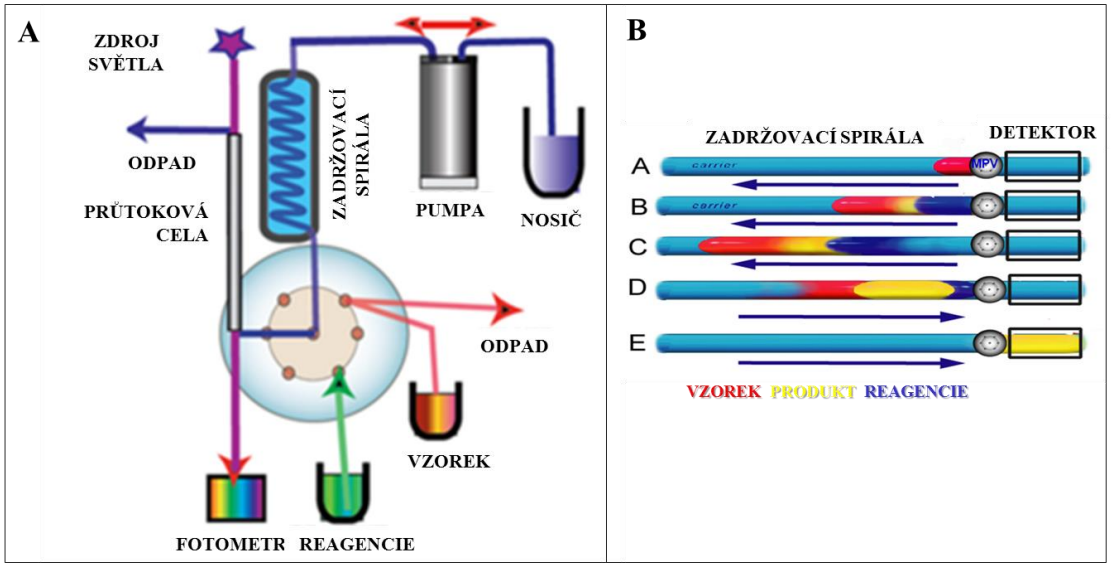

Obrázek 3. Schéma SIA systému s absorpčním detektorem (spektrofotometr) (A) a proces disperze reagencie (modrá) do vzorku (červená) za vzniku produktu (žlutá) během SIA analýzy. Převzato z: http://www.flowinjectiontutorial.com/index.html

3.1.4 Částicová injekční analýza

Částicová injekční analýza (bead injection analysis, BIA) byla vyvinuta Růžičkou a kol. na začátku 90. let *(Ruzicka a kol., 1993)*. V nejjednodušším uspořádání BIA je roztok definovaného množství mikročástic vstříknut do proudu nosiče. Tyto částice jsou v určité části systému zachyceny. Vzorek je následně injektován a jeho zóna prochází mikročásticemi, kde buď analyt reaguje s molekulami reagencie na povrchu částic, nebo je analyt imobilizován a následně derivatizován promytím reagencií (Obr. 4). Detekce zachyceného analytu probíhá buď přímo na samotných částicích, nebo může být derivatizovaný analyt z částic eluován a standardně nesen na detektor *(Ruzicka a kol., 1993; Ruzicka, 1994)*. Obnova reaktivního povrchu mikročástic (pevné fáze) je

atraktivní vlastností této metody, protože umožňuje selektivní imobilizaci analytu z matrice. Pro efektivní využití této metody musí být aparatura speciálně konstruována - v injekčním ventilu musí být mikrokanál s imobilizovanými mikročásticemi. Tento design se nazývá lab-on-valve (laboratoř ve ventilu).

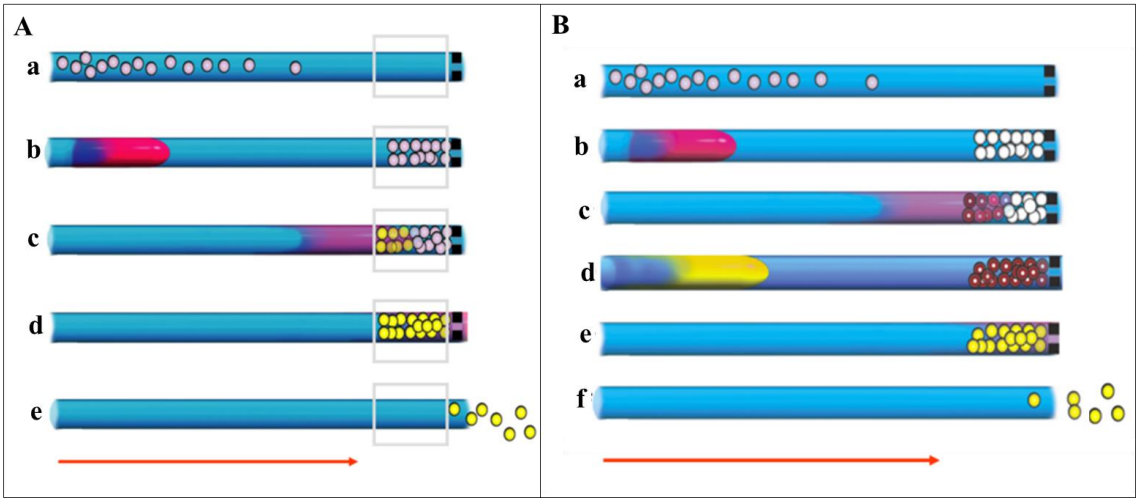

Obrázek 4. Schéma procesů probíhajících při BIA s reagencií imobilizovanou na částicích (A). Částice jsou aplikovány do proudu nosiče (a). Následně je nastříknut vzorek (b), který je unášen k detektoru. Když je vzorek dopraven k částicím, reaguje s jejich funkčními skupinami a je zde imobilizován (c). Naopak zóna vzorku je unášena dále a matrice vzorku je odplavena (d). Částice mohou být odmyty do odpadu (e) nebo ponechány na detektoru pro další analýzy. Schéma procesů probíhajících při BIA s analytem imobilizovaným na částicích. Nejprve jsou nastříknuty částice do proudu nosiče s reagenciemi (a). Následně je nastříknut vzorek (b) a je unášen proudem k detektoru, kde je zachycen na částicích a matrice je odmyta (c). Následně je nastříknuta reagencie (např. chromogenní látka) (d) a když dosáhne částic, vzniká detekovatelný substrát (e). Částice mohou být odmyty (f) nebo ponechány pro další analýzu. Převzato z: http://www.flowinjectiontutorial.com/index.html

3.1.5 Miniaturizace průtokových analýz

Počátky mikrofluidních analýz lze spojit s vývojem prvních kapilárních kolon pro plynové chromatografy na počátku 70. let. První on-chip plynový chromatograf představil Terry a kol. v roce 1979 *(Terry a kol., 1979)*. Toto zařízení bylo vyrobeno standardními litografickými technikami na křemíkové destičce a skládalo se z 1,5 m dlouhé kolony, injekčního ventilu a z křemíku vyrobeného vodivostního detektoru. Navzdory schopnosti provádět velmi rychlé separace a minimální velikosti těchto zařízení, reakce vědecké komunity byly spíše vlažné (jako v případě každé nové technologie) a do konce 80. let se mikrofluidní technologie vyvíjely poměrně pomalu. Už v této době však byla pozornost věnována výrobě pomocných, nicméně neméně důležitých součástí mikroprůtokových zařízení - mikropumpám a mikroventilům

(Vanlintel a kol., 1988; Esashi a kol., 1989; Vandepol a kol., 1990). S vědomím, že v případě dostatečné miniaturizace průměru průtokového kanálu postačí difuze k promíchání reagencií a vzorku, se Růžička a kol. v tomto období zabýval integrací miniaturních detektorů do mikrokanálů *(Ruzicka a kol., 1984).*

Po roce 1990, kdy vznikl koncept miniaturizovaných komplexních analytických zařízení (micro total analytical systems, μTAS), nastal prudký rozvoj mikroprůtokových technik *(Manz a kol., 1990).* Původní smysl miniaturizací těchto zařízení nebyl snížení spotřeby mobilní fáze, nosiče, reagencií aj., ale ve zlepšení celkového analytického výkonu. V této době již vznikala první zařízení, která lze označit za mikrofluidní, kdy vnitřní průměry průtokových kanálů klesaly k desítkám μm *(Lichtenberg a kol., 2002).* Whitesides považuje mikrofluidiku za obor, který manipuluje s objemy 10^{-9} – 10^{-18} l v kanálech o průměru od desítek po stovky μm *(Whitesides, 2006).* Tyto zařízení často využívají separační techniky a umožňovaly provádět analýzy více složek vzorku v jednom zařízení *(Manz, Grabera Widmer, 1990).* Elektroforéza (elektroosmotická pumpa) byla navíc vhodným nástrojem, jak zajistit konstantní průtok v zařízení, protože konvenční pumpy v 90. letech měly problémy s vytvořením dostatečného tlaku pro transport v mikrokanálech.

V současnosti jsou dostupná již komerční mikrofluidní zařízení (ačkoli pouze specializovaná na konkrétní aplikaci) a v odborné literatuře je publikováno velké množství článků zabývající se touto tematikou *(Sivasamy a kol., 2010; Aibaidula a kol., 2016; Carugo a kol., 2016; Gao a kol., 2016; Zheng a kol., 2016).* Mikrofluidní zařízení již nejsou jen analytickým nástrojem, ale byla využita v celé řadě biologických disciplín – DNA sekvenování, klonování, PCR amplifikace, analýza aminokyselin, peptidů i proteinů, manipulace s buňkami aj. *(Tao a kol., 2015; Yehezkel a kol., 2016; Cui a kol., 2016; Lin, Zhao a kol., 2016; Lin, Leung a kol., 2016).*

3.2 Elektrochemie a fluidní zařízení

3.2.1 Souhrnný článek

KUDR, J., ZITKA, O., KLEJDUS, B., VRBA, R. a ADAM, V. Hazardous Materials Detected by Microfluidic Electrochemical Devices – Review. *Journal of Hazardous Materials* [odesláno do redakce].

Podíl autora Kudr J.: 70 % textové části práce

Hazardous Materials Detected by Microfluidic Electrochemical Devices – Review

Jiri Kudr [1,2], Ondrej Zitka [1,2], Borivoj Klejdus [1,2], Radimir Vrba [2] and Vojtech Adam [1,2,*]

[1] Department of Chemistry and Biochemistry, Mendel University in Brno, Zemedelska 1, Brno CZ-613 00, Czech Republic, European Union

[2] Central European Institute of Technology, Brno University of Technology, Technicka 3058/10, Brno CZ-616 00, Czech Republic, European Union

*****Correspondence: Department of Chemistry and Biochemistry, Mendel University in Brno, Zemedelska 1, 613 00 Brno, Czech Republic. Tel.: +420 5 4513 3350; fax: +420 5 4521 2044. E-mail address: vojtech.adam@mendelu.cz

Abstract

Pollution of environment represents serious issue, which deserves increased attention. Conventional laboratory techniques, which rely on bench-top devices, do not satisfy nowadays demands for *in situ* analysis. Progresses in microfabrication technologies enabled significant miniaturization of fluidic analytical devices and laid the foundations of microfluidics. This review focuses on electrochemical microfluidic analysers for environmental applications with emphasis on direct electrochemical detection without any separation step. Particularly, we paid the attention to advantages and disadvantages of the developed device and summarized their application for detection of pH, metals, nitrate and nitrite ions, phenols, pesticides and herbicides, and bacteria.

Keywords: automation; chip; electroanalysis; electrode; electrophoresis; heavy metals; microelectrode; pollution; sensors; voltammetry

1. Introduction

Worldwide pollution of environment belongs to the crucial issues mainly in developing countries. A releasing of harmful substances to environment and increasing concentrations of naturally occurring compounds above their common levels alter biogeochemical cycles represent two main mechanisms contributing to the pollution. Monitoring of pollutants levels in air, soil and water is the only way to meet national and international legislative measures and to protect environment, food sources and public health. It is not, thus, surprising that analytical chemistry is rapidly growing and pushes technical developments of online, automatic and fluidic analysis, which provide results without substantial delay [1]. Although fixed-site laboratory analysis is broadly used in environmental monitoring and industrial analysis, this review mainly focuses on one specific analytical branch, electrochemistry having great potential to be miniaturized.

Electrochemistry has been evolving nearly one century and during this period became valuable and versatile analytical method [2]. It deals with measurement of electrical quantities such as current, potential or charge and their relations to chemical parameters of an analysed sample [3]. To fundamentally describe the principles of various electrochemical is not the aim of this review, since there have been described elsewhere [3, 4]. However, it is worth to note that especially pulse techniques succeeded in lowering detection limits due to increase of faradaic vs. nonfaradaic currents ratio. Substantial improvement of electrochemical techniques sensitivity especially for trace metals detection was caused by an integration of pre-concentration step on an electrode followed by measurement of the pre-concentrated analyte so called stripping analysis [5, 6]. It was not only electrochemical signal generation, which changed significantly over the time and made electroanalysis more user-friendly and power-full method, but also progresses in microfabrication, electronics and software data evaluation significantly contributed to development of the field of electroanalysis.

In comparison with other analytical methods, electroanalytical ones provide several attractive properties. Among others, there is nearly limitless possibility of substantial miniaturization of electrodes and whole detection device, which is the most important in the field of microfluidics and *in situ* analysis. The first part of presented review is aimed to the progresses in electrode materials and geometries. Subsequent, we summarize electrochemistry in fluidic analysis. However, due to extensiveness of this topic, several cross-references for review articles are supplied, too. Finally, the text is enriched by description of several applications of microfluidic sensors in detection of inorganic, organic and biological pollutants.

2. Electrodes

2.1. Advanced working electrode geometries

The first step in the pathway having user-friendly and robust electrochemical analysers has been developing electrode materials and geometries. Although electroanalysis is performed using three-electrode system (working, reference and counter electrode), its performance is influenced especially by working electrode properties. The choice of electrode material depends on redox analyte properties since low background current at analyte oxidation/reduction potential is required (potential window of electrode).

From the electrochemical point of view, mercury electrodes possess superior properties. High hydrogen overvoltage, smooth surface or surface recovery is some of them. On the other hand the possibilities of measurement at positive potentials and miniaturization are limited, where, in the case of miniaturization, mechanical properties of mercury and need to use capillary make the manipulation with mercury-based electrodes very challenging. Although these electrodes connected with adsorptive stripping voltammetry have superior sensitivity, possibility to use them in online/remote sensing is very limited. In order to lower

susceptibility of mercury electrode to be damaged and increase their mechanical resistance, mercury-film electrodes (MFE) have been used in several applications [7]. Unlike dropping mercury electrode (DME) and hanging mercury drop electrode (HMDE), MFE lack their fragility and decrease mercury consumption, which is consistent with current trends in analysis to use environment friendly materials. Glassy carbon mostly serves as a support material, however other carbon-based materials or metals have been also used [8]. An electrode is obviously plated at cathodic potential in mercury nitrate solution (*ex situ*), however, *in situ* plating, when mercury ions are added directly to a sample, was reported, too [9, 10]. It was proved that MFE performance depends on homogeneity (roughness) of electrodeposited film and on solution composition, therefore, electroplating represents the crucial step to obtain satisfactory results [11, 12], when renewable mercury film electrode was also found [8, 13]. This was based on silver, wire which was pressed by piston through chamber containing silver amalgam and limited by o-rings prior to a measurement. Foster *et al.* concluded that metallic modifiers improved electrode sensitivity towards lead(II) and cadmium(II) only when the film substrate performed slow electron transfer kinetics like glassy carbon or boron-doped diamond [14]. Instead of mercury, bismuth, lead, antimony or gallium films are used as a safe alternative to create so called MFE [15-17]. Especially bismuth film electrodes (BiFE) possesses comparable performance with MFE [18].

From solid state electrodes, mostly carbon, silver and gold ones are used. Solid materials enable to measure highly positive potentials, which is advantage compared to mercury based ones. If one may continue in comparing these types of electrodes, surface of solid state ones is heterogeneous and needs to be carefully pretreated before measurement, which limits its repeated on-site use in field-portable instrumentation. Actually, this is also case of MFEs and other film electrodes, since the glassy carbon or other solid materials mostly serve as support, where mercury covers the surface of support material with many

droplets rather than homogenous film [19-21]. Solid electrodes are mostly presented in stationary planar disk geometry, i.e. the electrode material of cylindrical shape is fitted within tube of insulating material. However, wire-shape electrodes and advanced electrode geometries like screen-printed electrode (SPE) or interdigitated microelectrodes (IDE) are emerging.

Screen-printed electrodes (SPEs) were suggested to overcome demands for pretreatment. Fabrication of SPE is based on required paste casting through a mask (Fig. 1A). Portability of these electrodes is obtained by introduction of working, reference and counter electrode into one solid support, however printing on flexible substrates and paper was also reported [22-24]. Although they can't compete with classical electrodes sensitivity, their disposable use due to inexpensive fabrication and effective performance makes them attractive for broad range of routine applications. Rapid development of screen-printing technology caused mass production of SPE in different configurations and from various materials according to demands. Moreover, SPE arrays, which enable simultaneous amperometric detection of different analytes, can be fabricated [25], which is one of the biggest advantages of SPEs.

Other electrodes with miniaturized geometries like (ultra)microelectrodes (one dimension not greater than 25 μm) and interdigitated microelectrodes arrays (IDE) were suggested to improve analysis sensitivity and to enhance their practical applicability compared to SPEs. When dimension of working electrode is comparable with electrode diffusion layer, it provides several advantages for electrochemical measurements [26]. Among others, the rate of mass transport to microelectrode surface increases, double layer capacity decreases and as a consequence it possesses superb signal-to-background characteristics. Application of these electrodes reaches from a using in microfluidic devices, as an amperometric detector in electrophoretic capillaries (CE-AD), to be used directly *in vivo* [27,

28]. In addition, electrodes dimensions were pushed forward from micro- to nanometers, however their use is restricted to laboratories [29, 30]. IDE represents further step in the search for an ideal electrode. Since diffusion layers of several adjacent microelectrodes in array are overlapping, current amplification is obtained by redox cycling, i.e. one electrode performs analyte reduction and reduced analyte diffuse to adjacent electrode where oxidation to original form take place (Fig. 1B).

Chemical modification and functionalization of electrode surface is another possibility to enhance electrode sensitivity and selectivity. Boom of nanotechnology attracted attention of electrochemists since nanoparticles help to increase electrodes surface area, fasten mass transport, control electrode microenvironment and enable efficient catalysis [31, 32]. They pave the way for cheap fabrication of electrodes from expensive materials and for biosensors construction. This broad topic was previously reviewed in [33, 34].

2.2. Reference electrode

From the miniaturization point of view, not just working electrode but also reference electrode requires considerable attention [35]. The potential of working electrode is expressed in *V* against reference electrode potential, hence the reference electrode has significant influence on measurement reliability. The main requirement for reference electrode is that its potential remains constant (non-polarizable) during the electroanalysis. Shinwari *et al.* suggested that reproducibility of potential between individual reference electrodes and minimization of potential drift during measurement should be taken into account when reference electrode is miniaturized [35]. Ag/AgCl is definitely the most used reference electrode in industry and research due to its simplicity and low price. The macroscopic one mostly consists of Ag wire closed in glass tube, covered with AgCl and immersed in saturated solution of KCl (liquid-junction reference electrodes). The internal solution is separated from

analysed solution by salt bridge and membrane. Kitade *et al.* reported needle-type reference electrode with outer and inner diameter 1.0 μm and 0.5 ± 0.2 μm, respectively, with an agar gel containing potassium chloride as a salt bridge [36]. Although, the miniaturized reference electrode with ordinary geometry was reported, the quasi-reference electrode (QRE) AgCl (sometimes also called pseudo-reference since are not non-polarizable) electrodes without filling are used in order to simplify the fabrication step [36-38]. The potential of such electrodes is unknown, hence the comparison of QRE with true reference electrode using measurement of inner standard (e.g. ferrocene/ferrocenium) is needed [39]. Since the electrode is directly in contact with measured solution (no salt bridge and membrane) its ohmic resistance is minimal. Potential is considered not to change during series of measurements in limited range of conditions (mainly pH). Microfabrication techniques like lithography, thin-film metallization, etching, electroplating, screen printing and their combinations have been used to produce miniaturized reference electrode, however fabrication of these electrodes consisted of several relatively complicated steps, thus, their mass production seems to be hardly possible now [40-42]. The fabrication method of QRE must be carefully selected especially when the monitoring for long period is required since the thin electrode material is connected with decrease of electrode stability and lifetime. Standard hydrogen electrode (SHE) or saturated calomel electrode (SCE) can be also miniaturized, nevertheless the need of hydrogen controlled pressure and use of mercury makes fabrication of them challenging [43, 44]. Single step microfabricated QRE from palladium hydride was used by Webster & Goluch [45].

3. Electrochemistry in fluidics

In the previous chapter, the evolution of electrode materials and geometries was discussed since it represents necessary step in development of automatic electroanalytical

devices. In this pathway, an integration of electrodes to fluidic devices represents further step, however, manipulation and control over sample and reagent delivery are key features of fluidic microdevices. The fluidic analysis is considered as an analysis where liquid sample is continuously flowed over a detector. But mostly, a sample is also processed (aspirated or injected, moved to waste etc.) by controlled flowing stream. The common fluidic devices consist of pumps and detection flow-through cell connected with tubes of various lengths and diameters. However, additional components like bubble-traps or valves can be integrated, too [46]. For fluidic analysers, techniques like liquid chromatography or chip electrophoresis also fit. These techniques often benefit from electrochemical detection however these will not be described here extensively since they were reviewed elsewhere [47, 48].

In order to lower sample and reagents consumption, fast processing, low cost, automation and improved portability microfluidics was introduced. This attractive filed of science has been defined in number of ways based on manipulated solution volumes or diameter of fluidic channel. For example Whitesides defines microfluidics as a science and technology of systems that process or manipulate small (10^{-9} to 10^{-18} litres) amounts of fluids, using channels with dimensions of tens to hundreds of micrometres [49]. When the higher volumes than 10^{-9} litres are operated, it is defined like milifluidics [50-52].

3.1 Fluidic chips fabrication

Silicon and glass belong to common substrate for fluidic/microfluidic devices fabrication. Processing of silicon benefited from decades of semiconductor microelectronics production. These techniques based on photolithography and etching nowadays reached high degree of precision, nevertheless they are still very time-consuming (unique mask for every pattern is needed etc.) and expensive [53]. The introduction of soft lithography (poly(dimethylsiloxane) (PDMS) moulding), 3D printing and micromilling significantly

lowered the price of microstructures fabrication [54-56]. PDMS possesses several advantages, it is easily moulded, possesses good physicochemical properties, and enables fabrication of small and fast pumps and valves [57, 58]. Au *et al.* suggest that among others PDMS-moulding processes are not easily commercialized since high-throughput fabrication is expensive [55]. Mukhopadhyay broadly discussed PDMS properties for microfluidic application and highlighted its drawbacks like absorption of small hydrophobic molecules and hydrocarbons, its innate hydrophobicity and gas-permeability, which can be, however, an advantage for cell-based studies [59-61]. From polymeric materials poly(methylmethacrylate) and polycarbonate were commonly used to fabricate a chip, too [62-64].

Integration of electrodes to mentioned devices are achieved in the form of thin or thick-film patterns. Electrodes are deposited on flat substrate and subsequently bounded with part with desired channels [65, 66], which is shown in Fig. 2A. Common electrodes material for working and counter electrodes are carbon, platinum, gold and Ag/AgCl for reference electrode. Alternatively, metal microwires (Pt, Au or modified with carbon) can be incorporated within a chip and aligned to patterned electrode pad [67-69].

Since the introduction in 2007, paper-based microfluidic analytical devices (μPADs) have attracted significant attention [70]. They represent low-cost disposable instrumentation with an integrated simple separation step. Although conventional microfluidic systems rely on hollow channels liquid transport, μPADs are completely based on capillary flow just like in the case of paper chromatography, hence external pumps are not necessary (Fig. 2B). The μPAD topic is young, but very comprehensive and the focused literature is highly recommended [71, 72]. The basic methods of μPADs fabrication are based on creating wax barriers within the paper or selective removal of paper. Different types of detectors can be incorporated in μPADs. Colorimetric detection is common due to its simplicity, however electrodes provide further more selective and sensitive platform [73-75]. Electrodes can be

formed by noble metal sputtering, directly printed within μPADs using ink or paste or they can be combined with external SPE [76, 77]. Dossi *et al.* successfully used simple hand-drawing of desired electrodes geometry on paper using pencil lead [78]. Graphite-based pencil leads doped with suitable modifiers can be fabricated using extruder and serve instead of commercial pencil lead [79]. In addition, an incorporation of reference electrode is an issue as in the case of other micro applications. Lan *et al.* introduced μPAD using advanced geometry in order to provide stable reference potential, which is necessary for voltammetric analysis [80]. The sample and reference zone is separated by microfluidic channel that includes mixing zone. Microfluidic channel enables ionic contact between a sample and reference zone but slow diffusive convection-free transport prevents interchange of ions between sample and reference zones. Alternative method based on hand-drawing reference electrode using pencil lead doped with Ag and AgCl was developed by Dossi *et al.* [81]. A drawback of μPADs is nonspecific absorption of molecules to cellulose (lowers the amount of analyte reaching detector), which is needed to be compensated by calibration [82].

3.2. Sample handling

Understanding the principles of microfluidic is essential for developing more sophisticated analytical systems [83]. An ideal fluidic/microfluidic system represents a device, which is able to perform complete analysis. It includes several steps like sample injection, concentrating/dilution, mixing with reagents and final analysis where timing and transport must be accurately controlled. Small amounts of analytes require proper handling and minimal dispersion only can results in loss of sensitivity. In addition, low flow pulsation is required due to low flow rates.

In the case of macroelectrodes, it is needed to mix sample with inert supporting electrolyte to ensure that electric field in solution is homogenous and near-zero and not

affected by analyte oxidation/reduction (suppress migration of electroactive species). The only exception is microelectrodes in some applications (see [84] and [85]).

Fluid manipulation is mostly achieved by electrical techniques (e.g. electroosmotic flow) or by pressure. Pleasure-driven flow produces characteristic parabolic profile [86], but electroosmotic slightly differ, as it is shown in Fig. 3A and 3B, respectively. Syringe, piston or peristaltic pumps can be used to obtain such flow. Peristaltic pumps are able to provide constant flow rate and possibility of bidirectional flow is one of their advantages. Nevertheless at low flow rates, pulsating is obvious and performance in low flow rates is not reliable [87]. For some applications macroscale pumps are sufficient however microfluidic systems with self-contained flow generation are emerging. The field of micropumps was extensively reviewed by Laser & Santiago previously [88].

Instead of mechanical ones, pumps without moving parts are emerging due to pulsation free flow and higher reliability. Different actuation methods were used in this field as thermal, chemical (osmotic), acoustic, magnetic or electric. Electrical control of flow provides several possibilities, i.e. electrochemical, electrohydrodynamic and/or electrokinetic. In order to induce flow, an electrochemical way uses electrolysis creating bubbles causing movement [89]. Electrohydrodynamic way is being used in the case of dielectric movement (see [90] for review).

Electrokinetic pumps use electroosmotic and electrophoretic effects. They are the most popular due to simple design and fabrication. Stable electroosmotic flow (EOF) can be obtained by simple integration of high current/voltage circuit with integrated electrodes within channel (Fig. 3B). Flow is obtained by ionization of ionizable surface groups within channel. Charge double layer with counterions is created and current (DC or AC)/voltage application induces cations or anions in diffuse layer movement to cathode or anode. In the same time solvent molecules are dragged together [91]. EOF flow profile possesses shape of plug, which

allows separation of ionic species. The flow rate can be controlled using optimization of potential (applied current or voltage). This phenomenon is used in electroosmotic pumps, which possesses advantage of pulse-free working without back pressure. In capillary electrophoresis, electrodes are simply placed within solutions reservoirs, however, in microfluidics, an integration of electrodes within channels is preferred. Electroosmotic pumps possess two fundamental modes (i) open channel and (ii) packed-bed electroosmotic pumps. Open channel pumps consist of multiple (4 – 100) open channels with small diameter, which supply larger channel with electroosmotic flow. Open channel pumps are able to transport fluid with high flow rate, however they are not suitable for high pressure application due to low hydraulic resistance. Packed-bed pumps exhibit better performance in terms of overall output pressure. They are based on packing of small particles within channels and holding them on place. Electroosmotic pumps occupy only part of channel and pump for the rest of device. It is worth to note that high potentials on electrodes within microchannel for long period of time can lead to creation of bubbles due to water electrolysis in these arrangements.

Janasek *et al.* described differences between large channels and microfluidic systems and highlighted the major difference, mainly flow characteristics [92]. In the case of large scale channels when two solutions come together, they are mixed spontaneously by convection. However, the absence of turbulences in microfluidics causes that this two solutions mix only due to diffusion. Hence, development of special mixing devices is needed.

3.3. Methods

Electrochemical detectors are very popular in case of fluidic devices and since their significant miniaturization is possible, they are also used in microfluidic devices. Features inherent to electrochemical microfluidic devices are low sample and reagent consumption, low waste production, rapid analysis, portability, and incorporation of pretreatment process

[93]. The development of microfluidics is tightly connected with progresses in micromachining technology. Not just in case of electrodes, but also in case of other part of devices like pumps, valves, mixers or microchannels chips. Current trend is to use highly sophisticated analytical devices like Micro Total Analysis Systems (μTAS) or Lab-on-a-Chip. However the requirement to simplify their structure and functions in order to increase robustness is evident.

Four electrochemical techniques are broadly used in fluidic devices – potentiometry, amperometry, conductometry and voltammetry. Conductometry is general method, where two electrode systems are used for simultaneous measurement of all electroactive compounds in a solution. Conductivity measurement is common in two different electrode configurations. Direct contact of electrodes with analysed solution is possible. However for microfluidic applications contactless conductivity detection is preferred due to the electrodes fouling, bubble formation due to water electrolysis and interference with high voltages used to drive electroosmotic flow [94]. Instead of faradaic current measurement this method uses electrodes insulated from the solution (electrodes are capacitively coupled to the electrolyte) [95]. Since conductivity sensors lack any selectivity, their integration with capillary electrophoresis (CE) to provide microfluidic chips became powerful tool where conductivity detector high sensitivity is used [96]. It must be mentioned that electrochemical detection (potentiostat circuit) requires small power sources, electrokinetic processes such as CE require high-voltage power supplies [97].

In comparison with conductometry, amperometric detection is commonly performed using three electrode system. Reference electrode is used to apply required potential on working electrode in order to polarize it and the current between working and auxiliary electrode limited by analyte diffusion to working electrode surface is measured. Amperometry is common technique used in sensing/biosensing. The current dependence on time (*I-t* curve)

is detected hence it is able to monitor real-time changes. An integration of amperometric detector with fluidic device in comparison with static applications brings several advantages. Among them, due to enhanced convective mass transport to working electrode the increase of current or faster gain of steady state signal can be observed. It is good to highlight that amperometric detection can be used for measurement of electroactive or non-electroactive compounds (indirect amperometry). In the latter case, signal is observed as a decrease of amperometric current of electrolyte in the background [98, 99].

The potentiometric analysis is based on measurement of potentials difference on membrane, which separate two solutions with different ionic activities, where ions are detected. This method is applied in the case of no separation step via zone electrophoresis. Potentiometric sensors consist of reference and indicator electrode. The potential on indicator electrode is changing proportionally to the logarithm of ion activity hence potential stability and reliability represents key part of analysis. The critical problem of these analyses still remains in the reference electrode rather than in indicator electrode (simple metallic electrodes in non-selective analysis) [89]. The selective quantification of ions in electrolyte is performed using ion-selective electrode (ISE) as an indicator electrode – inner part of electrode is separated from sample by membrane. The application in the field of conventional ISE is limited due their price and fragility. However due to potentiometry simple operation and instrumentation is broadly used in clinical laboratories (electrolyte analysis in sweat or serum) representing universal approach to measure pH or to find out the end of titration [100, 101]. In order to lower sample volumes, make the maintenance easier and especially miniaturize potentiometric sensor, solid-contact ion-selective electrodes (SC-ISE) have been developed [102, 103]. Solid contact instead of filling solution is used as the ion-to-electron transducer in indicator electrode, here. Significant effort is also dedicated to obtain simple,

reproducible ISE with valid results with no or at least one point calibration, which would make point-of-care and environmental analysis easy-to-use [102, 104].

Voltammetric measurements in flow analysis are more broadly described in literature than potentiometric since possesses better dynamic response properties, due to the fact that membrane requires time to equilibrate with a measured sample in potentiometry [105]. In voltammetry, the potential between electrodes varies over a time and current response dependent on potential is recorded. The resulted peaks are used to identify and quantify the analyte undergoing redox reaction in sufficiently different potentials. In contrast to amperometric and conductometric detection, voltammetry is able to quantify several analytes simultaneously if they substantially differ in redox potentials [106]. However this selectivity is not needed in fluidic applications, where separation step is implemented. Voltammetric analysis implemented to fluidic (hydrodynamic approach) devices in comparison with stationary analysis is connected with improved detection limits, where faradaic current increases due to increased analyte transport rate to electrode surface however background current changes less [107].

3.4. Detection strategies

As it was mentioned previously, electrochemical on-chip detection is often connected with a separation step. Especially when environmental samples with complex matrix are analysed, a sample is purified and concentrated. Integration of electrochemical detectors within chips with electrophoretic separation can be challenging and three distinct approaches can be recognized. It is evident that potential of several thousand V, which is used in order to induce EOF, must be prevented from coupling with electrochemical detection (potential around 1 V), since it is responsible for noise creating and can damage circuitry of conventional potentiostats [108]. Firstly, end-channel approach represents simple way how to

separate voltages and is based on alignment of electrode outside of separation channel (10–20 μm from channel end), since electric field strength rapidly decreases there [109, 110]. On contrary, in the case of in-channel, detection electrode can be directly placed within channel due to electrically isolated potentiostat [108, 111]. Alternatively decouplers can ground the separation voltage in channel prior to the detector (off-channel configuration) [112]. Each of these options possesses their own advantages and disadvantages. Alignment of end-channel electrode is simple, however separation efficiency decreases due to dispersion of analyte plug. Resolving closely migrating peaks can be complicated and it can lower detection sensitivity. Since Pt or Pd decouplers can adsorb only H_2 generated by cathode (not O_2) they can be used in the case of normal polarity separations only [113]. In-channel alternative reduces peak broadening and retain high sensitivity, and enables reverse polarity separation without decoupler.

4. Applications of electrochemistry in microfluidic environmental analysis

4.1. pH measurement

The hydrogen ion exponent (pH) is one of the main water quality indicators. Measurement of pH provides information about acidity/alkalinity of substances thus is of great interest of environmental analysis and biomedical applications [114]. Life exists in precise pH range since physiological system of most organisms is affected by pH. In water systems, the pH is lowered by generation of H_2CO_3 from atmospheric CO_2 and causes other problems like increase of heavy metals mobility.

Compared to colorimetric pH detection in microfluidics, electrochemical measurement based on Nernst equation (e.g. hydrogen electrode, glass electrode, field-effect transistors) represents golden standard [115]. Nie *et al.* fabricated flexible microfluidic device in order to potentiometrically monitor pH in sweat with sensitivity 61 mV/pH (~gate voltage variation

per pH unit) [116]. The device used no pump since capillary action and evaporative pumping principle was used to take liquid and induce flow through chip. Moreover, microfabrication methods were used to fabricate IrO_x as an indicative electrode and AgCl as QRE. However as the authors highlighted and is also discussed in previous text, ions and especially Cl^- occurred in sweat would influence performance of these reference electrode and true reference electrode (e.g. like Safari *et al.* reported [117]) is needed to improve sensor accuracy.

Chemical sensitive field effect transistors (CHEMFET) nowadays represents broad group of transistor-based sensors (the circuit is comparable with metal oxide field effect transistors – MOSFETs) produced by microtechnologies. In the case of CHEMFETs, gates are covered with ion sensitive layers according to target analyte. Integration of pH sensitive FET within microfluidic channel was previously reported [118]. Microfluidic channel drives H_3O^+/OH^- between sensing electrical channels of FET and suspended membrane (gap between gate and bridge is low) hence modulate charges concentration within FET gap (induces change of charge transfer characteristics). The sensitivity of sensor 290 mV/pH and linear response between pH 5 and 10 was obtained. Sensitivity of pH sensitive FET sensors, which exceeds the maximum limit predicted by electrostatic gating effect of H^+ (59 mV/pH from Nernst equation), was also reported in the case of other suspended bridge pH-sensing device and device based electrolyte gated graphene [119-121].

Li *et al.* reported microfluidic chip, which used film of single wall carbon nanotubes (SWCNTs) as a pH-sensitive electrode and selective membrane [122]. Potentiometric pH response was observed as a change in electronic structure change in semiconducting SWCNTs. The sensor showed more or less ideal Nernstian response (59 mV/pH) in pH range 3 – 11 and flow rates from 0.1 to 15 $\mu l \cdot min^{-1}$.

4.2. Metals

Detection of toxic metals and extreme concentration of essential metals is broadly discussed topic due to their negative effects on public health [123]. Although these effects are known for long time and knowledge about their toxicity is still extending, exposure to them continues [124, 125]. Conventional methods for heavy metal analysis are atomic absorption spectrometry (AAS) and inductively coupled plasma mass spectrometry (ICP-MS). Further, enormous amount of biosensors for heavy metals have been introduced, too [126-128]. However, their use in online and *in situ* analysis is not possible due to size, cost and analysis time. Undoubtedly, electrochemistry is suitable method for heavy metal analysis and several reviews aim to this topic (see [128-131]). For this reason, we describe only several examples connected with the topic of this review.

Microfluidic sensor of Pb(II) suited for mass production and low cost analysis was reported by Jung *et al.* [132]. Particularly, microfabricated chip from cyclic olefin copolymer (COC) was equipped with silver working and silver counter electrode/QRE. Hence, Cl^- ions are needed to be within sample (the analysis was performed in 10 mM HNO_3 and 10 mM NaCl). In addition, square wave anodic stripping voltammetry (SWASV – preconcentration of metal phase on electrode and their selective oxidation during anodic sweep) was used in order to detect Pb(II) ions and limit of detection (LOD) of 0.55 ppb and linearity over a range 1 - 1000 ppb was obtained. The advantage of SWASV is that detection of Pb(II) can be performed without oxygen removal (oxygen is reduced at Pb(II) deposition potential around -0.7 V). Surprisingly, the performance of silver working electrode in respect of Pb(II) was excellent also in comparison with static mercury electrodes [133]. It is assumed to be due to continuous renewal of silver working electrode surface, since the silver ions dissolved on the counter silver electrode are redeposited on working electrode surface. The reason why Ag(I) ions reach working electrode during their dissolving is described by Kirowa-Eisner *et al.*

[133]. They claim that part of Ag(I) reaches working electrode due to working electrode and reference electrode proximity, finite rate of $Ag(I)^+ + Cl(I)^- \leftrightarrow AgCl$ reaction and Ag(I) ions presence within solution.

The work of Zou *et al.* aimed to Pb(II) and Cd(II) [66]. They used e-beam evaporation in order to create Bi working electrode, AgCl QRE and Au counter electrode within microfluidic microfabricated chip made of COC. E-beam evaporation represents alternative to *in situ* Bi plating of solid electrodes, i.e. introduction of Bi ions into sample is not needed. Using SWASV they obtained linear response for Pb(II) within range from 25 to 400 pb and from 28 to 280 ppb for Cd(II). As proof of their concept they measured Cd(II) in soil pore water, ground water and 10% serum supplemented DMEM and succeeded. Same analytes in sea water were measured by Zhou *et al.* [134]. They used platinum working and counter electrode, however instead of quasi-reference electrode true reference electrode, which is, in the case of microfabricated chip, relatively unusual.

Metals analysis by μPADs was reported, too. Conventional procedure of measurement with SPE is to dip electrode into sample or place droplet on the electrode when the physical contamination must be manually filtered out. Capillary pore within paper enables to skip this step, important in case of real samples. Shi *et al.* used a simple combination of chromatographic paper strip and commercial SPE in order to analyse real samples represented by soda water with dissolved gas and ground water with physical contamination [135]. Strip was left on SPE so as to fully cover all three electrodes. One end of paper strip was dipped within sample and sample flowed continuously through paper pores over electrodes while undissolved particles remained within sample cell and gasses within sample did not reach electrodes. They used Bi film electrode created by *in situ* plating of carbon SPE in order to simultaneously detect Pb(II) and Cd(II) and obtained linear response in range to 100 ppb with LOD 2.0 ppb and 2.3 ppb, respectively.

4.3. Nitrate and nitrite ions

Nitrite (NO_2^-) and nitrate (NO_3^-) ions are ubiquitous in environment, but both can induce detrimental effects on human (especially infants) health [136, 137]. Hence, World Health Organization considers their concentrations as important indicators of water quality. Techniques like colorimetry, fluorimetry, capillary electrophoresis or liquid chromatography are often used in order to detect nitrite/nitrate ions [138, 139]. Among these bench-top techniques, electrochemistry is suitable for low-cost real-time analysis. From electrochemical methods polarography/voltammetry and potentiometry were used to directly measure nitrite/nitrate ions [140-143]. Common problem in these techniques is low electrode's activity for nitrate reduction, whereas catalysts are often needed to achieve reduction at less negative potentials [144]. In addition, commercial ISEs are not able to recognize precise anion and their respond is based on their membrane lipophilicity (according to Hofmeister selectivity pattern) [145]. In order to create recognition conditions plasticized poly(vinyl chloride) membranes incorporating different lipophilic compounds and ionophores, which provide sufficient selectivity, were used [146].

Kim et al. fabricated microfludic chip and used electrochemical method called double-potential-step chronocoulometry (DPSC) in order to detect nitrate [147]. DPSC is amperometric technique, where current is integrated over period of time in order to increase signal-to-noise ratio and separate analyte signal from non-Faradaic currents and H_2O reduction current. They used thin-film silver electrode as a sensing electrode, silver-oxide as a reference electrode and platinum counter electrode and measured in 0.01 M NaOH. Reduction of nitrate was observed at -1.08 V, close to the hydroxide desorption potential at -1.00 V. They obtained LOD 4-75 μM, which includes chip-to-chip variation, but it is still enough taking into account by U.S. Environmental Protection Agency (EPA) maximum contaminant

level for nitrate at 0.7 mM. Several interferents commonly presented within groundwater were tested and their interference was found to be below 10 % of signal distortion except for Ca_2^+, Sr_2^+ and HPO_4^{2-}/PO_4^{3-} where it was more than 20 %.

Other microfluidic nitrate sensor based on doped polypyrrole nanowire electrode was reported by Aravamudhan *et al.* [148]. They obtained linear response in the range from 10 μM to 1 mM and LOD 4.5 ± 1.0 μM. The sensor selectivity which is not related to analyte lipophilicity is achieved using by electrochemical nitrate doping of polypyrrole as was suggested by Hutchins & Bachas [149]. The authors used nanowire geometry instead of standard polypyrrole film in order to increase surface-to-volume ratio and lower diffusion resistance [150]. No change in the sensor response was observed for 2 months. Authors suggested that pencil leads can be used as substrates for polypyrrole polymerisation instead of carbon nanowires.

Different approach to nitrate and other inorganic ions detection was used by Freitas *et al.* [96]. They used microchip electrophoresis to separate Cl^-, NO_3^-, SO_4^{2-} and NO_2^- ions and electrodes capacitively coupled to the electrolyte as a detector. They optimized separation condition (buffer and voltage) and with $Cr_2O_7^{2-}$ internal standard and separation for 60 s they obtained excellent repeatability of migration times (<1%) and peak areas (6.2 - 7.6%) (n=30).They determined ions levels in aquarium water, river water and biofertilizer samples with LODs ranging from 2.0 to 4.9 μM.

4.4. Phenolic compounds

Phenols are widely used in several branches of industry like chemical, tinctoral, petrol or pharmaceutical [151]. In addition, water bodies are contaminated by leakage of sewage waters and by release of biocides like pentachlorophenol. Phenols toxic effect is a result of their ability to generate free radicals and their hydrophobicity [152]. Conventional methods of

phenols analysis are chromatography, immunological ones and electroanalysis [153]. Previously, amperometric detector was integrated with flow analysis in liquid chromatography, FIA and CE and these devices were used in analysis of phenolic compounds [154-156]. Most phenols are oxidizable at moderate potentials hence amperometry represents suitable methods for phenols detection. Electrooxidation of phenols is complex process, where several further oxidizable intermediates like phenoxy-type radicals are formed [157]. The pathway of phenols oxidation products depends on electrode material. Although simple organic compounds like maleic or oxalic acids were reported as final product of reaction, further reaction with radicals or quinones is expectable. This can induce creation of dimers or oligomers and result in fouling of electrode surface [158, 159]. The presence of surfactants within measured solution was shown to help phenols detection on electrodes [160, 161]. Other approach was reported by Stoytcheva *et al.* [162]. They applied pulse potential waveform on electrode for continuous electrode cleaning and reactivation.

Nowadays enzyme-based electrochemical biosensors for phenolic compounds are emerging. They utilize commonly known advantages of biosensors where biomolecule (enzyme in this case) provides selectivity and simple amperometric detection. Enzymes tyrosinase, laccase and polyphenol oxidase have been tested in this case [163-165]. As an example, tyrosinase catalyzes hydroxylation of monophenols to o-diphenols and o-diphenols to o-quinones (possesses monophenolase and catecholase activity). O-quinone is subsequently electrochemically reduced to catechol [166]. Laccase possesses broader substrate specificity since catalyses oxidation of several phenolic compounds as o-, p- and some m-diphenols, aminophenols, polyphenols, as well as phenol. However, it is worth to note that biosensors have stability shortcomings with continuous measurements and their fabrication requires several subsequent steps. In addition, immobilization of macromolecules like enzymes while retain their activity is still key challenge [167].

Mayorga-Martinez *et al.* reported the sensing phenol using microfluidic device with SPE modified with $CaCO_3$-poly(ethyleneimine) microparticles and with tyrosinase [168]. The performance of amperometric device was linear within the range from 0.5 to 5.0 μM. In that study, PEI layer on particles enabled creation of hydrogen bonds between nitrogen of PEI amino groups and hydrogen of OH, NH or SH presented in all biomolecules. Further, laccase was immobilized on electrode using polyvinyl alcohol photopolymer or polyazetidine prepolymer [169, 170]. In general, enzyme immobilization is the most important aspect that affects sensor performance. On contrary, Gonzales-Rivera *et al.* reported direct electrodeposition of laccase from microchannel on working electrode by application of potential +1.2 V [171].

Direct oxidation of catechol together with copper and parathion (organophosphorous pesticide) in microfluidic device was reported by Gutiérrez-Capitán [172]. The analytes were detected using different chronoamperometric methods at three electrode system made of gold – anodic stripping chronoamperometry was used for Cu^{2+} (deposition at -0.40 V and stripping at +0.05 V), anodic chronoamperometry at +0.25 V for catechol and cathodic chronoamperometry at -0.60 V for parathion.

Further, several papers reported phenols analysis using electrophoresis with electrochemical detection [67, 173, 174]. Godoy-Caballero *et al.* reported phenolic compound (tyrosol, hydroxytyrosol and oleuropein glucoside) analysis in samples of extra virgin olive oil using microchip electrophoresis with end-channel amperometric detection on golden wire electrode [175].

4.5. Pesticides and herbicides

Pesticides represent broad group of synthetic or natural organic compounds or their mixtures that are used in order to control pests and plants. However their repeated and

increasing usage caused spread through environment and contaminated natural resources. Only the small fraction of applied pesticide reaches target pests and their trace amounts can be found in water, soil and air. Due to their low solubility, high stability and inherent toxicity including their residues and metabolites are called persistent organic pollutants (POPs) [176].

Since pesticides often possess electroactive functional groups direct electrochemistry can be used for their analysis and monitoring. In the past several electrochemical sensors for pesticides have been developed. Most of these methods utilized enzymes in order to obtain sufficient selectivity of sensor [177-179]. Acetylcholinesterase (AChE), bytyrylcholinesterase (BChE), organophosphorus hydrolase (OPH) etc. are being used in pesticide biosensing. From practical point of view biosensors suffer from many disadvantages. Mainly, the enzymes are expensive and their chemical/physical stability in time is an issue. In addition, environmental samples often include contamination, which can affect biosensor performance, where an enzyme activity can be lowered by metals and can give false positive results [180]. In general, concentration of pesticides in environmental samples is low and the analytical result can be affected by sample matrix hence sample pretreatment using solid-phase extraction is common [181-183].

Although direct electrochemical analysis of pesticides is possible and several publications dealt with enzyme-based microfluidic electrochemical or optical sensing of pesticides, we are not aware of any publication, which aims to integration of direct electrochemical sensing of pesticides in microfluidic configuration [184-186].

Electrochemical submicromolar detection of organosphosphate compounds (OP) on thick-film electrodes integrated with CE microchip was reported by Wang *et al.* [187]. They demonstrated the suitability of their method for OP detection by detection of 1.4×10^{-5} M paraoxon, 1.5×10^{-5} M methylparathion and 2.8×10^{-4} M fenitrothion in spiked river water.

Similar method was used in order to detect three most common triazine herbicides – simazine, atrazine and ametryn [188].

4.6. Bacteria

Bacterial contamination of drinking water still remains serious problem. Bacterial infection caused by eating contaminated food and drinking contaminated water represents a leading cause of death in developing countries. Several methods as cell culturing test, immune-based methods, polymerase chain reaction and mass spectrometry in order to identify and quantify bacterial contamination have been reported [189-191]. However, they possess drawbacks like labour-demanding procedures or expensive laboratory equipment. Further, several microfluidic methods capable of bacterial analysis was introduced. Tian *et al.* reported impedimetric detection of *E. Coli O157:H7* and *S. aureus* in microfluidic device, which used antibody in order to immobilize bacteria [192]. Safavieh *et al.* used microfluidic chip for *E. Coli* detection based on isothermal amplification of bacterial DNA and linear sweep voltammetric measurement of Hoechst 33258 as a redox probe [193]. When the target DNA was amplified, the more redox molecules are bound to DNA molecule and cause decrease of signal in comparison with negative control. However, as it was mentioned previously, biomolecules integration within microfluidic devices lowers their robustness and cause several troubles.

Dielectrophoretic impedance measurement of bacteria in drinking water was shown by Kim *et al.* [194]. The reported microfluidic device increased bacteria concentration using dielectrophoretic focusing, whereas cells are focused at the end of 40 pairs of passivated interdigitated electrodes with precise geometry). Subsequently, cell passed towards sensing electrode, where are trapped also using dielectrophoretic force. The trapped cells created a

bridge over the electrodes gap hence decrease impedance. They obtained detection limit for *E. Coli* of 300 CFU/ml in 100ul of sample.

Different approach was reported by Nejdl *et al.* [195]. They developed device capable of detection of bacteria producing alkaline phosphatase. The concept was tested on *S. aureus* however *E. coli*, *Bacillus cereus*, *Bacillus amyloliquefaciens* produce this enzyme. The bacteria were immobilized within cultivation chamber using non-specific interaction with magnetic particles and after cultivation, which improved detection sensitivity, were detected using cleavage of non-electroactive 1-napthylphosphate by alkaline phosphatase to electroactive 1-naphthol on screen-printed electrode.

5. Conclusion

Microfludic platforms with integrated electrochemical detectors have proved to be successful tool for detection of pollutants. Electrochemistry provides advantages for both, electrically and pressure-driven microfluidic devices, but also for emerging μPADs. Such devices can be utilized for *in situ* analysis and we believe that their put into practice will help with decreasing of anthropogenic pressure on environment, whereas we demonstrated the suitability of these methods for detection of several pollutants, however this field is rapidly growing and the list is broadening quickly.

Acknowledgement

This research has been financially supported by the Ministry of Education, Youth and Sports of the Czech Republic under the project CEITEC 2020 (LQ1601).

Figures

Figure 1

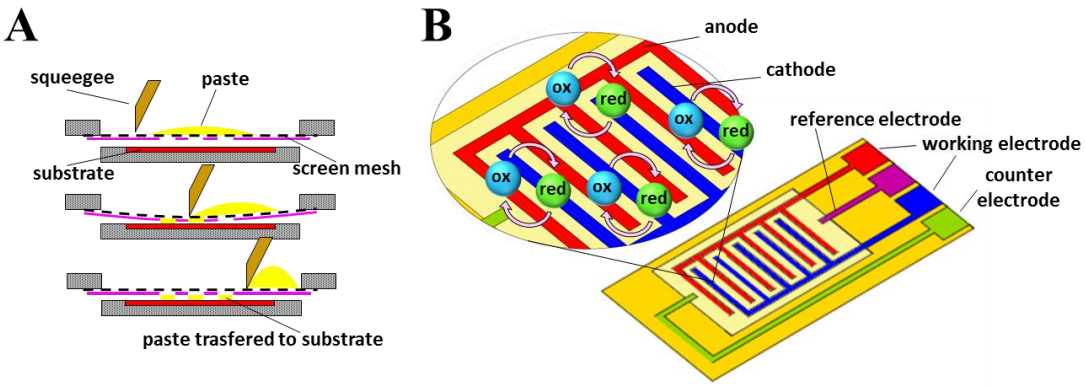

(**A**) Scheme of the screen-printed electrode fabrication outlining the basic processes involved. Adapted from [196] with permission. (**B**) Scheme of IDE layout with highlighted redox cycling.

Figure 2

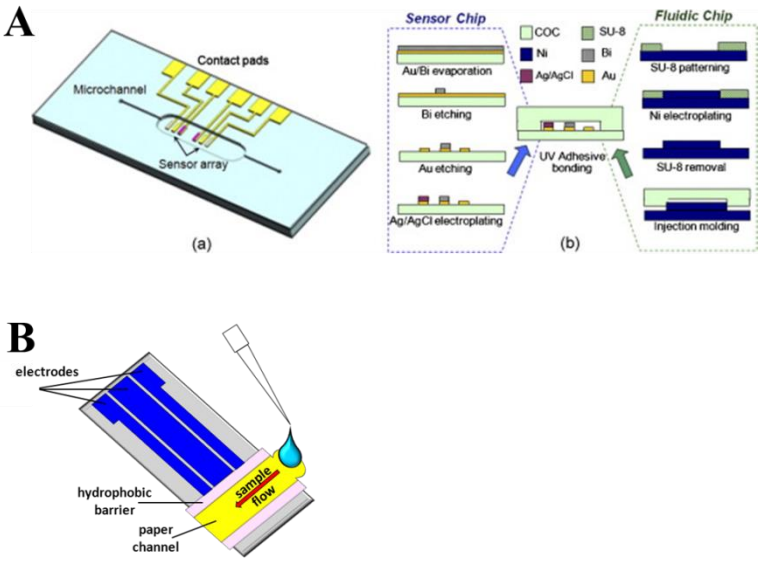

(**A**) The scheme of on-chip microfluidic electrochemical sensor array (a) and its fabrication processes (b). Adapted from [66] with permission. (**B**) The scheme of μPAD with

electrochemical sensing. The device consists of three electrodes printed on paper substrate and paper channel, which is in contact with electrodes.

Figure 3

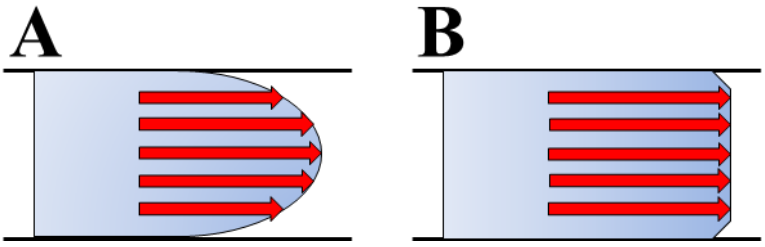

Profile of (**A**) pressure-driven and (**B**) electroosmotic flow.

References

[1] J. Workman, B. Lavine, R. Chrisman, M. Koch, Process Analytical Chemistry, Anal. Chem. 83 (2011) 4557-4578.
[2] J. Heyrovsky, Electrolysis with mercury dropping cathode (In Czech), Chem. Listy 16 (1922) 256-304.
[3] J. Wang, Analytical electrochemistry, Second edition, Wiley, New York, 2000.
[4] B. Uslu, S.A. Ozkan, Electroanalytical methods for the determination of pharmaceuticals: A review of recent trends and developments, Anal. Lett. 44 (2011) 2644-2702.
[5] S.M. Rosolina, J.Q. Chambers, C.W. Lee, Z.L. Xue, Direct determination of cadmium and lead in pharmaceutical ingredients using anodic stripping voltammetry in aqueous and DMSO/water solutions, Anal. Chim. Acta 893 (2015) 25-33.
[6] H. Huang, T. Chen, X.Y. Liu, H.Y. Ma, Ultrasensitive and simultaneous detection of heavy metal ions based on three-dimensional graphene-carbon nanotubes hybrid electrode materials, Anal. Chim. Acta 852 (2014) 45-54.
[7] R.R. Chillawar, K.K. Tadi, R.V. Motghare, Voltammetric techniques at chemically modified electrodes, J. Anal. Chem. 70 (2015) 399-418.
[8] B. Bas, Z. Kowalski, Preparation of silver surface for mercury film electrode of prolonged analytical application, Electroanalysis 14 (2002) 1067-1071.
[9] S. Zbeda, K. Pokpas, S. Titinchi, N. Jahed, P.G. Baker, E.I. Iwuoha, Few-layer Binder Free Graphene Modified Mercury Film Electrode for Trace Metal Analysis by Square Wave Anodic Stripping Voltammetry, Int. J. Electrochem. Sci. 8 (2013) 11125-11141.
[10] J. Kudr, L. Nejdl, S. Skalickova, B. Ruttkay-Nedecky, M.A.M. Rodrigo, S. Dostalova, A.M.J. Jinemez, D. Chudobova, K. Cihalova, M. Konecna, P. Kopel, J. Kynicky, V. Adam, R. Kizek, Plasmid HIV p24 Gene Detection on Mercury Film Electrode using Osmium Labelling, Int. J. Electrochem. Sci. 9 (2014) 3409-3418.
[11] L.M.S. Nunes, R.C. Faria, The Influence of the Electrodeposition Conditions on the Electroanalytical Performance of the Bismuth Film Electrode for Lead Determination, Electroanalysis 20 (2008) 2259-2263.
[12] S. Dal Borgo, V. Jovanovski, B. Pihlar, S.B. Hocevar, Operation of bismuth film electrode in more acidic medium, Electrochim. Acta 155 (2015) 196-200.
[13] J. Smajdor, R. Piech, B. Paczosa-Bator, A Novel Method of High Sensitive Determination of Prednisolone on Renewable Mercury Film Silver Based Electrode, Electroanalysis 28 (2016) 394-400.
[14] C.W. Foster, A.P. de Souza, J.P. Metters, M. Bertotti, C.E. Banks, Metallic modified (bismuth, antimony, tin and combinations thereof) film carbon electrodes, Analyst 140 (2015) 7598-7612.
[15] M. Grabarczyk, J. Wasag, Adsorptive Cathodic Stripping Voltammetric Method for Determination of Gallium Using an In Situ Plated Lead Film Electrode, Electroanalysis 27 (2015) 2596-2600.
[16] M. Korolczuk, K. Tyszczuk, M. Grabarczyk, Determination of uranium by adsorptive stripping voltammetry at a lead film electrode, Talanta 72 (2007) 957-961.
[17] K. Tyszczuk, M. Korolczuk, M. Grabarczyk, Application of gallium film electrode for elimination of copper interference in anodic stripping voltammetry of zinc, Talanta 71 (2007) 2098-2101.
[18] Z.Y. Guo, F. Feng, Y.X. Hou, N. Jaffrezic-Renault, Quantitative determination of zinc in milkvetch by anodic stripping voltammetry with bismuth film electrodes, Talanta 65 (2005) 1052-1055.

[19] Y. Temerk, M. Ibrahim, H. Ibrahim, M. Kotb, Adsorptive stripping voltammetric determination of anticancer drug lomustine in biological fluids using in situ mercury film coated graphite pencil electrode, J. Electroanal. Chem. 760 (2016) 135-142.
[20] D. Yang, L. Wang, Z.L. Chen, M. Megharaj, R. Naidu, Determination of Trace Lead and Cadmium in Water Samples by Anodic Stripping Voltammetry with a NafionIonic Liquid-Coated Bismuth Film Electrode, Electroanalysis 26 (2014) 639-647.
[21] M.K. Dey, A.K. Satpati, A.V.R. Reddy, Electrodeposited antimony and antimony-gold nanocomposite modified carbon paste electrodes for the determination of heavy metal ions, Anal. Methods 6 (2014) 5207-5213.
[22] J.P. Metters, S.M. Houssein, D.K. Kampouris, C.E. Banks, Paper-based electroanalytical sensing platforms, Anal. Methods 5 (2013) 103-110.
[23] A.P. Ruas de Souza, M. Bertotti, C.W. Foster, C.E. Banks, Back-to-Back Screen-Printed Electroanalytical Sensors: Extending the Potential Applications of the Simplistic Design, Electroanalysis 27 (2015) 2295-2301.
[24] S.L. Wang, N.S. Liu, C.X. Yang, W.J. Liu, J. Su, L.Y. Li, C.P. Yang, Y.H. Gao, Fully screen printed highly conductive electrodes on various flexible substrates for asymmetric supercapacitors, RSC Adv. 5 (2015) 85799-85805.
[25] A. Crew, D. Lonsdale, N. Byrd, R. Pittson, J.P. Hart, A screen-printed, amperometric biosensor array incorporated into a novel automated system for the simultaneous determination of organophosphate pesticides, Biosens. Bioelectron. 26 (2011) 2847-2851.
[26] D.E. Tallman, Microelectrodes for voltammetry-a personal historical perspective, J. Solid State Electrochem. 15 (2011) 1703-1710.
[27] J.J.P. Mark, P. Piccinelli, F.M. Matysik, Very fast capillary electrophoresis with electrochemical detection for high-throughput analysis using short, vertically aligned capillaries, Anal. Bioanal. Chem. 406 (2014) 6069-6073.
[28] G. Marton, G. Orban, M. Kiss, R. Fiath, A. Pongracz, I. Ulbert, A Multimodal, SU-8-Platinum - Polyimide Microelectrode Array for Chronic In Vivo Neurophysiology, PLoS One 10 (2015) 1-16.
[29] J. Kudr, S. Skalickova, L. Nejdl, A. Moulick, B. Ruttkay-Nedecky, V. Adam, R. Kizek, Fabrication of solid-state nanopores and its perspectives, Electrophoresis 36 (2015) 2367-2379.
[30] C.S. Lau, H. Sadeghi, G. Rogers, S. Sangtarash, P. Dallas, K. Porfyrakis, J. Warner, C.J. Lambert, G.A.D. Briggs, J.A. Mol, Redox-Dependent Franck-Condon Blockade and Avalanche Transport in a Graphene-Fullerene Single-Molecule Transistor, Nano Lett. 16 (2016) 170-176.
[31] E. Katz, I. Willner, J. Wang, Electroanalytical and bioelectroanalytical systems based on metal and semiconductor nanoparticles, Electroanalysis 16 (2004) 19-44.
[32] J. Kudr, L. Richtera, L. Nejdl, K. Xhaxhiu, P. Vitek, B. Rutkay-Nedecky, D. Hynek, P. Kopel, V. Adam, R. Kizek, Improved Electrochemical Detection of Zinc Ions Using Electrode Modified with Electrochemically Reduced Graphene Oxide, Materials 9 (2016) 1-12.
[33] C.M. Welch, R.G. Compton, The use of nanoparticles in electroanalysis: a review, Anal. Bioanal. Chem. 384 (2006) 601-619.
[34] L. Rassaei, M. Amiri, C.M. Cirtiu, M. Sillanpaa, F. Marken, Nanoparticles in electrochemical sensors for environmental monitoring, Trac-Trends Anal. Chem. 30 (2011) 1704-1715.
[35] M.W. Shinwari, D. Zhitomirsky, I.A. Deen, P.R. Selvaganapathy, M.J. Deen, D. Landheer, Microfabricated Reference Electrodes and their Biosensing Applications, Sensors 10 (2010) 1679-1715.

[36] T. Kitade, K. Kitamura, S. Takegami, Y. Miyata, M. Nagatomo, T. Sakaguchi, M. Furukawa, Needle-type ultra micro silver/silver chloride reference electrode for use in micro-electrochemistry, Anal. Sci. 21 (2005) 907-912.
[37] M.R. Majidi, Y. Omidi, P. Karami, M. Johari-Ahar, Reusable potentiometric screen-printed sensor and label-free aptasensor with pseudo-reference electrode for determination of tryptophan in the presence of tyrosine, Talanta 150 (2016) 425-433.
[38] A. Cazale, W. Sant, F. Ginot, J.C. Launay, G. Savourey, F. Revol-Cavalier, J.M. Lagarde, D. Heinry, J. Launay, P. Temple-Boyer, Physiological stress monitoring using sodium ion potentiometric microsensors for sweat analysis, Sens. Actuator B-Chem. 225 (2016) 1-9.
[39] H. Kahlert, Reference electrodes, in: F. Scholz (Ed.) Electroanalytical methods, Second edition, Springer, Heidelberg, 2010, pp. 456.
[40] R. Zielinska, E. Mulik, A. Michalska, S. Achmatowicz, M. Maj-Zurawska, All-solid-state planar miniature ion-selective chloride electrode, Anal. Chim. Acta 451 (2002) 243-249.
[41] K.S. Yun, H.J. Kim, S. Joo, J. Kwak, E. Yoon, Analysis of heavy-metal ions using mercury microelectrodes and a solid-state reference electrode on a Si wafer, Jpn. J. Appl. Phys. Part 1 - Regul. Pap. Brief Commun. Rev. Pap. 39 (2000) 7159-7163.
[42] M.A. Nolan, S.H. Tan, S.P. Kounaves, Fabrication and characterization of a solid state reference electrode for electroanalysis of natural waters with ultramicroelectrodes, Anal. Chem. 69 (1997) 1244-1247.
[43] M. Shibata, B. Siegfried, J.P. Huston, Miniature calomel electrode for recording DC potential changes accompanying spreading depression in freely moving rat, Physiol. Behav. 18 (1977) 1171-1174.
[44] M. Kunimatsu, H. Qiao, T. Okada, Microtubular hydrogen electrode, a reference electrode for electrochemical analyses, J. Electrochem. Soc. 152 (2005) E161-E166.
[45] T.A. Webster, E.D. Goluch, Electrochemical detection of pyocyanin in nanochannels with integrated palladium hydride reference electrodes, Lab Chip 12 (2012) 5195-5201.
[46] J.D. Stucki, O.T. Guenat, A microfluidic bubble trap and oscillator, Lab Chip 15 (2015) 4393-4397.
[47] F.M. Matysik, End-column electrochemical detection for capillary electrophoresis, Electroanalysis 12 (2000) 1349-1355.
[48] J. Dobes, O. Zitka, J. Sochor, B. Ruttkay-Nedecky, P. Babula, M. Beklova, J. Kynicky, J. Hubalek, B. Klejdus, R. Kizek, V. Adam, Electrochemical Tools for Determination of Phenolic Compounds in Plants. A Review, Int. J. Electrochem. Sci. 8 (2013) 4520-4542.
[49] G.M. Whitesides, The origins and the future of microfluidics, Nature 442 (2006) 368-373.
[50] J. Ruzicka, E.H. Hansen, Retro-review of flow-injection analysis, Trac-Trends Anal. Chem. 27 (2008) 390-393.
[51] J. Ruzicka, Discovering flow-injection - Journey from sample to a live cell and from solution to suspension, Analyst 119 (1994) 1925-1934.
[52] J. Ruzicka, L. Scampavia, From flow injection to bead injection, Anal. Chem. 71 (1999) 257A-263A.
[53] S.W. Lee, R.M. Sankaran, Direct writing via electron-driven reactions, Mater. Today 16 (2013) 117-122.
[54] Y.N. Xia, G.M. Whitesides, Soft lithography, Angew. Chem.-Int. Edit. 37 (1998) 550-575.
[55] A.K. Au, W. Huynh, L.F. Horowitz, A. Folch, 3D-Printed Microfluidics, Angew. Chem.-Int. Edit. 55 (2016) 3862-3881.

[56] D.J. Guckenberger, T.E. de Groot, A.M.D. Wan, D.J. Beebe, E.W.K. Young, Micromilling: a method for ultra-rapid prototyping of plastic microfluidic devices, Lab Chip 15 (2015) 2364-2378.
[57] S.K. Sia, G.M. Whitesides, Microfluidic devices fabricated in poly(dimethylsiloxane) for biological studies, Electrophoresis 24 (2003) 3563-3576.
[58] I.E. Araci, S.R. Quake, Microfluidic very large scale integration (mVLSI) with integrated micromechanical valves, Lab Chip 12 (2012) 2803-2806.
[59] R. Mukhopadhyay, When PDMS isn't the best. What are its weaknesses, and which other polymers can researchers add to their toolboxes?, Anal. Chem. 79 (2007) 3248-3253.
[60] J.N. Lee, C. Park, G.M. Whitesides, Solvent compatibility of poly(dimethylsiloxane)-based microfluidic devices, Anal. Chem. 75 (2003) 6544-6554.
[61] M.W. Toepke, D.J. Beebe, PDMS absorption of small molecules and consequences in microfluidic applications, Lab Chip 6 (2006) 1484-1486.
[62] M.R.F. Cerqueira, D. Grasseschi, R.C. Matos, L. Angnes, A novel functionalisation process for glucose oxidase immobilisation in poly(methyl methacrylate) microchannels in a flow system for amperometric determinations, Talanta 126 (2014) 20-26.
[63] L.M.C. Ferreira, E.T. da Costa, C.L. do Lago, L. Angnes, Miniaturized flow system based on enzyme modified PMMA microreactor for amperometric determination of glucose, Biosens. Bioelectron. 47 (2013) 539-544.
[64] P. Jankowski, D. Ogonczyk, L. Derzsi, W. Lisowski, P. Garstecki, Hydrophilic polycarbonate chips for generation of oil-in-water (O/W) and water-in-oil-in-water (W/O/W) emulsions, Microfluid. Nanofluid. 14 (2013) 767-774.
[65] X.F. Zhang, H.K. Chu, Y. Zhang, G.H. Bai, K.Q. Wang, Q.L. Tan, D. Sun, Rapid characterization of the biomechanical properties of drug-treated cells in a microfluidic device, J. Micromech. Microeng. 25 (2015) 1-9.
[66] Z.W. Zou, A. Jang, E. MacKnight, P.M. Wu, J. Do, P.L. Bishop, C.H. Ahn, Environmentally friendly disposable sensors with microfabricated on-chip planar bismuth electrode for in situ heavy metal ions measurement, Sens. Actuator B-Chem. 134 (2008) 18-24.
[67] Y.S. Ding, A. Ayon, C.D. Garcia, Electrochemical detection of phenolic compounds using cylindrical carbon-ink electrodes and microchip capillary electrophoresis, Anal. Chim. Acta 584 (2007) 244-251.
[68] J.A. Vickers, C.S. Henry, Simplified current decoupler for microchip capillary electrophoresis with electrochemical and pulsed amperometric detection, Electrophoresis 26 (2005) 4641-4647.
[69] Y.S. Ding, C.D. Garcia, Pulsed amperometric detection with poly(dimethylsiloxane)-fabricated capillary electrophoresis microchips for the determination of EPA priority pollutants, Analyst 131 (2006) 208-214.
[70] A.W. Martinez, S.T. Phillips, M.J. Butte, G.M. Whitesides, Patterned paper as a platform for inexpensive, low-volume, portable bioassays, Angew. Chem.-Int. Edit. 46 (2007) 1318-1320.
[71] D.M. Cate, J.A. Adkins, J. Mettakoonpitak, C.S. Henry, Recent Developments in Paper-Based Microfluidic Devices, Anal. Chem. 87 (2015) 19-41.
[72] Y.Y. Xia, J. Si, Z.Y. Li, Fabrication techniques for microfluidic paper-based analytical devices and their applications for biological testing: A review, Biosens. Bioelectron. 77 (2016) 774-789.
[73] M. Ariza-Avidad, A. Salinas-Castillo, L.F. Capitan-Vallvey, A 3D mu PAD based on a multi-enzyme organic-inorganic hybrid nanoflower reactor, Biosens. Bioelectron. 77 (2016) 51-55.

[74] K. Talalak, J. Noiphung, T. Songjaroen, O. Chailapakul, W. Laiwattanapaisal, A facile low-cost enzymatic paper-based assay for the determination of urine creatinine, Talanta 144 (2015) 915-921.
[75] S.H. Im, K.R. Kim, Y.M. Park, J.H. Yoon, J.W. Hong, H.C. Yoon, An animal cell culture monitoring system using a smartphone-mountable paper-based analytical device, Sens. Actuator B-Chem. 229 (2016) 166-173.
[76] P.D. Sinawang, V. Rai, R.E. Ionescu, R.S. Marks, Electrochemical lateral flow immunosensor for detection and quantification of dengue NS1 protein, Biosens. Bioelectron. 77 (2016) 400-408.
[77] T. Rungsawang, E. Punrat, J. Adkins, C. Henry, O. Chailapakul, Development of Electrochemical Paper-based Glucose Sensor Using Cellulose-4-aminophenylboronic Acid-modified Screen-printed Carbon Electrode, Electroanalysis 28 (2016) 462-468.
[78] N. Dossi, R. Toniolo, A. Pizzariello, F. Impellizzieri, E. Piccin, G. Bontempelli, Pencil-drawn paper supported electrodes as simple electrochemical detectors for paper-based fluidic devices, Electrophoresis 34 (2013) 2085-2091.
[79] N. Dossi, R. Toniolo, F. Terzi, F. Impellizzieri, G. Bontempelli, Pencil leads doped with electrochemically deposited Ag and AgCl for drawing reference electrodes on paper-based electrochemical devices, Electrochim. Acta 146 (2014) 518-524.
[80] W.J. Lan, E.J. Maxwell, C. Parolo, D.K. Bwambok, A.B. Subramaniam, G.M. Whitesides, Paper-based electroanalytical devices with an integrated, stable reference electrode, Lab Chip 13 (2013) 4103-4108.
[81] N. Dossi, R. Toniolo, F. Impellizzieri, G. Bontempelli, Doped pencil leads for drawing modified electrodes on paper-based electrochemical devices, J. Electroanal. Chem. 722 (2014) 90-94.
[82] K. Yamada, T.G. Henares, K. Suzuki, D. Citterio, Paper-Based Inkjet-Printed Microfluidic Analytical Devices, Angew. Chem.-Int. Edit. 54 (2015) 5294-5310.
[83] N.A. Polson, M.A. Hayes, Microfluidics - Controlling fluids in small places, Anal. Chem. 73 (2001) 312A-319A.
[84] E.J.F. Dickinson, J.G. Limon-Petersen, N.V. Rees, R.G. Compton, How Much Supporting Electrolyte Is Required to Make a Cyclic Voltammetry Experiment Quantitatively "Diffusional"? A Theoretical and Experimental Investigation, J. Phys. Chem. C 113 (2009) 11157-11171.
[85] M. Ciszkowska, Z. Stojek, Voltammetry in solutions of low ionic strength. Electrochemical and analytical aspects, J. Electroanal. Chem. 466 (1999) 129-143.
[86] L. Marle, G.M. Greenway, Microfluidic devices for environmental monitoring, Trac-Trends Anal. Chem. 24 (2005) 795-802.
[87] W.E. Morf, O.T. Guenat, N.F. de Rooij, Partial electroosmotic pumping in complex capillary systems - Part 1: Principles and general theoretical approach, Sens. Actuator B-Chem. 72 (2001) 266-272.
[88] D.J. Laser, J.G. Santiago, A review of micropumps, J. Micromech. Microeng. 14 (2004) R35-R64.
[89] F. Sassa, K. Morimoto, W. Satoh, H. Suzuki, Electrochemical techniques for microfluidic applications, Electrophoresis 29 (2008) 1787-1800.
[90] J. Seyed-Yagoobi, Electrohydrodynamic pumping of dielectric liquids, J. Electrost. 63 (2005) 861-869.
[91] F. Foret, L. Krivankova, P. Bocek, Capillary zone electrophoresis, John Wiley & Sons, Chichester, 1993.
[92] D. Janasek, J. Franzke, A. Manz, Scaling and the design of miniaturized chemical-analysis systems, Nature 442 (2006) 374-380.

[93] H.F. Li, J.M. Lin, Applications of microfluidic systems in environmental analysis, Anal. Bioanal. Chem. 393 (2009) 555-567.
[94] P. Kuban, P.C. Hauser, Contactless conductivity detection for analytical techniques-Developments from 2012 to 2014, Electrophoresis 36 (2015) 195-211.
[95] W.K.T. Coltro, R.S. Lima, T.P. Segato, E. Carrilho, D.P. de Jesus, C.L. do Lago, J.A.F. da Silva, Capacitively coupled contactless conductivity detection on microfluidic systems-ten years of development, Anal. Methods 4 (2012) 25-33.
[96] C.B. Freitas, R.C. Moreira, M.G.D. Tavares, W.K.T. Coltro, Monitoring of nitrite, nitrate, chloride and sulfate in environmental samples using electrophoresis microchips coupled with contactless conductivity detection, Talanta 147 (2016) 335-341.
[97] A.P. Lewis, A. Cranny, N.R. Harris, N.G. Green, J.A. Wharton, R.J.K. Wood, K.R. Stokes, Review on the development of truly portable and in-situ capillary electrophoresis systems, Meas. Sci. Technol. 24 (2013) 1-20.
[98] D. Dutta, S. Chandra, A.K. Swain, D. Bahadur, SnO2 Quantum Dots-Reduced Graphene Oxide Composite for Enzyme-Free Ultrasensitive Electrochemical Detection of Urea, Anal. Chem. 86 (2014) 5914-5921.
[99] M. Cernanska, P. Tomcik, Z. Janosikova, M. Rievaj, D. Bustin, Indirect voltammetric detection of fluoride ions in toothpaste on a comb-shaped interdigitated microelectrode array, Talanta 83 (2011) 1472-1475.
[100] G. Matzeu, C. O'Quigley, E. McNamara, C. Zuliani, C. Fay, T. Glennon, D. Diamond, An integrated sensing and wireless communications platform for sensing sodium in sweat, Anal. Methods 8 (2016) 64-71.
[101] E. Ota, S. Sakasegawa, S. Ueda, K. Konishi, M. Akimoto, T. Tateishi, M. Kawano, E. Hokazono, Y. Kayamori, Preliminary evaluation of an improved enzymatic assay method for measuring potassium concentrations in serum, Clin. Chim. Acta 446 (2015) 73-75.
[102] U. Vanamo, J. Bobacka, Electrochemical control of the standard potential of solid-contact ion-selective electrodes having a conducting polymer as ion-to-electron transducer, Electrochim. Acta 122 (2014) 316-321.
[103] J.J. Ye, F.H. Li, S.Y. Gan, Y.Y. Jiang, Q.B. An, Q.X. Zhang, L. Niu, Using sp(2)-C dominant porous carbon sub-micrometer spheres as solid transducers in ion-selective electrodes, Electrochem. Commun. 50 (2015) 60-63.
[104] X.U. Zou, J.H. Cheong, B.J. Taitt, P. Buhlmann, Solid Contact Ion-Selective Electrodes with a Well-Controlled Co(II)/Co(III) Redox Buffer Layer, Anal. Chem. 85 (2013) 9350-9355.
[105] M. Trojanowicz, Recent developments in electrochemical flow detections-A review Part I. Flow analysis and capillary electrophoresis, Anal. Chim. Acta 653 (2009) 36-58.
[106] J. Kudr, H.V. Nguyen, J. Gumulec, L. Nejdl, I. Blazkova, B. Ruttkay-Nedecky, D. Hynek, J. Kynicky, V. Adam, R. Kizek, Simultaneous Automatic Electrochemical Detection of Zinc, Cadmium, Copper and Lead Ions in Environmental Samples Using a Thin-Film Mercury Electrode and an Artificial Neural Network, Sensors 15 (2015) 592-610.
[107] K. Toth, K. Stulik, W. Kutner, Z. Feher, E. Lindner, Electrochemical detection in liquid flow analytical techniques: Characterization and classification - (IUPAC Technical Report), Pure Appl. Chem. 76 (2004) 1119-1138.
[108] D.B. Gunasekara, M.K. Hulvey, S.M. Lunte, In-channel amperometric detection for microchip electrophoresis using a wireless isolated potentiostat, Electrophoresis 32 (2011) 832-837.
[109] P. Batalla, A. Martin, M.A. Lopez, M.C. Gonzalez, A. Escarpa, Enzyme-Based Microfluidic Chip Coupled to Graphene Electrodes for the Detection of D-Amino Acid Enantiomer-Biomarkers, Anal. Chem. 87 (2015) 5074-5078.

[110] B.G. Lucca, S.M. Lunte, W.K.T. Coltro, V.S. Ferreira, Separation of natural antioxidants using PDMS electrophoresis microchips coupled with amperometric detection and reverse polarity, Electrophoresis 35 (2014) 3363-3370.
[111] D.J. Fischer, M.K. Hulvey, A.R. Regel, S.M. Lunte, Amperometric detection in microchip electrophoresis devices: Effect of electrode material and alignment on analytical performance, Electrophoresis 30 (2009) 3324-3333.
[112] N.A. Lacher, S.M. Lunte, R.S. Martin, Development of a microfabricated palladium decoupler/electrochemical detector for microchip capillary electrophoresis using a hybrid glass/poly(dimethylsiloxane) device, Anal. Chem. 76 (2004) 2482-2491.
[113] M.L. Kovarik, M.W. Li, R.S. Martin, Integration of a carbon microelectrode with a microfabricated palladium decoupler for use in microchip capillary electrophoresis/electrochemistry, Electrophoresis 26 (2005) 202-210.
[114] A.P. Timbo, P.V.F. Pinto, H.A. Pinho, L.P. de Moura, J.B. Chretien, F.W. Viana, R.G. Diogenes, E.B. da Silva, M.E.R. da Silva, J.W.M. Menezes, G.D. Guimaraes, W.B. Fraga, pH optical sensor based on thin films of sol-gel with bromocresol purple, Sens. Actuator B-Chem. 223 (2016) 406-410.
[115] I.M.P.D. Sansalvador, C.D. Fay, J. Cleary, A.M. Nightingale, M.C. Mowlem, D. Diamond, Autonomous reagent-based microfluidic pH sensor platform, Sens. Actuator B-Chem. 225 (2016) 369-376.
[116] C. Nie, A. Frijns, M. Zevenbergen, J. den Toonder, An integrated flex-microfluidic-Si chip device towards sweat sensing applications, Sens. Actuator B-Chem. 227 (2016) 427-437.
[117] S. Safari, P.R. Selvaganapathy, M.J. Deen, Microfluidic Reference Electrode with Free-Diffusion Liquid Junction, J. Electrochem. Soc. 160 (2013) B177-B183.
[118] I. Bouhadda, O. De Sagazan, F. Le Bihan, Field effect transistor with integrated microfluidic channel as pH sensor, Microsyst. Technol. 21 (2015) 289-294.
[119] F. Bendriaa, F. Le Bihan, A.C. Salaun, T. Mohammed-Brahim, O. Bonnaud, Study of mechanical stability of suspended bridge devices used as pH sensors, J. Non-Cryst. Solids 352 (2006) 1246-1249.
[120] P.K. Ang, W. Chen, A.T.S. Wee, K.P. Loh, Solution-Gated Epitaxial Graphene as pH Sensor, J. Am. Chem. Soc. 130 (2008) 14392-14393.
[121] S.S. Kwon, J. Yi, W.W. Lee, J.H. Shin, S.H. Kim, S.H. Cho, S. Nam, W.I. Park, Reversible and Irreversible Responses of Defect-Engineered Graphene-Based Electrolyte-Gated pH Sensors, ACS Appl. Mater. Interfaces 8 (2016) 834-839.
[122] C.A. Li, K.N. Han, X.H. Pham, G.H. Seong, A single-walled carbon nanotube thin film-based pH-sensing microfluidic chip, Analyst 139 (2014) 2011-2015.
[123] L. Jarup, Hazards of heavy metal contamination, Br. Med. Bull. 68 (2003) 167-182.
[124] R.K. Sharma, M. Agrawal, F.M. Marshall, Heavy metal (Cu, Zn, Cd and Pb) contamination of vegetables in urban India: A case study in Varanasi, Environ. Pollut. 154 (2008) 254-263.
[125] D.G. Bostwick, H.B. Burke, D. Djakiew, S. Euling, S.M. Ho, J. Landolph, H. Morrison, B. Sonawane, T. Shifflett, D.J. Waters, B. Timms, Human prostate cancer risk factors, Cancer 101 (2004) 2371-2490.
[126] H. Wang, Y.X. Wang, J.Y. Jin, R.H. Yang, Gold Nanoparticle-Based Colorimetric and "Turn-On" Fluorescent Probe for Mercury(II) Ions in Aqueous Solution, Anal. Chem. 80 (2008) 9021-9028.
[127] M.H. Wang, S. Zhang, Z.H. Ye, D.L. Peng, L.H. He, F.F. Yan, Y.Q. Yang, H.Z. Zhang, Z.H. Zhang, A gold electrode modified with amino-modified reduced graphene oxide, ion specific DNA and DNAzyme for dual electrochemical determination of Pb(II) and Hg(II), Microchim. Acta 182 (2015) 2251-2258.

[128] M.B. Gumpu, S. Sethuraman, U.M. Krishnan, J.B.B. Rayappan, A review on detection of heavy metal ions in water - An electrochemical approach, Sens. Actuator B-Chem. 213 (2015) 515-533.
[129] G. March, T.D. Nguyen, B. Piro, Modified electrodes used for electrochemical detection of metal ions in environmental analysis, Biosensors 5 (2015) 241-275.
[130] M. Li, Y.T. Li, D.W. Li, Y.T. Long, Recent developments and applications of screen-printed electrodes in environmental assays-A review, Anal. Chim. Acta 734 (2012) 31-44.
[131] W. Yantasee, Y.H. Lin, K. Hongsirikarn, G.E. Fryxell, R. Addleman, C. Timchalk, Electrochemical sensors for the detection of lead and other toxic heavy metals: The next generation of personal exposure biomonitors, Environ. Health Perspect. 115 (2007) 1683-1690.
[132] W. Jung, A. Jang, P.L. Bishop, C.H. Ahn, A polymer lab chip sensor with microfabricated planar silver electrode for continuous and on-site heavy metal measurement, Sens. Actuator B-Chem. 155 (2011) 145-153.
[133] E. Kirowa-Eisner, M. Brand, D. Tzur, Determination of sub-nanomolar concentrations of lead by anodic-stripping voltammetry at the silver electrode, Anal. Chim. Acta 385 (1999) 325-335.
[134] J.H. Zhou, K.N. Ren, Y.Z. Zheng, J. Su, Y.H. Zhao, D. Ryan, H.K. Wu, Fabrication of a microfluidic Ag/AgCl reference electrode and its application for portable and disposable electrochemical microchips, Electrophoresis 31 (2010) 3083-3089.
[135] J.J. Shi, F. Tang, H.L. Xing, H.X. Zheng, L.H. Bi, W. Wang, Electrochemical Detection of Pb and Cd in Paper-Based Microfluidic Devices, J. Braz. Chem. Soc. 23 (2012) 1124-1130.
[136] L. Fewtrell, Drinking-water nitrate, methemoglobinemia, and global burden of disease: A discussion, Environ. Health Perspect. 112 (2004) 1371-1374.
[137] M.T. Gladwin, A.N. Schechter, D.B. Kim-Shapiro, R.P. Patel, N. Hogg, S. Shiva, R.O. Cannon, M. Kelm, D.A. Wink, M.G. Espey, E.H. Oldfield, R.M. Pluta, B.A. Freeman, J.R. Lancaster, M. Feelisch, J.O. Lundberg, The emerging biology of the nitrite anion, Nat. Chem. Biol. 1 (2005) 308-314.
[138] N.S. Bryan, M.B. Grisham, Methods to detect nitric oxide and its metabolites in biological samples, Free Radic. Biol. Med. 43 (2007) 645-657.
[139] M. Jimidar, C. Hartmann, N. Cousement, D.L. Massart, Determination of nitrate and nitrite in vegetables by capillary electrophoresis with indirect detection, J. Chromatogr. A 706 (1995) 479-492.
[140] M.I.N. Ximenes, S. Rath, F.G.R. Reyes, Polarographic determination of nitrate in vegetables, Talanta 51 (2000) 49-56.
[141] R. Ojani, J.B. Raoof, E. Zarei, Electrocatalytic reduction of nitrite using ferricyanide; Application for its simple and selective determination, Electrochim. Acta 52 (2006) 753-759.
[142] M. Shamsipur, M. Javanbakht, A.R. Hassaninejad, H. Sharghi, M.R. Ganjali, M.F. Mousavi, Highly selective PVC-membrane electrodes based on three derivatives of (Tetraphenylporphyrinato) cobalt(III) acetate for determination of trace amounts of nitrite ion, Electroanalysis 15 (2003) 1251-1259.
[143] S.S.M. Hassan, H.E.M. Sayour, S.S. Al-Mehrezi, A novel planar miniaturized potentiometric sensor for flow injection analysis of nitrates in wastewaters, fertilizers and pharmaceuticals, Anal. Chim. Acta 581 (2007) 13-18.
[144] H. Zhad, R.Y. Lai, Comparison of nanostructured silver-modified silver and carbon ultramicroelectrodes for electrochemical detection of nitrate, Anal. Chim. Acta 892 (2015) 153-159.
[145] A. Bianchi, K.J. Bowman, E. Gracia, Supramolecular Chemistry of Anions, Wiley, New York, 1997.

[146] J.T. Mitchell-Koch, M. Pietrzak, E. Malinowska, M.E. Meyerhoff, Aluminum(III) porphyrins as ionophores for fluoride selective polymeric membrane electrodes, Electroanalysis 18 (2006) 551-557.
[147] D. Kim, I.B. Goldberg, J.W. Judy, Microfabricated electrochemical nitrate sensor using double-potential-step chronocoulometry, Sens. Actuator B-Chem. 135 (2009) 618-624.
[148] S. Aravamudhan, S. Bhansali, Development of micro-fluidic nitrate-selective sensor based on doped-polypyrrole nanowires, Sens. Actuator B-Chem. 132 (2008) 623-630.
[149] R.S. Hutchins, L.G. Bachas, Nitrate-selective electrode developed by electrochemically mediated imprinting doping of polypyrrole, Anal. Chem. 67 (1995) 1654-1660.
[150] X.L. Zhang, J.X. Wang, Z. Wang, S.C. Wang, Improvement of amperometric sensor used for determination of nitrate with polypyrrole nanowires modified electrode, Sensors 5 (2005) 580-593.
[151] J. Michalowicz, W. Duda, Phenols - Sources and toxicity, Pol. J. Environ. Stud. 16 (2007) 347-362.
[152] C. Hansch, S.C. McKarns, C.J. Smith, D.J. Doolittle, Comparative QSAR evidence for a free-radical mechanism of phenol-induced toxicity, Chem.-Biol. Interact. 127 (2000) 61-72.
[153] F. Karim, A.N.M. Fakhruddin, Recent advances in the development of biosensor for phenol: a review, Rev. Environ. Sci. Bio-Technol. 11 (2012) 261-274.
[154] C.D. Garcia, P.I. Ortiz, Glassy carbon electrodes modified with different electropolymerized resol prepolymer mixtures for phenol and derivatives quantification, Anal. Sci. 15 (1999) 461-465.
[155] K. Sato, Studies on novel electrochemical detection in liquid chromatography, Bunseki Kagaku 51 (2002) 199-200.
[156] M. Scampicchio, J. Wang, S. Mannino, M.P. Chatrathi, Microchip capillary electrophoresis with amperometric detection for rapid separation and detection of phenolic acids, J. Chromatogr. A 1049 (2004) 189-194.
[157] H. Lund, M.M. Baizer, Organic Chemistry, Marcel Dekker, New York, 1991.
[158] X.Y. Li, Y.H. Cui, Y.J. Feng, Z.M. Xie, J.D. Gu, Reaction pathways and mechanisms of the electrochemical degradation of phenol on different electrodes, Water Res. 39 (2005) 1972-1981.
[159] C. Comninellis, C. Pulgarin, Anodic oxidation of phenol for waste-water treatment, J. Appl. Electrochem. 21 (1991) 703-708.
[160] F.T. Hu, S.Q. Liu, Enhanced Effects of Surfactant on Sensing of Phenol on a Graphene Nano-sheet Paste Electrode, Int. J. Electrochem. Sci. 7 (2012) 11338-11350.
[161] M.F. Brugnera, M.A.G. Trindade, M.V.B. Zanoni, Detection of bisphenol A on a screen-printed carbon electrode in CTAB micellar medium, Anal. Lett. 43 (2010) 2823-2836.
[162] M. Stoytcheva, R. Zlatev, V. Gochev, Z. Velkova, G. Montero, M.T. Beleno, Amperometric biosensors precision improvement. Application to phenolic pollutants determination, Electrochim. Acta 147 (2014) 25-30.
[163] F. Gutierrez, F.N. Comba, A. Gasnier, A. Gutierrez, L. Galicia, C. Parrado, M.D. Rubianes, G.A. Rivas, Graphene Paste Electrode: Analytical Applications for the Quantification of Dopamine, Phenolic Compounds and Ethanol, Electroanalysis 26 (2014) 1694-1701.
[164] A.N. Sekretaryova, A.V. Volkov, I.V. Zozoulenko, A.P.F. Turner, M.Y. Vagin, M. Eriksson, Total phenol analysis of weakly supported water using a laccase-based microband biosensor, Anal. Chim. Acta 907 (2016) 45-53.
[165] Z.L. Hua, Q. Qin, X. Bai, X. Huang, Q. Zhang, An electrochemical biosensing platform based on 1-formylpyrene functionalized reduced graphene oxide for sensitive determination of phenol, RSC Adv. 6 (2016) 25427-25434.

[166] C.C. Mayorga-Martinez, M. Cadevall, M. Guix, J. Ros, A. Merkoci, Bismuth nanoparticles for phenolic compounds biosensing application, Biosens. Bioelectron. 40 (2013) 57-62.
[167] S. Cosnier, Biomolecule immobilization on electrode surfaces by entrapment or attachment to electrochemically polymerized films. A review, Biosens. Bioelectron. 14 (1999) 443-456.
[168] C.C. Mayorga-Martinez, L. Hlavata, S. Miserere, A. Lopez-Marzo, J. Labuda, J. Pons, A. Merkoci, Nanostructured CaCO3-poly(ethyleneimine) microparticles for phenol sensing in fluidic microsystem, Electrophoresis 34 (2013) 2011-2016.
[169] P. Ibarra-Escutia, J.J. Gomez, C. Calas-Blanchard, J.L. Marty, M.T. Ramirez-Silva, Amperometric biosensor based on a high resolution photopolymer deposited onto a screen-printed electrode for phenolic compounds monitoring in tea infusions, Talanta 81 (2010) 1636-1642.
[170] C. Tortolini, M. Di Fusco, M. Frasconi, G. Favero, F. Mazzei, Laccase-polyazetidine prepolymer-MWCNT integrated system: Biochemical properties and application to analytical determinations in real samples, Microchem J. 96 (2010) 301-307.
[171] J.C. Gonzalez-Rivera, J.F. Osma, Fabrication of an Amperometric Flow-Injection Microfluidic Biosensor Based on Laccase for In Situ Determination of Phenolic Compounds, Biomed Res. Int. 2015 (2015) 1-9.
[172] M. Gutierrez-Capitan, A. Ipatov, A. Merlos, C. Jimenez-Jorquera, C. Fernandez-Sanchez, Compact Electrochemical Flow System for the Analysis of Environmental Pollutants, Electroanalysis 26 (2014) 497-506.
[173] R. Castaneda, D. Vilela, M.C. Gonzalez, S. Mendoza, A. Escarpa, SU-8/Pyrex microchip electrophoresis with integrated electrochemical detection for class-selective electrochemical index determination of phenolic compounds in complex samples, Electrophoresis 34 (2013) 2129-2135.
[174] J. Wang, M.P. Chatrathi, B.M. Tian, Capillary electrophoresis microchips with thick-film amperometric detectors: separation and detection of phenolic compounds, Anal. Chim. Acta 416 (2000) 9-14.
[175] M.D. Godoy-Caballero, M.I. Acedo-Valenzuela, T. Galeano-Diaz, A. Costa-Garcia, M.T. Fernandez-Abedul, Microchip electrophoresis with amperometric detection for a novel determination of phenolic compounds in olive oil, Analyst 137 (2012) 5153-5160.
[176] K. Fenner, S. Canonica, L.P. Wackett, M. Elsner, Evaluating Pesticide Degradation in the Environment: Blind Spots and Emerging Opportunities, Science 341 (2013) 752-758.
[177] E.X. Luan, Z.Z. Zheng, X.Y. Li, H.X. Gu, S.Q. Liu, Inkjet-assisted layer-by-layer printing of quantum dot/enzyme microarrays for highly sensitive detection of organophosphorous pesticides, Anal. Chim. Acta 916 (2016) 77-83.
[178] N. Nesakumar, S. Sethuraman, U.M. Krishnan, J.B.B. Rayappan, Electrochemical acetylcholinesterase biosensor based on ZnO nanocuboids modified platinum electrode for the detection of carbosulfan in rice, Biosens. Bioelectron. 77 (2016) 1070-1077.
[179] Y.H. Song, J.Y. Chen, M. Sun, C.C. Gong, Y. Shen, Y.G. Song, L. Wang, A simple electrochemical biosensor based on AuNPs/MPS/Au electrode sensing layer for monitoring carbamate pesticides in real samples, J. Hazard. Mater. 304 (2016) 103-109.
[180] J.H. Zhou, C.Y. Deng, S.H. Si, S.E. Wang, Zirconia electrodeposited on a self-assembled monolayer on a gold electrode for sensitive determination of parathion, Microchim. Acta 172 (2011) 207-215.
[181] N. Lezi, A. Economou, Voltammetric Determination of Neonicotinoid Pesticides at Disposable Screen-Printed Sensors Featuring a Sputtered Bismuth Electrode, Electroanalysis 27 (2015) 2313-2321.

[182] P. Chorti, J. Fischer, V. Vyskocil, A. Economou, J. Barek, Voltammetric Determination of Insecticide Thiamethoxam on Silver Solid Amalgam Electrode, Electrochim. Acta 140 (2014) 5-10.
[183] Y. Liu, S.L. Yang, W.F. Niu, Simple, rapid and green one-step strategy to synthesis of graphene/carbon nanotubes/chitosan hybrid as solid-phase extraction for square-wave voltammetric detection of methyl parathion, Colloid Surf. B-Biointerfaces 108 (2013) 266-270.
[184] F.W.P. Ribeiro, F.W.D. Lucas, L.H. Mascaro, S. Morais, P.N.D. Casciano, P. de Lima-Neto, A.N. Correia, Electroanalysis of formetanate hydrochloride by a cobalt phthalocyanine functionalized multiwalled carbon nanotubes modified electrode: characterization and application in fruits, Electrochim. Acta 194 (2016) 187-198.
[185] M. Medina-Sanchez, C.C. Mayorga-Martinez, T. Watanabe, T.A. Ivandini, Y. Honda, F. Pino, K. Nakata, A. Fujishima, Y. Einaga, A. Merkoci, Microfluidic platform for environmental contaminants sensing and degradation based on boron-doped diamond electrodes, Biosens. Bioelectron. 75 (2016) 365-374.
[186] S. Nouanthavong, D. Nacapricha, C.S. Henry, Y. Sameenoi, Pesticide analysis using nanoceria-coated paper-based devices as a detection platform, Analyst 141 (2016) 1837-1846.
[187] J. Wang, M.P. Chatrathi, A. Mulchandani, W. Chen, Capillary electrophoresis microchips for separation and detection of organophosphate nerve agents, Anal. Chem. 73 (2001) 1804-1808.
[188] K. Islam, R. Chand, D. Han, Y.S. Kim, Microchip Capillary Electrophoresis Based Electroanalysis of Triazine Herbicides, Bull. Environ. Contam. Toxicol. 94 (2015) 41-45.
[189] D. Chudobova, K. Cihalova, R. Guran, S. Dostalova, K. Smerkova, R. Vesely, J. Gumulec, M. Masarik, Z. Heger, V. Adam, R. Kizek, Influence of microbiome species in hard-to-heal wounds on disease severity and treatment duration, Braz. J. Infect. Dis. 19 (2015) 604-613.
[190] Y.C. Xu, H. Yan, Y. Zhang, K.W. Jiang, Y. Lu, Y.H. Ren, H. Wang, S. Wang, W.L. Xing, A fully sealed plastic chip for multiplex PCR and its application in bacteria identification, Lab Chip 15 (2015) 2826-2834.
[191] P. Fach, S. Perelle, J. Grout, F. Dilasser, Comparison of different PCR tests for detecting Shiga toxin-producing Escherichia coli O157 and development of an ELISA-PCR assay for specific identification of the bacteria, J. Microbiol. Methods 55 (2003) 383-392.
[192] F. Tian, J. Lyu, J.Y. Shi, F. Tan, M. Yang, A polymeric microfluidic device integrated with nanoporous alumina membranes for simultaneous detection of multiple foodborne pathogens, Sens. Actuator B-Chem. 225 (2016) 312-318.
[193] M. Safavieh, M.U. Ahmed, M. Tolba, M. Zourob, Microfluidic electrochemical assay for rapid detection and quantification of Escherichia coli, Biosens. Bioelectron. 31 (2012) 523-528.
[194] M. Kim, T. Jung, Y. Kim, C. Lee, K. Woo, J.H. Seol, S. Yang, A microfluidic device for label-free detection of Escherichia coli in drinking water using positive dielectrophoretic focusing, capturing, and impedance measurement, Biosens. Bioelectron. 74 (2015) 1011-1015.
[195] L. Nejdl, J. Kudr, K. Cihalova, D. Chudobova, M. Zurek, L. Zalud, L. Kopecny, F. Burian, B. Ruttkay-Nedecky, S. Krizkova, M. Konecna, D. Hynek, P. Kopel, J. Prasek, V. Adam, R. Kizek, Remote-controlled robotic platform ORPHEUS as a new tool for detection of bacteria in the environment, Electrophoresis 35 (2014) 2333-2345.
[196] J.P. Metters, R.O. Kadara, C.E. Banks, New directions in screen printed electroanalytical sensors: an overview of recent developments, Analyst 136 (2011) 1067-1076.

4 METODIKA

4.1 Chemikálie

Všechny chemikálie byly v ACS čistotě pořízeny od firmy Sigma-Aldrich (St. Louis, MO, USA), pokud není uvedeno jinak. MilliQ voda použitá pro experimentální práci byla získána reverzní osmózou systému Aqual 25 (Aqual, Brno, Česká Republika) a purifikována purifikačním systémem Direct-Q 3 UV (Millipore, Billerica, MA, USA) na čistotu 18 $M\Omega \cdot cm^{-1}$.

4.2 Metody

4.2.1 Příprava elektrody ze skelného uhlíku k měření

Elektroda ze skelného uhlíku (GCE) s průměrem 3 mm (CH Instruments, Austin, TX, USA) byla mechanicky leštěna pomocí suspenze hliníkových částic (CH Instruments, Austin, TX, USA) na leštící tkanině do získání skelného povrchu. Následně byly nečistoty odstraněny z povrchu GCE pomocí ultrazvukové lázně Sonorex digital 10 P (Bandelin, Berlín, Německo).

4.2.2 Elektrochemická měření

Elektrochemická měření byla prováděna na potenciostatech PGSTAT302N (Metrohm, Herisau, Switzerland) a PGSTAT 101 (Metrohm, Herisau, Švýcarsko). Získané záznamy byly vyhodnocovány pomocí softwaru NOVA 1.8 (Metrohm, Herisau, Švýcarsko). Potenciály jsou s výjimkou tištěných elektrod vztahovány k Ag/AgCl/3 M KCl referenční elektrodě (CH Instruments, Austin, TX, USA) a jako pomocná elektroda byl používán platinový drátek (CH Instruments, Austin, TX, USA). Není-li uvedeno jinak, jako podpůrný elektrolyt byl používán acetátový pufr (0,2 $mol \cdot l^{-1}$ CH_3COONa a CH_3COOH, pH 5). Impedanční spektra byla měřena v roztoku $Fe(CN)_6^{3-/}Fe(CN)_6^{4-}$ a KCl. V publikacích byly používány metody diferenční pulzní voltametrie a cyklické voltametrie. Parametry měření a podrobnější informace jsou uvedeny v jednotlivých publikacích.

4.2.3 Výroba tištěných elektrod

Tištěné elektrody (tříelektrodový plochý sensor) byly navrženy a vyráběny v laboratořích LabSensNano (Vysoké učení technické v Brně, Česká republika).

Povrchy jednotlivých elektrod byly navrženy následující: pracovní elektroda 7,1 mm^2, referenční elektroda 1,3 mm^2 a pomocná elektroda 6,2 mm^2. Elektrody byly vyráběny pomocí poloautomatického screen-printeru Aurel C880 (Aurel Automation, Modigliana, Itálie) a nanesené vrstvy fixovány pomocí pece firmy BTU (BTU, Severní Billerica, MT, USA). K výrobě jednotlivých vrstev elektrod byly použity následující: vodivá vrstva z pasty 9562-G obsahující Ag, Pt a Pd (Electroscience, Reading, Spojené království), ochranná vrstva z dielektrické pasty ESL 4917 (Electroscience, Berkshire, Spojené království), pomocná elektroda z pasty ESL 5545 obsahující Pt. Pasty byly vytvrzeny v peci při 850 °C. Pracovní elektroda byla natištěna pomocí uhlíkové pasty pro elektrochemické senzory DuPont BQ221 (DuPont Company, Wilmington, DE, USA) a fixována při 130 °C. Referenční elektroda byla vytvořena nanesením speciálního polymeru s Ag/AgCl v poměru 65:35 DuPont 5874 (DuPont Company, Wilmington, DE, USA) a vytvrzena při 120 °C. Další podrobnosti o senzoru mohou být nalezeny v publikaci Prášek a kol. *(Prasek a kol., 2012).*

5 VÝSLEDKY A DISKUSE

Výsledková část předkládané disertační práce je přiložena ve formě publikací v odborných časopisech a dále doplněna o komentáře autora.

5.1 Využití nanomateriálů jako nástroje ke zlepšení vlastností elektrod

5.1.1 Vědecký článek I

Kudr, J.; Richtera, L.; Nejdl, L.; Xhaxhiu, K.; Vitek, P.; Ruttkay-Nedecky, B.; Hynek, D.; Kopel, P.; Adam, V.; Kizek, R. Improved electrochemical detection of zinc ions using electrode modified with electrochemically reduced graphene oxide. *Materials*, 2016, roč. 9. č. 4, s. 1-12. ISSN 1996-1944.

Podíl autora Kudr J.: 60 % textové části práce a 45 % experimentální práce

Kontaminace životního prostředí kovy a zejména těžkými kovy je v současnosti považována za jeden z nevíce znepokojujících environmentálních problémů *(Esashi, 1989)*. Těžké kovy představují vzhledem nemožnosti biologické degradace problematické polutanty. Důsledkem je jejich akumulace v živých organismech a vysoká mobilita potravními řetězci *(Luoma a kol., 2005)*. O tomto faktu svědčí velká pozornost, kterou této problematice věnuje WHO i vědecká komunita *(Mason a kol., 1996; Neff, 1997; Volesky, 2007; WHO, 2010).*

Zlatým standardem v kvantifikaci koncentrací těžkých kovů je atomová absorpční spektroskopie (AAS) a hmotnostní spektroskopie s indukčně vázaným plazmatem (ICP-MS) *(Sardans a kol., 2010; Habila a kol., 2016; Kojta a kol., 2016; Singh a kol., 2016).* Elektroanalytické metody pro tuto oblast reprezentují alternativu. Nicméně v porovnání s těmito metodami poskytují celou řadu výhod – instrumentace je finančně výrazně dostupnější, analýzy jsou rychlejší, spotřebují méně energie, umožňují miniaturizaci celého analytického zařízení a tím poskytují možnost *in situ* analýz *(Kang a kol., 2013; Zhang a kol., 2015; Kokkinos a kol., 2016)*. Elektroanalýza disponuje dostatečnou citlivostí a selektivitou pro stopovou analýzu těžkých kovů, i přes to je zlepšování vlastností elektrochemických zařízení stále aktuální *(Chaiyo a kol., 2016)*. Modifikace povrchů pracovních elektrod, kde při analýze probíhají samotné redoxní procesy, jsou

vhodným nástrojem jak zlepšit jejich vlastnosti. V současné době se v elektrochemii objevují dva trendy modifikací – biomolekulami a nanomateriály *(Wang a kol., 2015; Huang a kol., 2016; Chuang a kol., 2016; Khalilzadeh a kol., 2016)*. Úkolem nanomateriálů v této oblasti je především zvýšit povrch elektrod a umožnit lepší transport analytu k elektrodě.

Cílem předložené publikace bylo použít grafen oxid (uhlíkový nanomateriál) ke zlepšení elektroanalytických vlastností elektrody ze skelného uhlíku (GCE). Grafen oxid byl na elektrodu deponován za konstantního potenciálu (+1 V *vs.* Ag/AgCl/3 M KCl) a následně elektrochemicky redukován na redukovaný grafen oxid. Takto modifikovaná elektroda byla multi-instrumentálně charakterizována a použita k optimalizaci detekce Zn(II) iontů.

Z výsledků naší práce vyplývá, že elektrochemicky redukovaný grafen oxid je vhodným modifikátorem GCE pro detekci Zn(II) iontů. V porovnání s nemodifikovanou GCE, dosahuje větší citlivosti a nižšího limitu detekce. Interferenční studie navíc ukázala, že Zn(II) ionty mohou být tímto senzorem spolehlivě stanoveny i v přítomnosti Cd(II) iontů.

materials

MDPI

Article

Improved Electrochemical Detection of Zinc Ions Using Electrode Modified with Electrochemically Reduced Graphene Oxide

Jiri Kudr [1,2], Lukas Richtera [1,2], Lukas Nejdl [1,2], Kledi Xhaxhiu [1,2], Petr Vitek [3], Branislav Rutkay-Nedecky [1,2], David Hynek [1,2], Pavel Kopel [1,2], Vojtech Adam [1,2] and Rene Kizek [4,*]

Received: 11 November 2015; Accepted: 4 January 2016; Published: 7 January 2016
Academic Editor: Jung Ho Je

1 Department of Chemistry and Biochemistry, Mendel University in Brno, Zemedelska 1, Brno CZ-613 00, Czech Republic; george.kudr@centrum.cz (J.K.); oliver@centrum.cz (L.R.); lukasnejdl@gmail.com (L.N.); kledi.xhaxhiu@fshn.edu.al (K.X.); brano.ruttkay@seznam.cz (B.R.-N.); d.hynek@email.cz (D.H.); paulko@centrum.cz (P.K.); vojtech.adam@mendelu.cz (V.A.)
2 Central European Institute of Technology, Brno University of Technology, Technicka 3058/10, Brno CZ-616 00, Czech Republic
3 Global Change Research Institute, The Czech Academy of Sciences, v.v.i., Bělidla 4a, Brno CZ-603 00, Czech Republic; vitek.p@czechglobe.cz
4 Department of Biomedical and Environmental Analysis, Wroclaw Medical University, Borowska 211, Wrocław PL-50 556, Poland
* Correspondence: kizek@sci.muni.cz; Tel.: +420-545-133-350; Fax: +420-545-212-044

Abstract: Increasing urbanization and industrialization lead to the release of metals into the biosphere, which has become a serious issue for public health. In this paper, the direct electrochemical reduction of zinc ions is studied using electrochemically reduced graphene oxide (ERGO) modified glassy carbon electrode (GCE). The graphene oxide (GO) was fabricated using modified Hummers method and was electrochemically reduced on the surface of GCE by performing cyclic voltammograms from 0 to −1.5 V. The modification was optimized and properties of electrodes were determined using electrochemical impedance spectroscopy (EIS) and cyclic voltammetry (CV). The determination of Zn(II) was performed using differential pulse voltammetry technique, platinum wire as a counter electrode, and Ag/AgCl/3 M KCl reference electrode. Compared to the bare GCE the modified GCE/ERGO shows three times better electrocatalytic activity towards zinc ions, with an increase of reduction current along with a negative shift of reduction potential. Using GCE/ERGO detection limit 5 ng·mL^{-1} was obtained.

Keywords: carbon; cyclic voltammetry; electrochemical impedance spectroscopy; electrochemistry; graphene oxide; heavy metal detection; reduced graphene oxide

1. Introduction

Heavy metal pollution has become a major concern all over the world. Anthropogenic processes like urbanization and industrialization have led to their release from Earth's crust and their accumulation in the biosphere. The long-term monitoring of heavy metal pollution is the only way to meet the legislative demands and decrease pressure on the environment. However, most heavy metals like lead or cadmium are toxic even at low concentrations, others, which belong to a group of essential micronutrients, pose health risks in high supplementation only, but their monitoring is also needed [1–3]. Among essential micronutrients, zinc(II) plays one of the most important role. Zinc analysis is appealing not only from the environmental point of view but also from the biochemical one. Zinc(II) ions play

an important role in cell replication and nucleic acid metabolism, and its deficiency is connected with some pathological processes like retarded growth and immunity dysfunction [4]. As was shown recently, the enhanced zinc intake by drinking water in the case of mice caused zinc deficiency in the hippocampus, associated with memory deficit and decreased expression levels of learning and memory related receptors [5]. Zinc has these important roles and effects mainly as a co-factor of numerous proteins, therefore it is not surprising that metallomics and proteomics of zinc-containing proteins are emerging fields of science [6–8]. From these, metallothioneins are highlighted as maintainers and transporters of these proteins and their importance in zinc metabolism belongs to the interest of numerous researchers [9–18].

Atomic absorption spectrometry (AAS) and inductively coupled plasma mass spectrometry (ICP-MS) represent a gold standard in detection of trace heavy metals concentrations. Nevertheless, they require expensive instrumentation, experienced operators, and the analyses are time-consuming. On the contrary, electrochemistry offers superior features like portability, easy use, low price, miniaturization, and high sensitivity [19–23]. The great advantage of electroanalysis is also the possibility of electrode surface modification [24].

Mercury electrodes have been widely used in trace heavy metal analysis for decades; however, they do not correspond with current trends including miniaturization. Whereas material sciences are a rapidly developing field of science, several micro to nanosized materials like liquid metals/metal oxides in order to improve electrode properties are attracting the attention of analysts [25–28]. Graphene, theoretically perfect two-dimensional (one-atom-thick) material, is the ideal choice for electrochemistry since it possesses unusual electronic conductivity and high surface area [29]. However, it is worth noting that a one-atom-thick, defect-less graphene monolayer is difficult to prepare and standard graphene materials are far from perfectly structured, and therefore more often reduced graphene oxide (rGO) is used. The procedure of GO reduction influences subsequent rGO properties. Electrodes modified with rGO obtained using constant potential chemical and thermal reduction was previously compared [30]. From electrochemical methods for GO reduction cyclic voltammetry was also used [31]. Electrodes modified with rGO are not only desirable for just electroanalytical chemistry, but also for the removal of organic pollutants from wastewaters [32]. Various methods have been used to prepare electrodes modified with GO [33–36]. Among others, electrodeposition of GO or rGO attracted interest due to its efficiency, ease of use, and rapid procedure [37]. Potentiostatic methods and cyclic voltammetry (CV) were shown to be suitable tool for electrodeposition of these materials on electrodes [38,39]. Recently, pulse potential method based on changing of anodic deposition and cathodic reduction periods was developed too [40]. Moreover, an electrode surface modification with biomolecules or graphene-like nanomaterials can significantly improve detection sensitivity and selectivity [41–43].

In this work the GO film on glassy carbon electrode (GCE) was fabricated by the potentiostatic deposition of GO. Electrochemically deposited GO was subsequently subjected to electrochemical reduction to produce electrochemically reduced graphene oxide (ERGO) using CV. The properties of this modified electrode were compared with standard bare GCE using CV and electrochemical impedance spectroscopy (EIS). $[Fe(CN)_6]^{3-}/[Fe(CN)_6]^{4-}$ was used as a redox probe for electrode characterization and the performance of GCE/ERGO on detection of Zn(II) using differential pulse voltammetry (DPV) was examined.

2. Results and Discussion

2.1. Preparation of GCE/ERGO

Since the discovery of graphene, it has been attracting great attention due to its high conductivity and surface to volume ratio [44]. However, from an electrochemical point of view graphene suffers from a limited number of hydrophilic moieties and electroactive sites [45]. GO with randomly distributed oxygen groups benefits from structural similarity with graphene, nevertheless structure breaks cause

the decrease of conductivity [46]. Partially reduced GO represents an intermediate between ideal graphene structure and GO, whereas the amount of electroactive surface and reactive functionalities (epoxy, hydroxyl, carboxyl) are balanced.

The common method to fabricate rGO is exfoliation of graphite to produce GO followed by thermal or chemical reduction [47]. ERGO represents an alternative since no expensive equipment or use of toxic compounds is needed during its fabrication. Several procedures have been introduced to cover electrodes with a GO or GO/ERGO layer [34,38,48,49]. Direct electrodeposition from solution or drop-casting of GO or rGO on the surface of electrode can be used. If GO is used as a source material for electrode modification, deposition is followed by electrochemical reduction of GO to prepare ERGO. Previously, CV, potentiostatic or pulsed methods (several cycles of deposition in positive potential followed by GO reduction in negative potential) were used in order to cover the electrode with ERGO [50,51].

Here, GO was prepared according to the simplified Hummer's method (Figure 1A). It was revealed that our GO sample contains particles with hydrodynamic diameter of 848 ± 290 nm (Figure 1B). Negative charge of GO was confirmed using measurement of zetapotential (ζ = −43 mV), which enables to deposit GO particles on the electrode using application of positive potential on it. This value also suggests that GO particles possess good stability in colloid phase.

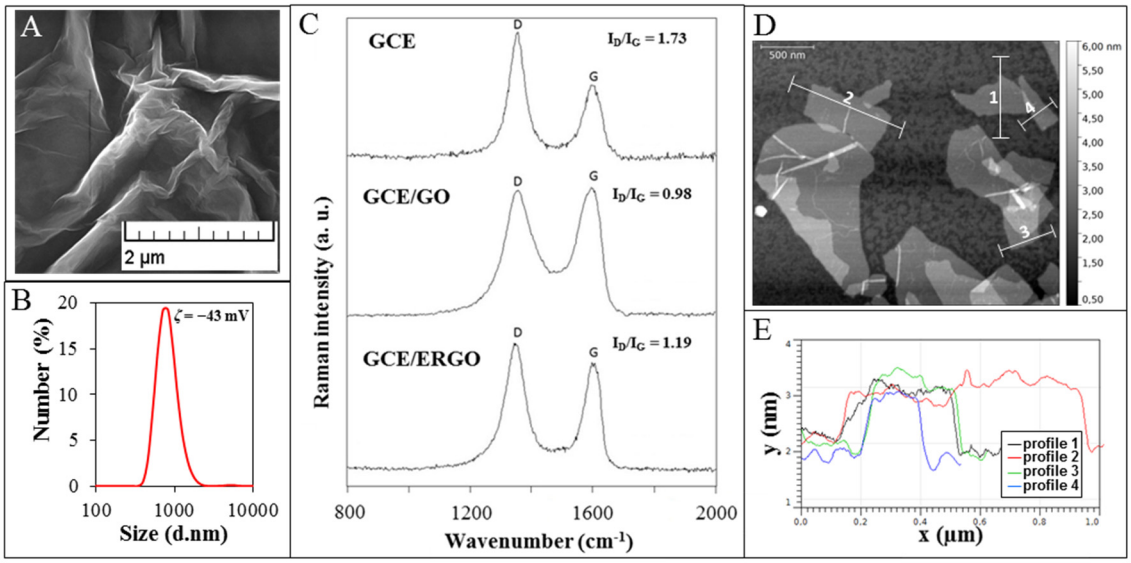

Figure 1. (**A**) Micrograph of GO used to modify GCE obtained by SEM; (**B**) GO size distribution including zetapotential; (**C**) Raman spectra of GCE, GCE modified with GO and GCE modified with ERGO; (**D**) AFM image of GO and (**E**) the height profiles along lines displayed in AFM image.

For the fabrication of GCE/ERGO, the constant potential +1.0 V *vs.* Ag/AgCl/3 M KCl reference electrode were applied to GCE in a previously sonicated water solution of GO (0.5 mg· mL^{-1}). Due to the presence of oxygen-containing functionalities negatively charged GO is electrostatically attracted to positively charge electrode. Subsequently, the working electrode was gently rinsed with water, transferred to acetate buffer and five CV cycles (from 0 to −1.50 V) were performed [52]. The irreversible reduction signals at −1.05 V and −0.85 V were observed in first cycle and completely disappeared in subsequent cycles (Figure 2A). It was shown previously that reduction of GO provides peak around −1.10 V [8,45,51]. Nevertheless different oxygen-containing moieties can be presented within GO, which can result in different reduction signals. The deposition (0–480 s) time of GO on electrode was optimized using detection of 20 µmol· L^{-1} Zn(II) signal and the deposition for 60 s was found as an optimal (Figure 2B). It was shown that although deposition of GO increased reduction signal of zinc slightly for 15 s, deposition of GO increased signal nearly three-fold for 30 s when compared

with bare GCE cathodized for precise time in water. The deposition time 60 s was able to sufficiently modify the surface of GCE with GO, and the increase of deposition time did not result in the increase of detection signal.

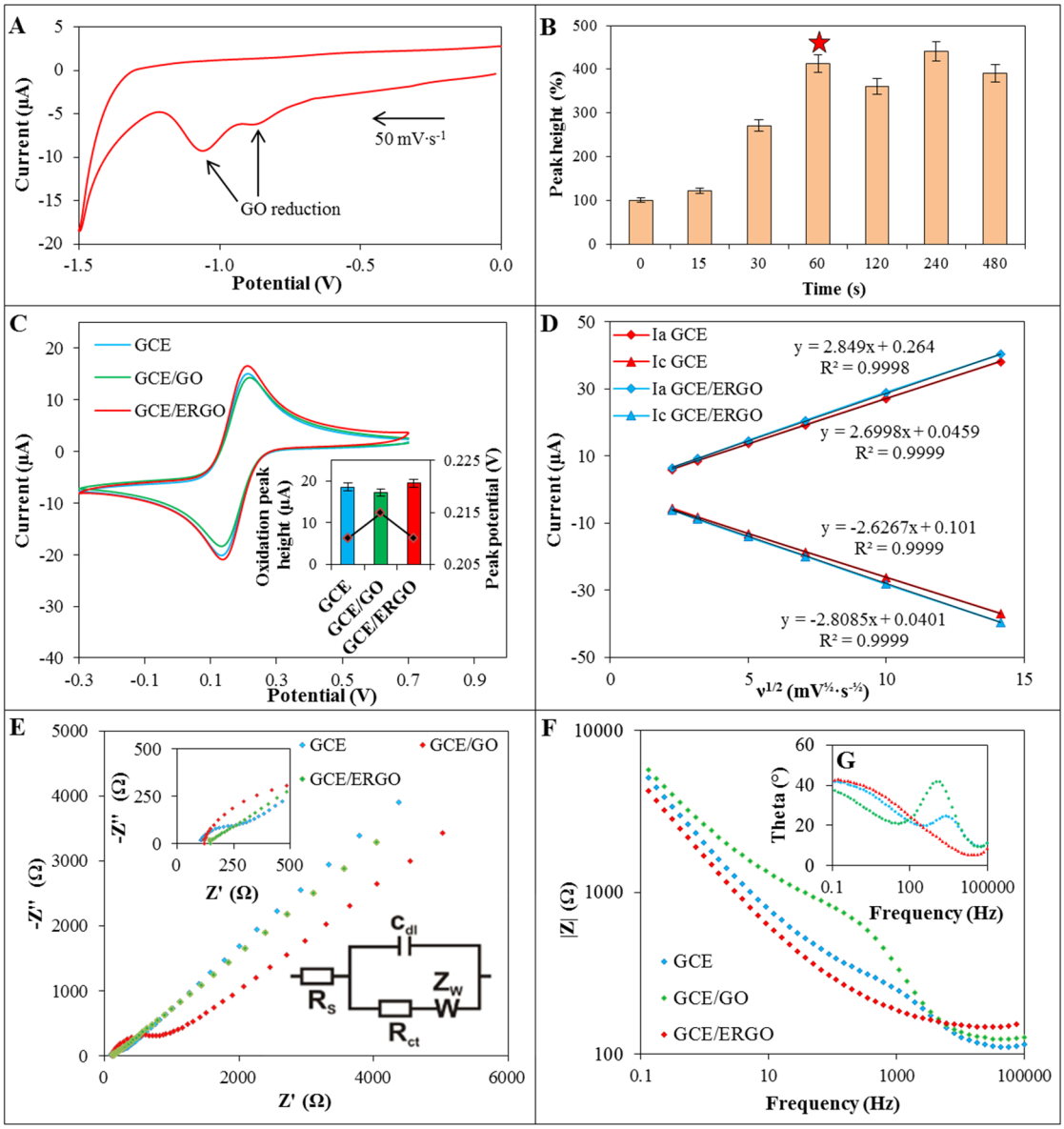

Figure 2. (**A**) The CV (0 − (−1.5) V) of GCE/GO in acetate buffer; (**B**) Dependence of Zn(II) reduction signal obtained using GCE/ERGO on deposition time of GO (0.5 mg· mL^{-1}) on the electrode (deposition time selected as optimal is marked with star); (**C**) CV of 2 mM $[Fe(CN)_6]^{3-}$/$[Fe(CN)_6]^{4-}$ in 0.1 M KCl (50 $mV{\cdot}s^{-1}$) recorded on bare GCE (blue line), GCE/GO (red line) and GCE/ERGO (green line) and corresponding peak current levels; (**D**) The dependence of $[Fe(CN)_6]^{3-}$/$[Fe(CN)_6]^{4-}$ anodic (Ia) and cathodic (Ic) peak heights on the square root of scan rate; (**E**) Nyquist plot, detail of nyquist plot high frequency region and equivalent circuit used for data evaluation in insets; (**F**) Bode modulus plot of bare GCE (blue line), GCE/GO (red line) and GCE/ERGO (green line); and (**G**) corresponding Bode phase diagram (same colours as previous figure).

Further, we analyzed the surface of the modified electrode by Raman spectroscopy. The D and G Raman bands were detected at 1355 cm^{-1} and 1595 cm^{-1} for GO and 1348 cm^{-1} and 1600 cm^{-1} for ERGO, both deposited on GCE. The Raman intensity ratio of the D and G bands (I_D/I_G) is increased

in the case of GCE/ERGO (1.19) compared to GCE/GO (0.98) (Figure 1C), which is in accordance with literature [53,54]. It is attributed to the modification of the GO structure by reduction resulting in removal of functional groups and creation of defects between the sp^2 domains [55]. Change of full width at half maximum (FWHM) was observed from 115 cm^{-1} for GO towards 78 cm^{-1} in the case of ERGO for D band. The value for ERGO points at high disorder with low distances between defects [55]. The image of GO obtained using AFM suggests that GO is presented within sample in sheet-like shapes (Figure 1D). The thickness of GO, deduced from the height profile of AFM image, is about 1 nm, which is comparable to GO monolayer thickness published previously [56,57].

2.2. Characterization of GCE/ERGO

In order to characterize GCE/ERGO, cyclic voltammograms of equimolar 2 mmol· L^{-1} $[Fe(CN)_6]^{3-}$/$[Fe(CN)_6]^{4-}$ as a redox probe was measured using bare GCE and GCE/GO and compared with the record measured using GCE/ERGO. As it is shown in Figure 2C, deposition of GO on GCE reduces the peak current by 5%. On the contrary, GCE/ERGO exhibited better detection properties by 10% (inset in Figure 2C). Based on these data, the Randles-Sevcik equation (Equation (1)) was used to calculate the electroactive surface area of bare GCE and subsequently compare it with GCE/ERGO. The areas of 6.4 mm^2 and 7.0 mm^2 were acquired, respectively, which means increase for about 9.4% and confirm successful deposition and reduction of GO. The values of reduction and oxidation peaks of $[Fe(CN)_6]^{3-}$/$[Fe(CN)_6]^{4-}$ were plotted against the square root of scan rates (Figure 2D). The linear dependence revealed diffusion controlled processes for both GCE and GCE/ERGO and slightly improved sensitivity of detection in case of GCE/ERGO. These results were also confirmed by EIS (Figure 2E).

The Randles circuit was used as an equivalent circuit for fitting the EIS data. It consisted of solution resistance Rs, charge transfer resistance Rct, double layer capacitance Cdl and Warburg impedance ZW (inset in Figure 2E). Nyquist diagram showed in case of bare GCE depressed semicircle with charge transfer resistance 2.1 kΩ· cm^{-1}. After deposition of GO on GCE, charge transfer resistance increased four-fold to 8.5 kΩ· cm^{-1}. Very small depressed semicircle was observed in the case of GCE/ERGO, where Rct decreased to 0.6 kΩ· cm^{-1} (32% of GCE Rct). Significantly lower charge transfer resistance of GCE/ERGO in comparison with GCE/GO was previously reported [58]. In Bode diagram the frequency dependence on absolute magnitudes of impedance modulus |Z| was plotted (Figure 2F). The peaks of Bode phase diagram in case of GCE and GCE/GO (1–3 kHz) suggests that charge transfer resistance takes place in the electrode/electrolyte interface. Phase peak of Bode plot of GCE/ERGO disappeared at higher frequencies as a result of high electron transfer, where charge transfer resistance decreased (Figure 2G).

2.3. Detection of Zn(II)

The detection of Zn(II) was performed using DPV. Firstly, deposition potentials ((−1.45) − (−0.65) V) of Zn(II) on the surface of GCE/ERGO was optimized. As it can be seen in Figure 3A, the obtained Zn(II) signal increased from potential −0.65 to −1.25 V. At potential −1.25 V the Zn(II) signal reached its higher value and was choose as an optimal. As the next step, deposition time (0–90 s) of Zn(II) was optimized (Figure 3B). It was revealed that the signal increased by 73% using deposition time 60 s and deposition potential −1.25 V in comparison with deposition time 0 s. After this optimization, different concentrations of Zn(II) were measured using GCE/ERGO and calibration curve was determined (Figure 3C). It exhibited linear section between 1.0 μmol· L^{-1} and 62.5 μmol· L^{-1} and other analytical parameters of detection are displayed in Table 1. The modification of GCE with ERGO improved the detection of zinc ions (35 μmol· L^{-1}) four-fold in comparison with bare GCE and slightly shifted peak potential from −1.18 V to −1.2 V (Figure 3D). Using GCE/ERGO, we obtained limit of detection (LOD) 0.1 μmol· L^{-1} Zn(II) (~5 ng· mL^{-1}).

Table 1. Analytical parameters of electrochemical detection of Zn(II).

Substance	Working Electrode	Regression Equation	Linear Dynamic Range (μmol· L^{-1})	R^2 [a]	LOD [b] (μmol· L^{-1})	LOQ [c] (μmol· L^{-1})	RSD (%)
Zn(II)	GCE/ERGO	$y = 0.1608x - 0.1231$	62.5 – 1.0	0.9999	0.1	0.4	4.8
Zn(II)	GCE	$y = 0.0539x - 0.0916$	500.0 – 2.0	0.9992	0.5	2.0	5.2

[a] Regression coefficient; [b] LOD ($S/N = 3$); [c] LOQ ($S/N = 10$).

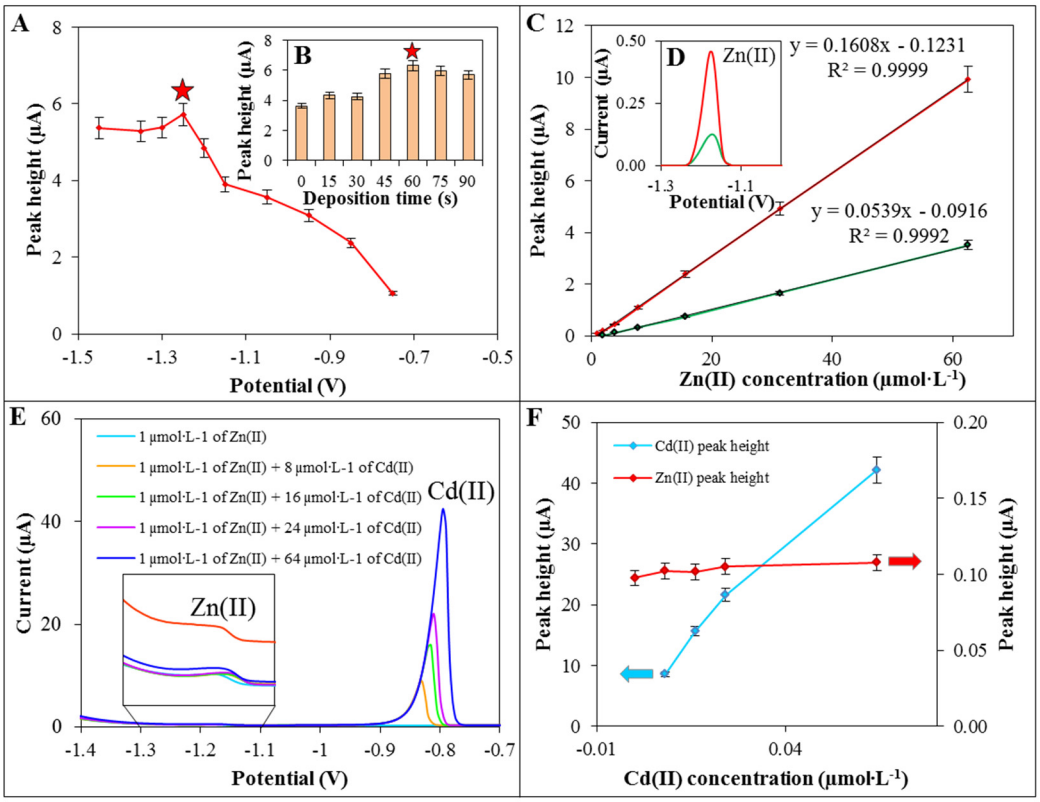

Figure 3. Dependence of Zn(II) reduction signal on deposition potential (**A**) and deposition time (**B**) of Zn(II) (35 μmol· L^{-1}) on GCE/ERGO (parameters marked with star was selected as an optimal); (**C**) Dependence of electrochemical signal on Zn(II) concentration (1.0–62.5 μmol· L^{-1}) and comparison of DPV reduction signals of Zn(II) (4 μmol· L^{-1}) (**D**) obtained using GCE/ERGO (red line) and bare GCE (blue line); (**E**) DPV voltammograms ((−1.40) − (−0.70) V) and comparison of Zn(II) and Cd(II) peak heights (**F**) of Zn(II) solution (1 μmol· L^{-1}) with different concentrations of Cd(II) (0–64 μmol· L^{-1}). Comparison of 10 μmol· L^{-1} Zn(II) electrochemical signal in acetate buffer with added 50 μmol· L^{-1} K(I), Ca(II) and Mg(II) in inset.

As the final step, the effect of interference with Zn(II) detections was examined. We chose Cd(II) since it is quite often presented in environmental samples and may affect Zn(II) detection [41,59]. Zn(II) solutions (1 μmol· L^{-1}) with different concentrations of Cd(II) (0–64 μmol· L^{-1}) were measured and the peak heights of Zn(II) (potential −1.15 V) were compared (Figure 3E). As it can be seen, peak of Cd(II) (about potential −0.80 V) is well separated from Zn(II) peak and did not significantly affect Zn(II) peak heights even at a 64-times higher concentration (Figure 3F). In addition, other monovalent and bivalent ions were tested as a possible interference in real sample. To Zn(II) solution five-times higher concentrations of K(I), Ca(II), and Mg(II) ions were added and their effects on Zn(II) were evaluated. All Zn(II) analysis presented here were performed in the acetate buffer where Na(I) ions were present in high concentration. Other tested ions showed no apparent interference in Zn(II) detection (Figure 3F inset).

3. Experimental Section

3.1. Chemicals and Material

ACS purity (*i.e.*, chemicals meet the specifications of the American Chemical Society) sodium acetate trihydrate, acetic acid, zinc nitrate, potassium hexacyanoferrate(III), potassium hexacyanoferrate(II) trihydrate, potassium chloride, water, and other chemicals were purchased from Sigma-Aldrich (St. Louis, MO, USA) unless noted otherwise.

3.2. Preparation of GO

GO was synthesized using chemical oxidation of graphite flakes (5.0 g, Sigma-Aldrich, and 100 mesh, ⩾75% min) in a mixture of concentrated H_2SO_4 (670 mL, ACS reagent 95.0%–98.0%) and 30.0 g $KMnO_4$ (>99%) according to the simplified Hummer's method [60]. The reaction mixture was stirred vigorously. After four days, the oxidation of graphite was terminated by slow adding of H_2O_2 solution (250 mL, 30 wt % in H_2O) and the colour of the mixture turned to bright yellow, indicating high oxidation level of graphite. Formed graphite oxide was washed three times with 1 M of HCl and washed with water several times (total volume used 12 L) until constant pH value (4–5) was achieved using a simple decantation. Then, it was possible to centrifuge this solution. During the washing process with deionized water, exfoliation of graphite oxide led to the thickening of solution and formation of a stable colloid of GO.

3.3. Glassy Carbon Electrode Modification with Graphene

GCE was mechanically polished by the 1.0 μm and 0.3 μm alumina suspension (CH Instruments, Austin, TX, USA) on polishing cloth to produce mirror-like surface. Then, the electrode was sonicated for 3 min in distilled water (25 °C) and acetone successively in the Sonorex digital 10 P ultrasonic bath (Bandelin, Berlin, Germany). As prepared, the electrode was rinsed with water solution of GO (0.5 mg· mL^{-1}) and potential +1.0 V was applied on working electrode *vs.* Ag/AgCl/3 M KCl. The deposited film of GO was reduced by performing CV from 0.0 V to −1.5 V in acetate buffer (0.2 M, pH = 5) to produce ERGO.

3.4. Instrumentation

Determination of Zn(II) and $[Fe(CN)_6]^{3-}/[Fe(CN)_6]^{4-}$ by DPV and CV respectively was performed using PGSTAT302N (Metrohm, Herisau, Switzerland) using a three electrode system. A 3 mm diameter GCE (CH Instruments, Austin, TX, USA) was employed as the working electrode. An Ag/AgCl/3 M KCl electrode was used as the reference and platinum wire served as auxiliary. For data processing NOVA 1.8 (Metrohm, Herisau, Switzerland) was employed. Acetate buffer (0.2 mol· L^{-1} CH_3COONa and CH_3COOH, pH = 5) and 0.2 mol· L^{-1} KCl were used as a supporting electrolyte in cases of Zn(II) and $[Fe(CN)_6]^{3-}/[Fe(CN)_6]^{4-}$ determination, respectively.

The parameters of the measurement by DPV were as it follows: initial potential −1.3 V, end potential −1.0 V, deposition time 60 s, time interval 0.03 s, step potential 5 mV, scan rate 50 mV· s^{-1}. Parameters of the measurement by CV were as it follows: initial potential of −0.3 V, upper vertex potential 0.7 V, lower vertex potential −0.3 V, step potential 2.4 mV, scan rate 50 mV· s^{-1}. All measurements were carried out at 25 ± 1 °C.

The value of formal potential of $[Fe(CN)_6]^{3-}$ in 0.1 mol· L^{-1} KCl was 0.25 V and we also adopted it at impedance measurements. Impedance spectra were measured from 0.1 Hz to 10^5 Hz with alternating current (AC) amplitude of 10 mV. PGSTAT302N (Metrohm, Herisau, Switzerland) was used for impedance measurements with the same three electrode system as mentioned previously. Individual elements of equivalent circuit were calculated using NOVA 1.8 (Metrohm, Herisau, Switzerland).

3.5. The Electroactive Surface Determination

In order to determine electroactive area of GCE and to compare it with GCE/ERGO, cyclic voltammograms of 2 mM $[Fe(CN)_6]^{3-}/[Fe(CN)_6]^{4-}$ in 0.1 M KCl were recorded using the aforementioned electrodes. Electroactive surface was calculated according to Randles-Sevcik equation:

$$I_p = 2.69 \cdot 10^5 A \cdot D^{\frac{1}{2}} n^{\frac{3}{2}} \nu^{\frac{1}{2}} C \quad (1)$$

where I_p is anodic current peak (A), A is the electroactive area (cm^2), D is the diffusion coefficient of $[Fe(CN)_6]^{4-}$ in solution (6.1×10^{-6} $cm^2 \cdot s^{-1}$ was taken according to Prathish *et al.* [61]), n is the number of electrons transferred in half-reaction (1 in case of $[Fe(CN)_6]^{4-}$), ν is scan rate (0.05 $V \cdot s^{-1}$ was chosen) and C is $[Fe(CN)_6]^{4-}$ concentration ($mol \cdot L^{-1}$).

3.6. Scanning Electron Microscopy (SEM)

Structure of carbon materials were characterized by SEM. For documentation of the structure, a MIRA3 LMU (Tescan, Brno, Czech Republic) was used. The SEM was fitted with In-Beam SE detector. For automated acquisition of selected areas a TESCAN proprietary software tool called Image Snapper was used. The software enabled automatic acquisition of selected areas with defined resolution. An accelerating voltage of 15 kV and beam currents about 1 nA gave satisfactory results.

3.7. Dynamic Light Scattering (DLS)

Average particle size, size distribution, and particle zetapotential were determined by dynamic light scattering method by Zetasizer Nano-ZS (Malvern Instruments Ltd., Worchestershire, UK) with a scattering angle θ = 173°. Samples were measured in water solution.

3.8. Raman Spectroscopy

All carbonaceous materials, bare GCE, GO, and ERGO deposited on GCE were characterized by Raman spectroscopy. Measurements were performed on a Renishaw *InVia* Reflex Raman microspectrometer equipped by the 514.5 nm line of an argon laser for excitation. A Leica microscope equipped with a standard 50× objective were used. The laser power was set to 1–2 mW at source to obtain an optimal Raman signal and simultaneously avoid any thermal alteration of the sample. Scans of 5–8 s were accumulated 10 times. Resulting spectra were baseline-corrected in GRAMS/AI 9.1.

3.9. Interference Measurement

$Zn(NO_3)_2$ was mixed with KCl, $CaCl_2$, and $MgCl_2$ to obtain a final concentration of 10 $\mu mol \cdot L^{-1}$ Zn(II) and 50 $\mu mol \cdot L^{-1}$ K(I), Ca(II) and Mg(II), respectively, in acetate buffer. Obtained Zn(II) reduction signals were compared with a signal of 10 $\mu mol \cdot L^{-1}$ Zn(II) in acetate buffer.

3.10. Atomic Force Microscopy Measurement

3.10.1. GO Immobilization

GO was immobilized on freshly cleaved mica surfaces grade V-1 (Structure Probe/SPI Supplies, West Chester, PA, USA). The mica surface was first modified by silanization in vapours of *N*-aminopropyldimethylethoxysilane (APDMES) with catalysis of *N*,*N*-diisopropylethylamine (DiPEA, both from Sigma Aldrich). Fifty microliters of GO stock solution 10-times diluted in double distilled water was subsequently transferred onto the modified mica surface and left to incubate for 15 min in a wet chamber under laboratory temperature. Then the surface was carefully washed with double distilled water and left to dry in desiccators for another 30 min (10 Pa vacuum).

3.10.2. Visualization of GO

The AFM images of GO fixed on mica sheets were taken by Bruker Dimension FastScan atomic force microscope (Bruker Nano Surface, Santa Barbara, CA, USA) operated in tapping mode. Basic parameters of the visualization process were as follows: set point value 3.5 nm, iGain 0.8, PGain 5.5, piezo *Z* scale range 500 nm. All images were collected under ambient conditions at 38% relative humidity and 22.5 °C with a scanning raster rate of 2.0 Hz. Silicon nitride triangular cantilevers "FastScan A" (Bruker Nano Surface) characterized by spring constant of 17 N/m and resonant frequency of 1397 kHz equipped with tetrahedral silicon tip with nominal tip radius 5 nm were used for imaging.

Gwyddion software [62] version 2.43 was used for AFM data post processing and for graphical output.

4. Conclusions

Modifications of electrode surface, where redox processes in electrochemical measurements take place, are promising techniques to improve detection sensitivity. Nanomaterials and different carbon materials among others are nowadays frequently used to meet this goal. As it was evident from our measurements, graphene modification of working electrodes is an easy way to enhance electrode properties. GO was electrodeposited from solution on GCE at constant positive potential and subsequently electrochemically reduced using cyclic voltammetry measurement at negative potentials. Proved by Raman and electrochemical impedance spectroscopy, successful modification of the electrode resulted in an increase of electroactive surface area by 9.4% compared with bare GCE. We found that GCE/ERGO possesses three-fold higher sensitivity for zinc ions in comparison with bare GCE. Acceptable selectivity towards interfering ions, such as K(I), Cd(II), Mg(II), and Ca(II) was achieved.

Acknowledgments: Financial support from IGA MENDELU TP-01-15 is greatly acknowledged. Petr Vitek gives thanks for the NPU I grant of Ministry of education, youth and sport (grant number LO1415). Authors would like to thank to Jan Pribyl from CEITEC Masaryk University for the AFM measurements.

Author Contributions: Jiri Kudr prepared the GCE/ERGO, performed the EIS measurements, and drafted the manuscript; Lukas Richtera prepared the GO for electrode modification; Lukas Nejdl performed DPV and CV measurements; Kledi Xhaxhiu carried out the dynamic light scattering measurements; Petr Vitek characterized the material by Raman spectroscopy; Branislav Rutkay-Nedecky was involved in DPV and CV measurements and manuscript correction; David Hynek provided SEM imaging; Pavel Kopel was involved in the design of the study; Vojtech Adam and Rene Kizek coordinated experiments and participated in design of the study.

Conflicts of Interest: The authors declare no conflict of interest.

References

1. Haider, S.; Anis, L.; Batool, Z.; Sajid, I.; Naqvi, F.; Khaliq, S.; Ahmed, S. Short term cadmium administration dose dependently elicits immediate biochemical, neurochemical and neurobehavioral dysfunction in male rats. *Metab. Brain Dis.* **2015**, *30*, 83–92. [CrossRef] [PubMed]
2. Mazzei, V.; Longo, G.; Brundo, M.V.; Sinatra, F.; Copat, C.; Conti, G.O.; Ferrante, M. Bioaccumulation of cadmium and lead and its effects on hepatopancreas morphology in three terrestrial isopod crustacean species. *Ecotoxical. Environ. Saf.* **2014**, *110*, 269–279. [CrossRef] [PubMed]
3. Blazovics, A.; Szentmihalyi, K.; Vinkler, P.; Kovacs, A. Zn overdose may cause disturbance in iron metabolism in inactive inflammatory bowel diseases. *Trace Elem. Electrolytes* **2004**, *21*, 240–247. [CrossRef]
4. Murakami, M.; Hirano, T. Intracellular zinc homeostasis and zinc signaling. *Cancer Sci.* **2008**, *99*, 1515–1522. [CrossRef] [PubMed]
5. Yang, Y.; Jing, X.P.; Zhang, S.P.; Gu, R.X.; Tang, F.X.; Wang, X.L.; Xiong, Y.; Qiu, M.; Sun, X.Y.; Ke, D.; *et al*. High dose zinc supplementation induces hippocampal zinc deficiency and memory impairment with inhibition of BDNF signaling. *PLoS ONE* **2013**, *8*, e55384. [CrossRef] [PubMed]

6. Krizkova, S.; Ryvolova, M.; Hynek, D.; Eckschlager, T.; Hodek, P.; Masarik, M.; Adam, V.; Kizek, R. Immunoextraction of zinc proteins from human plasma using chicken yolk antibodies immobilized onto paramagnetic particles and their electrophoretic analysis. *Electrophoresis* **2012**, *33*, 1824–1832. [CrossRef] [PubMed]
7. Ryvolova, M.; Hynek, D.; Skutkova, H.; Adam, V.; Provaznik, I.; Kizek, R. Structural changes in metallothionein isoforms revealed by capillary electrophoresis and Brdicka reaction. *Electrophoresis* **2012**, *33*, 270–279. [CrossRef] [PubMed]
8. Frederickson, C.J.; Koh, J.Y.; Bush, A.I. The neurobiology of zinc in health and disease. *Nat. Rev. Neurosci.* **2005**, *6*, 449–462. [CrossRef] [PubMed]
9. Masarik, M.; Gumulec, J.; Sztalmachova, M.; Hlavna, M.; Babula, P.; Krizkova, S.; Ryvolova, M.; Jurajda, M.; Sochor, J.; Adam, V.; *et al*. Isolation of metallothionein from cells derived from aggressive form of high-grade prostate carcinoma using paramagnetic antibody-modified microbeads off-line coupled with electrochemical and electrophoretic analysis. *Electrophoresis* **2011**, *32*, 3576–3588. [CrossRef] [PubMed]
10. Krizkova, S.; Ryvolova, M.; Gumulec, J.; Masarik, M.; Adam, V.; Majzlik, P.; Hubalek, J.; Provaznik, I.; Kizek, R. Electrophoretic fingerprint metallothionein analysis as a potential prostate cancer biomarker. *Electrophoresis* **2011**, *32*, 1952–1961. [CrossRef] [PubMed]
11. Krizkova, S.; Ryvolova, M.; Hrabeta, J.; Adam, V.; Stiborova, M.; Eckschlager, T.; Kizek, R. Metallothioneins and zinc in cancer diagnosis and therapy. *Drug Metab. Rev.* **2012**, *44*, 287–301. [CrossRef] [PubMed]
12. Gumulec, J.; Masarik, M.; Krizkova, S.; Adam, V.; Hubalek, J.; Hrabeta, J.; Eckschlager, T.; Stiborova, M.; Kizek, R. Insight to physiology and pathology of zinc(II) ions and their actions in breast and prostate carcinoma. *Curr. Med. Chem.* **2011**, *18*, 5041–5051. [CrossRef] [PubMed]
13. Adam, V.; Petrlova, J.; Wang, J.; Eckschlager, T.; Trnkova, L.; Kizek, R. Zeptomole electrochemical detection of metallothioneins. *PLoS ONE* **2010**, *5*, e11441. [CrossRef] [PubMed]
14. Babula, P.; Masarik, M.; Adam, V.; Eckschlager, T.; Stiborova, M.; Trnkova, L.; Skutkova, H.; Provaznik, I.; Hubalek, J.; Kizek, R. Mammalians' metallothioneins and their properties and functions. *Metallomics* **2012**, *4*, 739–750. [CrossRef] [PubMed]
15. Sobrova, P.; Vyslouzilova, L.; Stepankova, O.; Ryvolova, M.; Anyz, J.; Trnkova, L.; Adam, V.; Hubalek, J.; Kizek, R. Tissue specific electrochemical fingerprinting. *PLoS ONE* **2012**, *7*, e49654. [CrossRef] [PubMed]
16. Bonaventura, P.; Benedetti, G.; Albarede, F.; Miossec, P. Zinc and its role in immunity and inflammation. *Autoimmun. Rev.* **2015**, *14*, 277–285. [CrossRef] [PubMed]
17. Haase, H.; Rink, L. Zinc signals and immune function. *Biofactors* **2014**, *40*, 27–40. [CrossRef] [PubMed]
18. Zalewska, M.; Trefon, J.; Milnerowicz, H. The role of metallothionein interactions with other proteins. *Proteomics* **2014**, *14*, 1343–1356. [CrossRef] [PubMed]
19. Nejdl, L.; Kudr, J.; Cihalova, K.; Chudobova, D.; Zurek, M.; Zalud, L.; Kopecny, L.; Burian, F.; Ruttkay-Nedecky, B.; Krizkova, S.; *et al*. Remote-controlled robotic platform ORPHEUS as a new tool for detection of bacteria in the environment. *Electrophoresis* **2014**, *35*, 2333–2345. [CrossRef] [PubMed]
20. Prasek, J.; Adamek, M.; Hubalek, J.; Adam, V.; Trnkova, L.; Kizek, R. New hydrodynamic electrochemical arrangement for cadmium ions detection using thick-film chemical sensor electrodes. *Sensors* **2006**, *6*, 1498–1512. [CrossRef]
21. Krystofova, O.; Trnkova, L.; Adam, V.; Zehnalek, J.; Hubalek, J.; Babula, P.; Kizek, R. Electrochemical microsensors for the detection of cadmium(II) and lead(II) ions in plants. *Sensors* **2010**, *10*, 5308–5328. [CrossRef] [PubMed]
22. Krizkova, S.; Krystofova, O.; Trnkova, L.; Hubalek, J.; Adam, V.; Beklova, M.; Horna, A.; Havel, L.; Kizek, R. Silver(I) ions ultrasensitive detection at carbon electrodes—Analysis of waters, tobacco cells and fish tissues. *Sensors* **2009**, *9*, 6934–6950. [CrossRef] [PubMed]
23. Nejdl, L.; Ruttkay-Nedecky, B.; Kudr, J.; Kremplova, M.; Cernei, N.; Prasek, J.; Konecna, M.; Hubalek, J.; Zitka, O.; Kynicky, J.; *et al*. Behaviour of zinc complexes and zinc sulphide nanoparticles revealed by using screen printed electrodes and spectrometry. *Sensors* **2013**, *13*, 14417–14437. [CrossRef] [PubMed]
24. Adam, V.; Baloun, J.; Fabrik, I.; Trnkova, L.; Kizek, R. An electrochemical detection of metallothioneins at the zeptomole level in nanolitre volumes. *Sensors* **2008**, *8*, 2293–2305. [CrossRef]
25. Zhang, W.; Ou, J.Z.; Tang, S.Y.; Sivan, V.; Yao, D.D.; Latham, K.; Khoshmanesh, K.; Mitchell, A.; O'Mullane, A.P.; Kalantar-zadeh, K. Liquid metal/metal oxide frameworks. *Adv. Funct. Mater.* **2014**, *24*, 3799–3807. [CrossRef]

26. Cincotto, F.H.; Martinez-Garcia, G.; Yanez-Sedeno, P.; Canevari, T.C.; Machado, S.A.S.; Pingarron, J.M. Electrochemical immunosensor for ethinylestradiol using diazonium salt grafting onto silver nanoparticles-silica-graphene oxide hybrids. *Talanta* **2016**, *147*, 328–334. [CrossRef] [PubMed]
27. Hui, N.; Wang, S.Y.; Xie, H.B.; Xu, S.H.; Niu, S.Y.; Luo, X.L. Nickel nanoparticles modified conducting polymer composite of reduced graphene oxide doped poly(3,4-ethylenedioxythiophene) for enhanced nonenzymatic glucose sensing. *Sens. Actuators B Chem.* **2015**, *221*, 606–613. [CrossRef]
28. Campbell, J.L.; Breedon, M.; Latham, K.; Kalantar-Zadeh, K. Electrowetting of superhydrophobic ZnO nanorods. *Langmuir* **2008**, *24*, 5091–5098. [CrossRef] [PubMed]
29. Li, D.; Kaner, R.B. Materials science—Graphene-based materials. *Science* **2008**, *320*, 1170–1171. [CrossRef] [PubMed]
30. Le, T.X.H.; Bechelany, M.; Lacour, S.; Oturan, N.; Oturan, M.A.; Cretin, M. High removal efficiency of dye pollutants by electron-Fenton process using a graphene based cathode. *Carbon* **2015**, *94*, 1003–1011. [CrossRef]
31. Li, B.; Pan, G.H.; Avent, N.D.; Lowry, R.B.; Madgett, T.E.; Waines, P.L. Graphene electrode modified with electrochemically reduced graphene oxide for label-free DNA detection. *Biosens. Bioelectron.* **2015**, *72*, 313–319. [CrossRef] [PubMed]
32. Le, T.X.H.; Bechelany, M.; Champavert, J.; Cretin, M. A highly active based graphene cathode for the electro-Fenton reaction. *RSC Adv.* **2015**, *5*, 42536–42539. [CrossRef]
33. Kim, Y.R.; Bong, S.; Kang, Y.J.; Yang, Y.; Mahajan, R.K.; Kim, J.S.; Kim, H. Electrochemical detection of dopamine in the presence of ascorbic acid using graphene modified electrodes. *Biosens. Bioelectron.* **2010**, *25*, 2366–2369. [CrossRef] [PubMed]
34. Chen, L.Y.; Tang, Y.H.; Wang, K.; Liu, C.B.; Luo, S.L. Direct electrodeposition of reduced graphene oxide on glassy carbon electrode and its electrochemical application. *Electrochem. Commun.* **2011**, *13*, 133–137. [CrossRef]
35. Cheemalapati, S.; Palanisamy, S.; Chen, S.M. Electrochemical determination of isoniazid at electrochemically reduced graphene oxide modified electrode. *Int. J. Electrochem. Sci.* **2013**, *8*, 3953–3962.
36. Sehat, A.A.; Khodadadi, A.A.; Shemirani, F.; Mortazavi, Y. Fast immobilization of glucose oxidase on graphene oxide for highly sensitive glucose biosensor fabrication. *Int. J. Electrochem. Sci.* **2015**, *10*, 272–286.
37. Ping, J.F.; Wang, Y.X.; Fan, K.; Wu, J.; Ying, Y.B. Direct electrochemical reduction of graphene oxide on ionic liquid doped screen-printed electrode and its electrochemical biosensing application. *Biosens. Bioelectron.* **2011**, *28*, 204–209. [CrossRef] [PubMed]
38. Cui, F.; Zhang, X.L. A method based on electrodeposition of reduced graphene oxide on glassy carbon electrode for sensitive detection of theophylline. *J. Solid State Electrochem.* **2013**, *17*, 167–173. [CrossRef]
39. Li, G.N.; Li, T.T.; Deng, Y.; Cheng, Y.; Shi, F.; Sun, W.; Sun, Z.F. Electrodeposited nanogold decorated graphene modified carbon ionic liquid electrode for the electrochemical myoglobin biosensor. *J. Solid State Electrochem.* **2013**, *17*, 2333–2340. [CrossRef]
40. Wang, F.; Wu, Y.J.; Lu, K.; Ye, B.X. A sensitive voltammetric sensor for taxifolin based on graphene nanosheets with certain orientation modified glassy carbon electrode. *Sens. Actuator B Chem.* **2015**, *208*, 188–194. [CrossRef]
41. Adam, V.; Petrlova, J.; Potesil, D.; Zehnalek, J.; Sures, B.; Trnkova, L.; Jelen, F.; Kizek, R. Study of metallothionein modified electrode surface behavior in the presence of heavy metal ions-biosensor. *Electroanalysis* **2005**, *17*, 1649–1657. [CrossRef]
42. Kudr, J.; Nguyen, V.H.; Gumulec, J.; Nejdl, L.; Blazkova, I.; Ruttkay-Nedecky, B.; Hynek, D.; Kynicky, J.; Adam, V.; Kizek, R. Simultaneous automatic electrochemical detection of zinc, cadmium, copper and lead ions in environmental samples using a thin-film mercury electrode and an artificial neural network. *Sensors* **2015**, *15*, 592–610. [CrossRef] [PubMed]
43. Chao, M.Y.; Ma, X.Y.; Li, X. Graphene-modified electrode for the selective determination of uric acid under coexistence of dopamine and ascorbic acid. *Int. J. Electrochem. Sci.* **2012**, *7*, 2201–2213.
44. Novoselov, K.S.; Fal'ko, V.I.; Colombo, L.; Gellert, P.R.; Schwab, M.G.; Kim, K. A roadmap for graphene. *Nature* **2012**, *490*, 192–200. [CrossRef] [PubMed]
45. Davies, T.J.; Hyde, M.E.; Compton, R.G. Nanotrench arrays reveal insight into graphite electrochemistry. *Angew. Chem. Int. Ed.* **2005**, *44*, 5121–5126. [CrossRef] [PubMed]
46. Zhao, J.P.; Pei, S.F.; Ren, W.C.; Gao, L.B.; Cheng, H.M. Efficient preparation of large-area graphene oxide sheets for transparent conductive films. *ACS Nano* **2010**, *4*, 5245–5252. [CrossRef] [PubMed]
47. Chen, D.; Feng, H.B.; Li, J.H. Graphene oxide: Preparation, functionalization, and electrochemical applications. *Chem. Rev.* **2012**, *112*, 6027–6053. [CrossRef] [PubMed]

48. Castro, S.S.L.; de Oliveira, M.F.; Stradiotto, N.R. Study of the electrochemical behavior of histamine using a Nafion (R)-Copper(II) hexacyanoferrate film-modified electrode. *Int. J. Electrochem. Sci.* **2010**, *5*, 1447–1456.
49. Gilje, S.; Han, S.; Wang, M.; Wang, K.L.; Kaner, R.B. A chemical route to graphene for device applications. *Nano Lett.* **2007**, *7*, 3394–3398. [CrossRef] [PubMed]
50. Ye, W.C.; Zhang, X.J.; Chen, Y.; Du, Y.L.; Zhou, F.; Wang, C.M. Pulsed electrodeposition of reduced graphene oxide on glass carbon electrode as an effective support of electrodeposited Pt microspherical particles: Nucleation studies and the application for methanol electro-oxidation. *Int. J. Electrochem. Sci.* **2013**, *8*, 2122–2139.
51. Zhang, Z.P.; Yan, J.; Jin, H.Z.; Yin, J.G. Tuning the reduction extent of electrochemically reduced graphene oxide electrode film to enhance its detection limit for voltammetric analysis. *Electrochim. Acta* **2014**, *139*, 232–237. [CrossRef]
52. Guo, H.L.; Wang, X.F.; Qian, Q.Y.; Wang, F.B.; Xia, X.H. A green approach to the synthesis of graphene nanosheets. *ACS Nano* **2009**, *3*, 2653–2659. [CrossRef] [PubMed]
53. Stankovich, S.; Dikin, D.A.; Piner, R.D.; Kohlhaas, K.A.; Kleinhammes, A.; Jia, Y.; Wu, Y.; Nguyen, S.T.; Ruoff, R.S. Synthesis of graphene-based nanosheets via chemical reduction of exfoliated graphite oxide. *Carbon* **2007**, *45*, 1558–1565. [CrossRef]
54. Krishnamoorthy, K.; Veerapandian, M.; Mohan, R.; Kim, S.J. Investigation of Raman and photoluminescence studies of reduced graphene oxide sheets. *Appl. Phys. A Mater. Sci. Process.* **2012**, *106*, 501–506. [CrossRef]
55. Eigler, S.; Dotzer, C.; Hirsch, A. Visualization of defect densities in reduced graphene oxide. *Carbon* **2012**, *50*, 3666–3673. [CrossRef]
56. Bi, S.; Zhao, T.T.; Jia, X.Q.; He, P. Magnetic graphene oxide-supported hemin as peroxidase probe for sensitive detection of thiols in extracts of cancer cells. *Biosens. Bioelectron.* **2014**, *57*, 110–116. [CrossRef] [PubMed]
57. Huang, P.; Xu, C.; Lin, J.; Wang, C.; Wang, X.S.; Zhang, C.L.; Zhou, X.J.; Guo, S.W.; Cui, D.X. Folic acid-conjugated graphene oxide loaded with photosensitizers for targeting photodynamic therapy. *Theranostics* **2011**, *1*, 240–250. [CrossRef] [PubMed]
58. Casero, E.; Parra-Alfambra, A.M.; Petit-Dominguez, M.D.; Pariente, F.; Lorenzo, E.; Alonso, C. Differentiation between graphene oxide and reduced graphene by electrochemical impedance spectroscopy (EIS). *Electrochem. Commun.* **2012**, *20*, 63–66. [CrossRef]
59. Nejdl, L.; Kudr, J.; Ruttkay-Nedecky, B.; Heger, Z.; Zima, L.; Zalud, L.; Krizkova, S.; Adam, V.; Vaculovicova, M.; Kizek, R. Remote-controlled robotic platform for electrochemical determination of water contaminated by heavy metal ions. *Int. J. Electrochem. Sci.* **2015**, *10*, 3635–3643.
60. Hummers, W.S.; Offeman, R.E. Preparation of graphitic oxide. *J. Am. Chem. Soc.* **1958**, *80*, 1339–1339. [CrossRef]
61. Prathish, K.P.; Barsan, M.M.; Geng, D.S.; Sun, X.L.; Brett, C.M.A. Chemically modified graphene and nitrogen-doped graphene: Electrochemical characterisation and sensing applications. *Electrochim. Acta* **2013**, *114*, 533–542. [CrossRef]
62. Necas, D.; Klapetek, P. Gwyddion: An open-source software for SPM data analysis. *Cent. Eur. J. Phys.* **2012**, *10*, 181–188.

5.2 Automatizace elektrochemického měření směsi těžkých kovů

5.2.1 Vědecký článek II

Kudr, J.; Nguyen, H. V.; Gumulec, J.; Nejdl, L.; Blažková, I.; Ruttkay-Nedecky, B.; Hynek, D.; Kynicky, J.; Klejdus, B.; Kizek, R.; Adam, V. Simultaneous automatic electrochemical detection of zinc, cadmium, copper and lead ions in environmental samples using a thin-film mercury electrode and an artificial neural network. *Sensors*, 2015, roč. 15. č. 1, s. 592-610. ISSN 1424-8220.

Podíl autora Kudr J.: 65 % textové části práce a 35 % experimentální práce

Rtuť byla díky unikátním fyzikálně-chemickým vlastnostem nejvyužívanějším elektrodovým materiálem pro elektrochemickou analýzu kovů *(Suren a kol., 2007; Beltagi a kol., 2009; Huang a kol., 2016).* V současné době lze sledovat odklon od tohoto toxického materiálu k pevným elektrodám. Přechodem mezi těmito elektrodovými materiály jsou elektrody s tenkým filmem, kdy je materiál výhodných vlastností (např. rtuť) deponován na povrch pevné elektrody z roztoku o nízké koncentraci *(Lange a kol., 1997; Yan, 2008).* Tím se jednak sníží spotřeba toxické chemikálie, naopak výrazně se zvýší mechanická odolnost senzoru.

Monitorování stavu životního prostředí z hlediska znečištění souvidí s analýzou velkých množství vzorků. Automatizace operací se vzorkem je způsob, jak zkrátit čas nutný pro analýzu *(Ruhlig a kol., 2006; Intarakamhang a kol., 2013).* Jedním směrem automatizace elektrochemických měření jsou fluidní zařízení. Druhou možností je použít naprogramovaného polohovacího zařízení, které automaticky přemisťuje detektor mezi roztoky *(Intarakamhang a kol., 2013).*

Environmentální vzorky analyzované voltametrickými senzory poskytují vzhledem k časté přítomnosti složité matrice komplexní signály. Ke zlepšení selektivity elektrochemických senzorů se nabízí modifikace elektrod *(Adam a kol., 2005).* Druhou možností je pokročilé vyhodnocování signálů např. s využitím neuronové sítě. Bylo prokázáno, že vyhodnocení signálů na základě neuronových sítí je schopno vyhodnotit překrývající se píky a minimalizovat chyby při analýze interferujících těžkých kovů *(Wilson a kol., 2012; Wang a kol., 2014).*

Tato publikace popisuje použití automatického robotického ramene s tříelektrodovým systémem zahrnujícím uhlíkovou elektrodu pokrytou tenkou vrstvou

rtuťi jako nástroj pro simultání detekci iontů Cd(II), Pb(II), Zn(II) a Cu(II) v 24-polohové mikrotitrační destičce. Tato metoda byla použita na široké spektrum vzorků – samotné ionty ve vodném roztoku, mineralizované horniny, játra a mozek kuřecích embryí a lidskou plazmu s přídavkem iontů. Vzhledem k interferenci Zn(II) iontů při detekci Cu(II) a *vice versa* byla pro správné vyhodnocení výsledků použita neuronová síť *(Panteli a kol., 2009)*.

Sensors **2015**, *15*, 592-610; doi:10.3390/s150100592

OPEN ACCESS

sensors

ISSN 1424-8220

www.mdpi.com/journal/sensors

Article

Simultaneous Automatic Electrochemical Detection of Zinc, Cadmium, Copper and Lead Ions in Environmental Samples Using a Thin-Film Mercury Electrode and an Artificial Neural Network

Jiri Kudr [1,2], Hoai Viet Nguyen [1,2], Jaromir Gumulec [2], Lukas Nejdl [1,2], Iva Blazkova [1,2], Branislav Ruttkay-Nedecky [1,2], David Hynek [1,2], Jindrich Kynicky [3], Vojtech Adam [1,2] and Rene Kizek [1,2,*]

[1] Department of Chemistry and Biochemistry, Faculty of Agronomy, Mendel University in Brno, Zemedelska 1, CZ-613 00 Brno, Czech Republic; E-Mails: george.kudr@centrum.cz (J.K.); nguyenviethoai@hus.edu.vn (H.V.N.); lukasnejdl@gmail.com (L.N.); iva.blazkova@seznam.cz (I.B.); brano.ruttkay@seznam.cz (B.R.-N.); d.hynek@email.cz (D.H.); vojtech.adam@mendelu.cz (V.A.)

[2] Central European Institute of Technology, Brno University of Technology, Technicka 3058/10, CZ-616 00 Brno, Czech Republic; E-Mail: j.gumulec@gmail.com

[3] Karel Englis College, Sujanovo nam. 356/1, Brno CZ-602 00, Czech Republic; E-Mail: jindrak@email.cz

* Author to whom correspondence should be addressed; E-Mail: kizek@sci.muni.cz; Tel.: +420-5-4513-3350; Fax: +420-5-4521-2044.

Academic Editor: Libuše Trnková

Received: 23 October 2014 / Accepted: 11 December 2014 / Published: 30 December 2014

Abstract: In this study a device for automatic electrochemical analysis was designed. A three electrodes detection system was attached to a positioning device, which enabled us to move the electrode system from one well to another of a microtitre plate. Disposable carbon tip electrodes were used for Cd(II), Cu(II) and Pb(II) ion quantification, while Zn(II) did not give signal in this electrode configuration. In order to detect all mentioned heavy metals simultaneously, thin-film mercury electrodes (TFME) were fabricated by electrodeposition of mercury on the surface of carbon tips. In comparison with bare electrodes the TMFEs had lower detection limits and better sensitivity. In addition to pure aqueous heavy metal solutions, the assay was also performed on mineralized rock samples, artificial blood plasma samples and samples of chicken embryo organs treated with cadmium. An artificial

neural network was created to evaluate the concentrations of the mentioned heavy metals correctly in mixture samples and an excellent fit was observed (R^2 = 0.9933).

Keywords: automation; electrochemical detection; artificial neuronal network; robotic device; metal ions; environmental analysis

1. Introduction

Metals mainly occur in the Earth's crust, however, urbanization and industrialization lead to their releasing into the biosphere, where they have become part of the air, soil, water and biota [1–3]. As a consequence of the metabolic similarity of toxic metals with non-toxic elements, they bind to the sulfhydryl groups of proteins causing negative effects, including mutagenesis [4,5]. Some metals, such as copper (Cu) and zinc (Zn), are essential micronutrients, although they are also toxic in higher concentrations. On the other hand, other metals as cadmium, lead and mercury can damage numerous biochemical pathways, even at low concentration. Due to this fact and the fact that the one-half of the World's population lives now in urbanized areas, metals continue to present a serious issue for public health [6].

Several methods have been developed to detect trace amounts of heavy metals. Conventional heavy metal detection methods include atomic absorption spectrometry (AAS), inductively coupled plasma mass spectrometry (ICP-MS) or inductively coupled plasma optical emission spectroscopy (ICP-OES) [7–9]. However, they do not meet the demands for portable, easy-to-use, quick and cheap analysis. In this field, electrochemical analysis of heavy metals is an alternative to conventional methods and provides a few attractive properties, in addition to a high degree of sensitivity [10–12]. Electrochemistry offers unique application possibilities in the field of heavy metal analysis due to the compact, simple and portable instrumentation, electrode miniaturisation and easy electrode modification [13–15]. Electrochemistry was also proved to be suitable method to analyse heavy metal contents in biological and environmental samples like body fluids, tissues or rocks [16–18]. *Gallus domesticus* hen and its embryos are broadly used as a model organism [19], where the liver represents the organ of initial Cd accumulation and recent study shows that high levels of Cd can be presented also in brain [20].

Among other electrode materials suitable for these purposes, mercury and carbon have been used the most frequently. In spite of the fact that mercury has unique physico-chemical properties and are widely used in trace heavy metal analysis, neither the dropping mercury electrode nor the hanging mercury drop electrode are suitable for automated analysis methods because of their mechanical instability (the mercury drop is easily dislodged). High consumption of metallic mercury in these cases also does not correspond with current trends in heavy metal analysis, since much attention has been focused on the use of more eco-friendly solid materials like carbon and chemical modification of its surface to improve sensitivity [21,22]. Thin-film mercury electrodes (TFMEs) are able to resolve these limitations [23]. They decrease mercury consumption, enable electrode manipulation and preserve the key mercury electrode properties like a wide cathodic potential window. In this case, mercury is electrodeposited from a solution with low mercury concentration on the surface of a solid electrode, which serves as a mechanical support and enables easier manipulation. In the case of heavy metals

analysis, anodic stripping voltammetry (ASV) exhibits remarkable sensitivity [24,25]. A more negative potential than the standard redox potential of the heavy metal ions is used to preconcentrate them on the mercury surface. A subsequent linear increase of the potential stripps them back into the solution represented by increased current at a specific potential. Pulse techniques like differential pulse or square wave voltammetry suppressing the background current were successfully combined with ASV to lower the limits of detection [26]. The only alternatives to mercury for stripping techniques are Bi-modified electrodes, however, their limitations are low anodic potential [27].

Moreover, there are also demands on high throughput analysis in the field of environmental monitoring. The long-term monitoring of heavy metal pollution is the only way to meet national and international legislative measures implemented to decrease the anthropogenic pressure on the environment. The automatic handling of samples shortens time-consuming analysis, enables one to perform multiple analyses without continuous operator attention and is also consistent with current trends in analytical chemistry. Automatic flow-based voltammetric detections of heavy metals were proven to have good accuracy and reproducibility and succeeded in reducing analysis times [28,29]. Use of titre plates for automatic analysis enables one to avoid the need for complex microfluidics and electrochemical flow-cells [30]. The potential of the electrochemical robotic system for automated quantification of Ni^{2+} ion released from corroding nickel-titanium alloys was recently demonstrated [31]. The electrochemical robotic system was designed for automatically performing adsorptive stripping voltammetry in individual compartments of 24-well microtiter plates. Displacing the preloaded plates in the *x* and *y* directions, locating an electrode assembly into the solution in a selected well, conditioning the working electrode surface, and finally executing adsorptive stripping voltammetry are key actions that had to be automated for the sequential determination of Ni^{2+} concentrations in sample solutions in the different wells of the microtiter plate [31]. In another work, automatic ascorbic acid voltammetry was performed in 24-well microtiter plates. The automated assay used a movable assembly of a pencil rod working electrode, an Ag/AgCl reference electrode and a Pt counter electrode using differential pulse anodic stripping voltammetry (DPASV) for concentration-dependent current generation [30].

Data obtained by voltammetric sensors from multicomponent environments produces complex signals. To solve this problem, several electrode surface functionalizations were developed to improve the electrode selectivity [12,32]. Alternatively, a multivariate signal processing tool can be used. Among others, artificial neural network (ANN) software-based techniques were developed to analyse complex data sets, and they excel in modelling and calibrating complex analytical signals [33]. There are many types of ANNs that vary mostly in the architecture or in the way they learn. It was proved that using ANN data analysis interference between target heavy metals ions and the effect of sample matrix can be counterbalanced and this also enables evaluate overlapped voltammograms [34–36]. This paper describes a novel application of the electrochemical robotic device that provides a convenient electrochemical 24-well microtiter plate assay for the automated quantification of multiple heavy metal samples containing Cd(II), Cu(II), Pb(II) and Zn(II) in pure aqueous model solutions, mineralized rocks, chicken embryo liver and brain and human plasma samples spiked with metals. The choice of the carbon tip electrode modified with mercury film as a working electrode, signal stability and reproducibility of known metal solution levels are reported. Moreover, artificial neural networks software-based techniques developed to analyse the complex data sets were also used in this

study [37–40], because it was found that the presence of copper and zinc in samples may lead to the formation of intermetallic compounds on the mercury film and this affects analysis of both elements [41]. The correct zinc concentration in the presence of copper and *vice versa* can be, however, determined by ANN processing [42,43].

2. Experimental Section

2.1. Chemicals

ACS purity (*i.e.*, chemicals meet the specifications of the American Chemical Society) sodium acetate trihydrate, acetic acid, $Hg(NO_3)_2$, water and other chemicals were purchased from Sigma-Aldrich (St. Louis, MO, USA) unless noted otherwise.

2.2. Instrumentation

An electrochemical robotic device (Sensolytics, Bochum, Germany) performed the automatic positioning of electrodes. Carbon tips (1 mL) were purchased from Tosoh Corporation (Tokyo, Japan) and were used as working electrodes after modification. Ag/AgCl/3M KCl as reference electrode (Metrohm, Herisau, Switzerland) and platinum wire (Metrohm, Herisau, Switzerland) as counter electrode were used. Electrochemical signals were recorded using a PGSTAT 101 potentiostat (Metrohm) and the NOVA 1.8 software (Metrohm) was employed for data evaluation. The electrode holder was printed by a PROFI 3D MARKER printing system (3Dfactories, Straznice, Czech Republic). Samples were measured in flat bottomed TPP tissue culture 24-well plates (Sigma-Aldrich).

2.2.1. Electrochemical Robotic Device

Electrodes were placed into the holder fabricated using the 3D printer. The electrochemical robotic device (Sensolytics) positioning the electrodes included three motorized units ST4118M1804 (Nanotec, Munich, Germany) and positioning system (OWIS, Staufen, Germany). The first unit was rigidly connected to the vertical frame of the electrochemical robot. The electrode holder was attached to it and this enabled us to perform precise vertical (z) positioning of the electrode holder (up and down). The microtiter plate was placed on a horizontally (x/y) positioned board. Coordinates and the precise time of the holder and plate motion were controlled by the ELChemRo software (Sensolytics). We used the advanced settings of NOVA to prepare a script enabling us to set up the sequence of differential pulse voltammetric measurements with adjustable time intervals between individual measurements.

2.2.2. Working Electrode

Automatic electrochemical detection was performed using a three electrodes system. A pipette tip made from polymeric material and coated by graphite enabled us to use it as a working electrode due to its conductive resin. Based on the mentioned facts, these electrodes can be used for detection of substances undergoing reduction and/or oxidation on the surface of such electrodes. In this study, detection of Cd(II), Pb(II), and Cu(II) was carried out by a bare working electrode. Carbon tip

electrode modified with mercury film was employed for detection of Zn(II) ions (no reduction was observed using the bare electrode) and for detection of metal mixtures.

2.2.3. Modification of Carbon Tips

The carbon tips were inserted into 0.01 M $Hg(NO_3)_2$ solution, prepared by the dissolution of 0.086 g mecury(II) nitrate in 25 mL of acidified (5% HNO_3, *v*/*v*) Milli-Q water. A −0.9 V potential was applied to the electrodes for 60 s, which resulted in the formation of a thin-film of mercury on the surface of the working electrode [44].

2.2.4. Method

We used differential pulse voltammetry for all measurements and measurement parameters were as follows: deposition potential −1.6 V, initial potential −1.6 V, end potential 0.1 V, step potential 0.005 (scan rate 50 $mV \cdot s^{-1}$), modulation amplitude 0.1 V, modulation time 0.004 s, interval time 0.1 s. All experiments were carried out at room temperature. Acetate buffer (0.2 M CH_3COOH and 0.2 M CH_3COONa) was used as the supporting electrolyte. The limit of detection was calculated as LOD = (3.3 × SD)/S, where *SD* = standard deviation of the response and *S* = slope of the calibration curve.

2.3. Statistical Analysis

First, simple regression was performed for each metal peak value–metal concentration pair. The following functions were tested: linear, logarithmic and exponential. The correlation of each regression was tested and then the optimal function for each metal was used. Based on these results, a nonlinear estimation using a user-determined regression function was created and the goodness of fit of the model was tested again. In the third step, an automated neuronal network was created. The following methods were tested: radial basis function and multilayer perceptron. The following activation functions were used for hidden and output neurons: identity, logistic, tan, and exponential. The number of hidden neurons was limited to 20 and was optimized during after the primary learning cycle. Weight decay was used to prevent overfitting using the following setting: 0.0001–0.001 (min–max) for both hidden and output layer. Data (645 samples in total) was randomly divided into a training group (70%), testing group (15%) and verification group (15%). A Broyden-Fletcher-Goldfarb-Shanno (BFGS) training algorithm was used. Unless noted otherwise, *p*-level 0.05 was considered significant. The software Statistica 12 (StatSoft, Tulsa, OK, USA) was used for analysis.

2.4. Sample Preparations

Fertilized egg of ISA brown hen (Integra, a.s., Zabcice, Czech Republic) was incubated in a RCom 50 MAX incubator (Gyeongnam, Changwon, Korea) at 37.5 °C and humidity control (45% rH). After 16 days of the incubation the embryo vitality was checked and then a solution of $Cd(NO_3)_2 \bullet 4H_2O$ (4.5 $mg \cdot mL^{-1}$ in ACS water) was applied (500 μL) by injection using a Chirana T. injecta device (maximal volume: 1 mL, size: 0.33 × 12 mm) through a small hole in the egg shell into the air cell on the chorioallantoic membrane. After that the hole was covered by a plaster. The chicken embryo was incubated till the next day and then the brain and liver was extracted. From the chicken embryo, 10 mg

of tissue (brain, liver) was equally removed, weighed and added to 500 μL of a mixture consisting of 350 μL 65% nitric acid (*v*/*v*) and 150 μL 30% hydrogen peroxide (*v*/*v*). The solutions were subjected to digestion in a microwave reaction system Anton Paar (Anton Paar GmbH, Graz, Austria) using the following conditions: time 40 min (10 min power 50, 30 min power 100 and 10 min power 0), 60 °C, Rotor-64MG5-16. Mineralized solutions (200 μL) were transferred to a 96-well Deepwell plate 96 evaporation plate (Eppendorf, Hamburg, Germany) and evaporated. For evaporation of samples an Ultravap 96 nitrogen blow-down evaporator with spiral needles (Porvair Sciences, Leatherhead, UK) was used. Finally, the solutions were dissolved in 0.2 M acetate buffer (200 μL, pH 5.0) and were diluted 10-fold with the same acetate buffer prior to analysis. Rock samples (10 mg) were prepared in the same manner as chicken samples. For mineralization the following conditions were used: time 110 min (100 min power-100 and 10 min power-0), 100 °C, Rotor-64MG5-16 and samples were diluted 1000-fold. The plasma samples with random heavy metal concentrations (0–6 $\mu g \cdot mL^{-1}$) were prepared as follows: to 10 μL of human plasma specific amount of metals ion stock solutions were added. Mineralized and evaporated samples were diluted to the original volume, then they were diluted 10-fold with acetate buffer (0.2 M, pH 5.0) and used for ANN evaluation.

2.5. Determination of Cadmium by Atomic Absorption Spectrometry

Cadmium was also determined on an Agilent Technologies 80 Z atomic absorption spectrometer (Agilent, Santa Clara, CA, USA) with electrothermal atomization. The spectrometer was operated at the 228.8 nm resonance line with a spectral bandwidth of 0.5 nm. The sample volume (20 μL) was injected into the graphite tube. The flow of argon inert gas was 300 $mL \cdot min^{-1}$. Zeeman background correction was used with a field strength of 0.8 Tesla. The absorption signal was evaluated in peak height mode with seven point smoothing.

2.6. X-Ray Fluorescence Analysis (XRF)

The rock samples were measured on a Spectro Xepos apparatus (Spectro Analytical Instruments, Kleve, Germany) using an anode X-ray tube with Pd anode working at a voltage of 44.69 kV and a current of 0.55 mA. Signals were detected with Barkla scatter aluminium oxide for 300 s. For excitation three secondary targets (Mo, Al_2O_3 and high-ordered pyrolithic graphite crystal) were used. The excitation geometry was 90°. The crushed samples were measured through the PE bottle side wall 20 mm above the bottom. The Spectro Xepos software and TurboQuant method were applied for data analysis.

3. Results and Discussion

3.1. Automatic System for Heavy Metal Detection

Automation or semi-automation of analysis reduces time-consuming manual operations and costs. We used an electrochemical detection method (differential pulse voltammetry) with all its known advantages (easy-to-use, good sensitivity, cheap instrumentation) for automatic simultaneous detection of cadmium, zinc, copper and lead ions in various types of real samples. The whole system consisted of detection and positioning parts. Detection was performed using a classical three-electrode system (working, reference and auxiliary electrode). Electrodes were fitted to a movable holder and positioned

using an electrochemical robotic device schematically depicted in Figure 1A and photographed in Figure 1B. Scripts were created to precisely control the timing of electrochemical measurements and movements of the electrode holder with the electrodes. At first, we used a disposable carbon tip as a working electrode, nevertheless this electrode was not able to detect zinc ions. Hence, we fabricated thin-film mercury electrodes (TFMEs) by electrodeposition of mercury (II) ions from solution onto the carbon surface of electrodes (Figure 1C) and its sensitivity was compared with a disposable carbon tip electrode. Due to the fact that we focused on automation, the electrochemical robotic system was used to perform plating automatically and the automated pipetting device was used to prepare different heavy metal concentrations for calibration curve measurement and mixing samples with buffer. It is well known that oxidation/reduction of some metals on the surface of TFME can be affected by the presence of other metals by forming of intermetallic compounds [45]. Therefore, we used statistical methods (linear regression, multiregression model and finally a neural network) to reduce measurement errors and evaluate the detected concentrations of target heavy metals [42,43]. Complex analytical signals of mixture samples obtained by arrays of potentiometric electrodes or by voltammetric systems (not those based on specific receptors) mostly require application of chemometric tools [46,47]. We decided to use an artificial neural network for these purposes since it is an effective instrument to analyse these types of multivariate signals and is able to recognise specific patterns in data sets. It can be considered as one of the most important tools in this kind of analysis and is not only broadly used in evaluation of redox, but also optical signals [48,49]. Gutés *et al.* emphasized the need for voltammetric signal pre-processing before ANN modelling in order to reduce ANN training time and create a more accurate network [50]. A wavelet transform was previously used to extract the most relevant information from voltammograms [51]. We used individual ions peak heights as the ANN input data, because Cd(II) and Zn(II) ions in samples tended to affect the peak heights of each other instead of overlapping (peaks of Cd(II), Cu(II) and Pb(II) and Zn(II) are well separated) [41]. The neural network reliability was tested using 22 mineralized blood plasma samples with random heavy metal concentrations (0.0–6 $\mu g \cdot mL^{-1}$) and 20 randomly selected heavy metal mixtures (0.01–8 $\mu g \cdot mL^{-1}$). The automatic electrochemical robotic device and neural network were also used for evaluation of heavy metal content in rocks and chicken embryo tissues exposed to cadmium(II) ions. Addition of buffer to mineralized rock samples, chicken brain and liver and artificial plasma samples was performed by an automated pipetting device (Figure 1D). The way samples were treated is shown in Figure 1E.

3.2. Optimization of the Automatic System for Heavy Metal Detection

The automatic system for heavy metal detection was optimized for determination of the four metal ions (Cd(II), Cu(II), Pb(II) and Zn(II)). The optimization was focused on monitoring of the electrochemical response of the individual elements depending on the increasing accumulation time within the range from 0 to 300 s. Longer accumulation times were not investigated because of our desire to shorten the analysis to a maximum of 5 min. Thereafter, calibration curves were determined and limits of detection (LODs) were calculated. For values resulting from the calibration curve double-sided reliability bands were created, what is the part of the plane limited by straight lines, where the observed calibration points fall within with 95% probability [52]. Further, the sensitivity of the WE before and after modification with mercury film was compared by plotting the slopes of the calibration curves in

the column graph. Due to the fact that lower limits of detection were attained by the mercury-modified carbon tip, calibration curves were determined within a linear range of concentrations (0.6, 1.25, 2.5 and 10 $\mu g \cdot mL^{-1}$). This linear range is common for both unmodified and modified WE, and therefore all the slopes could be compared. Finally, the automatic system was verified by comparing the electrochemical results with atomic absorption spectrometry (AAS) data.

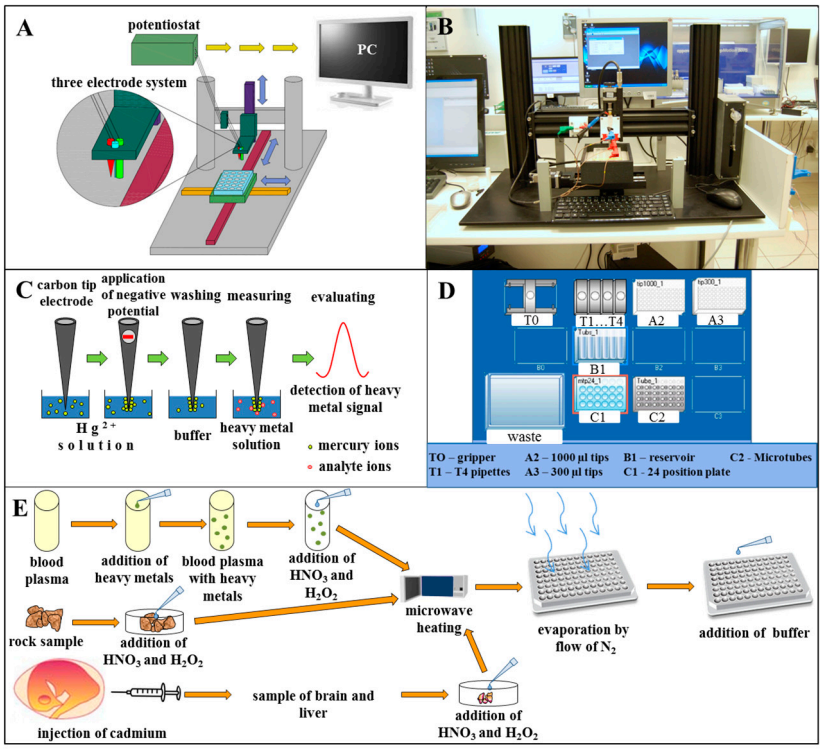

Figure 1. (**A**) Scheme and (**B**) photo of robotic device with electrochemical three-electrode detection system; (**C**) Individual steps of thin mercury film preparation on the surface of carbon tip electrode; (**D**) Scheme of automated pipetting system epMotion 5075 desktop, which was used to add buffer to mineralized samples of rocks; (**E**) The samples of blood plasma, stone and chicken embryo organs preparation prior to heavy metals detection.

At first, the electrochemical responses of the studied metals on the unmodified carbon tip WE were studied. Cd(II), Cu(II), and Pb(II) ion electrochemical signals were measured, but Zn(II) ions did not give any signal at the bare electrode. For this reason, the electrochemical optimization was performed only for the detected ions. The best electrochemical response of metal ions was achieved when using an accumulation time of 300 s. This accumulation was applied for all measurements. For the analysis of Cd(II) ions the electrochemical signal gave its maximum at a potential of −0.69 V and LOD was estimated as 0.1 $\mu g \cdot mL^{-1}$ (Figure 2A). For the analysis of Pb(II) ions the peak maximum was detected at a potential of −0.51 V and LOD = 0.2 $\mu g \cdot mL^{-1}$ was estimated (Figure 2B). For the analysis of Cu(II) ions the peak maximum was detected at a potential of −0.29 V and LOD = 0.1 $\mu g \cdot mL^{-1}$ was found (Figure 2C).

The next step was to estimate the LOD of electrochemical determination of metal ions when using mercury film modified carbon tip as WE. It was found that due to the modification of WE with mercury film the electrochemical signal of Zn(II) was recorded. The signal of Zn(II) ions showed a maximum at a potential of −1.07 V and LOD was estimated as 0.6 $\mu g \cdot mL^{-1}$ (Figure 2D). For the

analysis of Cd(II) ions the peak maximum was detected at a potential of −0.7 V and LOD as 0.06 μg·mL^{-1}, which is 21 times less than when measured with the unmodified WE, was found (Figure 2E). For the analysis of Pb(II) ions the peak maximum was detected at a potential of −0.54 V and LOD as 0.03 μg·mL^{-1}, which is five times less than when measured with the unmodified WE (Figure 2F). For the analysis of Cu(II) ions the peak maximum was detected at a potential of −0.29 V and LOD as 0.02 μg·mL^{-1}, which is five times less than when measured with the unmodified WE (Figure 2G).

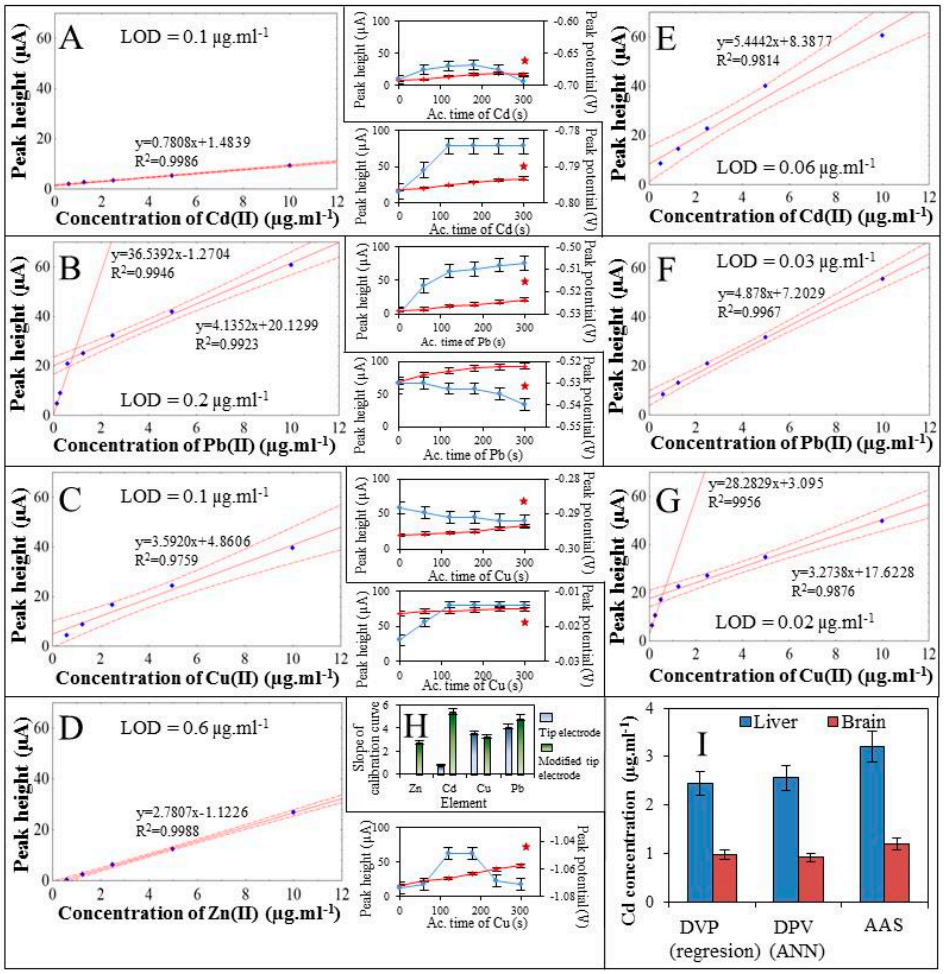

Figure 2. Calibration curves of (**A**) cadmium(II) (0.6–10 μg·mL^{-1}); (**B**) lead(II) (0.16–10 μg·mL^{-1}) and (**C**) copper(II) ions (0.6–10 μg·mL^{-1}) measured using carbon tip electrode. Calibration curves of (**D**) zinc(II); (**E**) cadmium(II); (**F**) lead(II) (all 0.6–10 μg·mL^{-1}) and (**G**) copper(II) ions (0.16–10 μg·mL^{-1}) measured using thin film mercury electrode. (**H**) The graph of optimized time of accumulation (0–300 s) (**red line**) is connected with appropriate calibration curve and shows the changes of peak potential (**blue line**). Comparison of slopes of calibration curves measured using carbon tip electrode (blue bar) and thin film mercury electrode (**green bar**); (**I**) The amount of cadmium ions detected (by AAS, DPV and ANN) in brain and liver of chicken embryo (16 day) exposed to cadmium (II) ions (0.5 mg) by injection to air cell.

Further, for the use of the slopes of the calibration curves (Figures 2A–2G), sensitivities of the unmodified and modified WE for analysis of individual metal ions were compared (Figure 2H). It was found that modification of WE with mercury film had the greatest effect on detection of Zn(II) and Cd(II) ions. Detection of Zn(II) ions was possible only due to the WE modification. For detection of Cd(II) ions the sensitivity was increased 7-fold. On the other hand an increase in sensitivity was not demonstrated for the detection of Cu(II) and Pb(II) ions within a 5% error bar. Finally, brain and liver samples of the real-chicken embryo treated with Cd(II) ions were analysed. For these samples Cd(II) ions were determined. Comparison of the results measured by both DPASV (without stirring since the samples were placed in a titre plate) and AAS coincided within 10% error, as shown in Figure 2I.

3.3. Rock Analysis

Four different rocks were analysed electrochemically using TFME and the obtained results were compared with the X-ray fluorescence analysis (XRF) ones. Two rock samples consisting predominantly of the minerals sphalerite (ZnS) and pyrite (FeS_2) were obtained in Madan in Croatia, and further galenite (PbS), and a mineral association of arsenopyrite (FeAsS) with pyrite and löllingite ($FeAs_2$) were obtained in Panasqueira in Portugal (Figure 3).

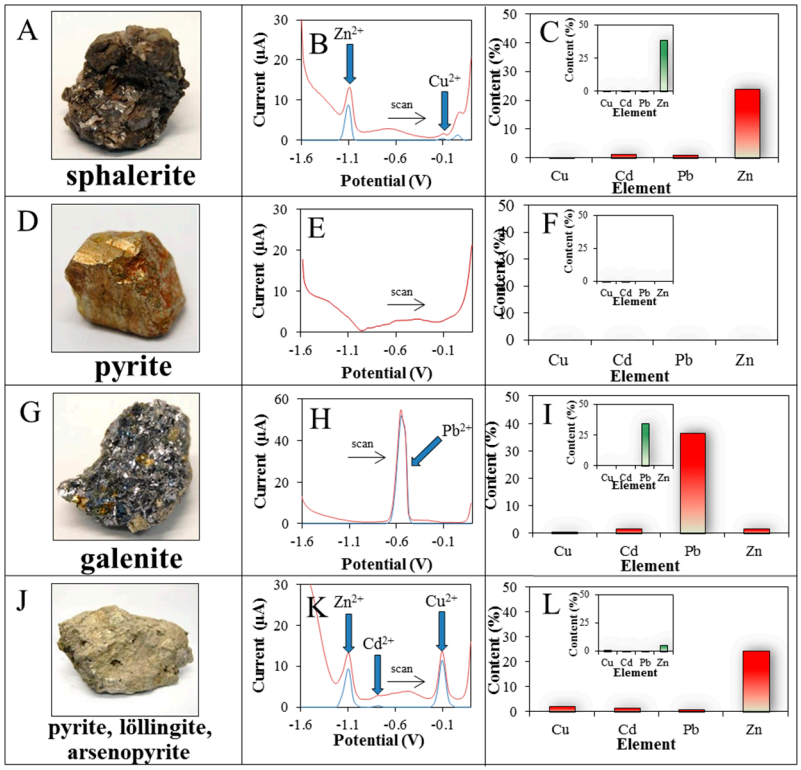

Figure 3. (**A**) Photo, original (red) and (**B**) baselined voltammogram (blue); (**C**) the element content in the rock calculated by neuronal network from voltammograms and element content measured using XRF (inserts) of rocks containing (**D**–**F**) sphalerite and pyrite; (**G**–**I**) galenite; and (**J**–**L**) arsenopyrite, pyrite, and löllingite.

For the first sample of analysed rock, which was composed predominantly of the mineral sphalerite (Figure 3A), the highest content of Zn(II) (24%) and traces of Cd(II) (1.5%), Pb(II) (1.0%) and

Cu(II) (0.3%) were determined electrochemically and evaluated by ANN (Figure 3B). Similar results were obtained by XRF analysis (Figure 3C). In addition the elements Fe (10%) and S (12% of detected elements) were further detected (not shown).

For the second sample of analysed rock composed mainly of pyrite (Figure 3D), none of the analysed metals was determined electrochemically (Figure 3E and F). Using XRF analysis the elements Fe (47%), S (30%), Mg (1.22%) and Cu (1.35%) were detected (not shown), which corresponds essentially to the elemental composition of pyrite.

For the third sample of analysed rock, which was composed mainly of the mineral galenite (Figure 3G), the highest content of Pb(II) (37%) was determined electrochemically and this corresponded to the composition of this mineral (Figure 3H). Further, Si (8.5%) and minor amounts of Zn (1.8%), Cd (1.6%), and Cu (0.6%) ions were also determined (Figure 3I). Similar results were obtained by XRF analysis (Figure 3H and I).

For the fourth sample of analysed rocks, consisting primarily of the minerals arsenopyrite, pyrite and löllingite (Figure 3J) the largest amount of Zn(II) (25%) and in smaller amounts Cu(II) (2.0%), Cd(II) (1.4%) and Pb(II) (1.0%) were determined electrochemically (Figure 3K and L). Similar results were obtained using XRF analysis, but the elements Fe (32%), As (>18.29%), S (8%) and Sn (>2.875%) were also found (not shown).

3.4. Identification of Regression Function

A total of 645 mixture combinations of Zn(II), Cd(II), Cu(II), and Pb(II) standard concentrations within the range 0–10 μg/mL were prepared (appropriate amounts of the corresponding nitrates were dissolved in water). First, simple linear regression was performed to reveal the associations between peak values and concentrations using the following equation

$$y_{Zn} = a_{Zn} + b_{Zn}x_{Zn} \quad (1)$$

where y indicates the concentration of each metal, x indicates the peak value for each metal and a and b are constants for each metal (Table 1). The goodness of fit of the model was as low as $R^2 = 0.87$ for copper. Therefore, other functions were tested. Highest R squared ($R^2 = 0.92$) was observed for the exponential function. Based on these results a multiple regression model using the following combined linear/exponential regression function was used:

$$y_{Zn} = b_{Zn}x_{Zn} + b_{Cd}x_{Cd} + b_{Pb}x_{Pb} + b_{Cu}e^{(a_{Cu}x_{Cu})} \quad (2)$$

where y indicates the concentration of each metal, x indicates the peak value for each metal, b is a constant (different for each metal), and e is the Euler constant (Table 1). The performance of this model was still weak for the calculation of copper concentration ($R^2 = 0.87$). Therefore, instead of fitting another higher order or other complex functions, regression using automated neural networks was performed.

Table 1. Parameter estimates for simple regression and nonlinear estimation used in the optimization steps of the model. Parameters *a* and *b* for each metals are those used in the Equations (1) and (2). * indicate parameter is significant for calculation and therefore was used for the model.

Model	Parameter	Parameter Estimates (95% Confidence Interval)			
		Zn(II)	Cd(II)	Pb(II)	Cu(II)
Simple linear regression					
	a	* −0.56	* −0.62	* −0.52	* −1.47
	b	* 0.72	* 0.67	* 0.18	* 0.20
	model R^2	0.98	0.98	0.98	0.87
Nonlinear estimation					
	b_{Zn}	* 0.72 (0.70–0.73)	* 0.12 (0.11–0.13)	* −0.02 (−0.03–−0.01)	* 0.03 (0.00–0.05)
	b_{Cd}	* 0.15 (0.13–0.16)	* 0.74 (0.73–0.76)	* −0.02 (−0.04–−0.01)	0.00 (−0.02–0.03)
	b_{Pb}	0.00 (0.00–0.01)	0.00 (0.00–0.00)	* 0.19 (0.18–0.19)	0.00 (−0.01–0.00)
	b_{Cu}	* −2.61 (−2.94–−2.28)	* −2.94 (−3.19–−2.7)	0.02 (−0.27–0.31)	* 0.46 (0.33–0.59)
	a_{Cu}	0.00 (0.00–0.00)	0.00 (0.00–0.00)	0.00 (−0.31–0.31)	* 0.06 (0.05–0.06)
	model R^2	0.98	0.98	0.98	0.87

3.5. Building a Neural Network Model

Both the radial basic function and multilayer perceptron approaches were used for training with the following activation functions, which were used for hidden and output neurons: identity, logistic, tan, and exponential. In the initial training set total 10,000 training cycles were performed with weight decay and the five best were retained. The number of hidden neurons was limited to 20. After the initial training, the highest observed network performance was observed in a network with 19 hidden neurons, and exponential and logistic hidden and output activation functions, respectively. The goodness of fit of the model was 0.9996 for both test and validation (Table 2).

Table 2. Results of the neuronal network learning optimization.

Training	Network Performance (R^2)			Network Error			Training	Activation Function	
Network Name	Training	Test	Validation	Training	Test	Validation	Cycle	Hidden	Output
Initial training									
MLP 4-17-4	0.9993	0.9993	0.9993	0.0362	0.0347	0.0367	210	Logistic	Exponential
MLP 4-19-4	0.9996	0.9996	0.9996	0.0261	0.0222	0.0291	699	Exponential	Logistic
MLP 4-19-4	0.9995	0.9995	0.9994	0.0292	0.0261	0.0320	232	Exponential	Logistic
MLP 4-14-4	0.9992	0.9990	0.9993	0.0 394	0.0461	0.0367	589	Tan	Identity
MLP 4-15-4	0.9993	0.9993	0.9993	0.0348	0.0333	0.0362	722	Tan	Exponential
Final network for further deployment									
MLP 4-8-4	0.9941	0.9924	0.9933	0.3744	0.3641	0.4275	1237	Exponential	Logistic

Based on this network, the number of hidden neurons was optimized using a custom network design with enabled training stopping conditions. The number of hidden neurons was optimized in a range 0–30. The activation function for hidden and output layer was exponential and logistic with weight decay activated. When the number of hidden neurons increased from 1 to 8, the validation performance of the network increased significantly from 0.36 to 0.995. Subsequent increase in number of hidden

neurons did not enhance the performance of the network significantly, therefore, eight hidden neurons was used as a model for final analyses (Table 2 and Figure 4A). Decreasing evaluation errors of training and testing samples were plotted against number of training cycles (Figure 4B).

Network name includes training method, and number of input-hidden-output neurons. MLP, multilayer perceptron. Training cycle indicates cycle number when the network was created (in the case of initial training) or the training was stopped by stopping conditions (in the case of final network design).

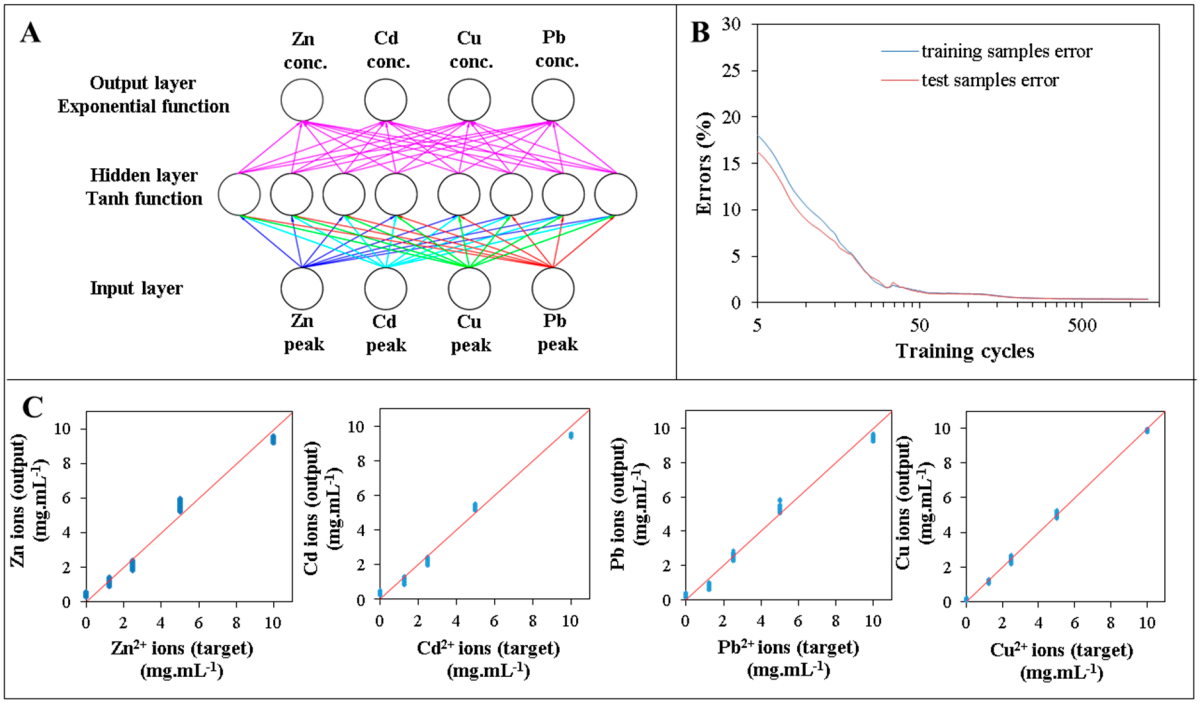

Figure 4. (**A**) Design of the final custom neuronal network model with four input, eight hidden and four output neurons. Note input layer neurons use identity functions; (**B**) Training of the network with the employment of the stopping conditions to prevent overfitting. Network was trained in the 1237th cycle, when the test error started to increase; (**C**) Testing the goodness of the fit of the target (known concentration) and output (neuronal network result).

3.6. Measurements of a Blood Plasma and Unknown Samples

Consequently, a model was employed for the measurement of the 22 blood plasma samples, to which defined heavy metal concentrations were added (Table 3). The goodness of fit for the neuronal network was 0.995, 0.998, 0.993 and 9.999 for Zn, Cd, Pb, and Cu ions, respectively. Consequently, the model was tested on validation sample and goodness of fit was tested again. The R^2 was as follows: 0.996, 0.998, 0.997, and 0.999 for Zn(II), Cd(II), Pb(II) and Cu(II), respectively. The results of these validations indicate significant improvement over using a general regression model with user defined function (compare the goodness of fit in Tables 1 and 2).

Table 3. Employment of the network on the measurement of the artificial blood plasma samples and set of validation samples.

Group No. of Sample	Concentration Targets				Neuronal Network Outputs			
	Zn(II) (μg·mL^{-1})	Cd(II) (μg·mL^{-1})	Pb(II) (μg·mL^{-1})	Cu(II) (μg·mL^{-1})	Zn(II) (μg·mL^{-1})	Cd(II) (μg·mL^{-1})	Pb(II) (μg·mL^{-1})	Cu(II) (μg·mL^{-1})
blood plasma samples measurement								
1	6.00	6.00	6.00	6.00	6.61	6.48	6.00	6.25
2	6.00	6.00	6.00	4.00	6.58	6.49	6.01	3.94
3	6.00	6.00	6.00	2.00	6.54	6.49	6.03	2.25
4	6.00	6.00	6.00	1.00	6.49	6.49	6.05	1.11
5	6.00	6.00	6.00	0.00	6.49	6.50	6.04	0.17
6	6.00	6.00	4.00	6.00	6.59	6.47	4.51	6.24
7	6.00	6.00	2.00	6.00	6.54	6.44	2.20	6.24
8	6.00	6.00	1.00	6.00	6.48	6.37	0.63	6.22
9	6.00	6.00	0.00	6.00	6.42	6.29	0.20	6.21
10	6.00	4.00	6.00	6.00	6.75	4.18	5.97	6.23
11	6.00	2.00	6.00	6.00	6.81	1.99	5.93	6.21
12	6.00	1.00	6.00	6.00	6.87	0.95	5.92	6.18
13	6.00	0.00	6.00	6.00	6.88	0.32	5.93	6.14
14	4.00	6.00	6.00	6.00	5.27	6.50	5.95	6.24
15	2.00	6.00	6.00	6.00	1.88	6.45	5.80	6.22
16	1.00	6.00	6.00	6.00	1.00	6.49	5.74	6.20
17	0.00	6.00	6.00	6.00	0.37	6.47	5.66	6.18
18	0.00	0.00	0.00	4.00	0.49	0.50	0.38	3.81
19	0.00	0.00	4.00	0.00	0.49	0.47	4.77	0.10
20	0.00	4.00	0.00	0.00	0.45	4.18	0.31	0.09
21	4.00	0.00	0.00	0.00	5.08	0.38	0.27	0.08
22	0.00	0.00	4.00	4.00	0.46	0.46	4.64	3.91
R^2 of the network				0.995	0.998	0.993	0.999	
Validation samples								
1	8.00	8.00	8.00	8.00	8.42	8.59	8.53	9.02
2	8.00	8.00	8.00	4.00	8.38	8.60	8.52	3.82
3	8.00	8.00	8.00	2.00	8.35	8.61	8.53	2.11
4	8.00	8.00	8.00	1.00	8.31	8.61	8.54	1.04
5	8.00	8.00	8.00	0.00	8.27	8.61	8.54	0.19
6	8.00	8.00	4.00	8.00	8.35	8.56	4.65	8.94
7	8.00	8.00	2.00	8.00	8.30	8.52	2.22	8.89
8	8.00	8.00	1.00	8.00	8.25	8.46	0.60	8.83
9	8.00	8.00	0.00	8.00	8.19	8.39	0.18	8.78
10	8.00	4.00	8.00	8.00	8.19	3.85	8.40	8.94
11	8.00	2.00	8.00	8.00	8.11	1.87	8.35	8.90
12	8.00	1.00	8.00	8.00	8.04	0.89	8.32	8.86
13	8.00	0.00	8.00	8.00	8.44	0.28	8.31	8.80
14	4.00	8.00	8.00	8.00	5.37	8.48	8.36	9.00
15	2.00	8.00	8.00	8.00	1.83	8.32	8.17	8.96
16	1.00	8.00	8.00	8.00	0.96	8.27	8.09	8.95
17	0.00	8.00	8.00	8.00	0.34	8.18	7.96	8.92
18	0.00	0.00	8.00	8.00	0.45	0.42	7.99	8.66

Table 3. *Cont.*

Group No. of Sample	Concentration Targets				Neuronal Network Outputs			
	Zn(II) (μg·mL^{-1})	Cd(II) (μg·mL^{-1})	Pb(II) (μg·mL^{-1})	Cu(II) (μg·mL^{-1})	Zn(II) (μg·mL^{-1})	Cd(II) (μg·mL^{-1})	Pb(II) (μg·mL^{-1})	Cu(II) (μg·mL^{-1})
19	0.00	4.00	4.00	0.00	0.39	3.94	4.39	0.14
20	2.00	2.00	0.00	0.00	2.04	2.10	0.27	0.09
R^2 of the network					0.996	0.998	0.997	0.999

Concentration targets are concentrations added to blood plasma samples and prepared as custom concentrations for validation samples. Goodness of fit was tested separately for both sample sets. Correlations analysis of input heavy metals concentrations and output results were performed (Figure 4C).

4. Conclusions

In this work electrochemical system for automatic detection of heavy metals was developed. Using this system rock samples, blood plasma samples and organs of chicken embryos were successfully analysed. The accuracy of the system was verified by atomic absorption spectrometer (AAS) and X-Ray fluorescence (XRF). Furthermore, the different mathematical models were used to calculate the mutual interactions between the individual electrochemical signals in the multi element analysis. The performance of simple linear regression and multiple regression models (combination of linear and exponential regression) for determining copper concentrations correctly was weak. Based on this fact, an artificial neural network model was built and used for the correction of results in mixtures of metal samples. Perfect fit of this model was found ($R^2 = 0.9933$).

Acknowledgments

Financial support from the project NANOLABSYS CZ.1.07/2.3.00/20.0148 is highly acknowledged. These results were presented at the 14th Workshop of Physical Chemists and Electrochemists.

Author Contributions

J. K. was responsible for electrochemical measurements automation and performed XRF analysis. H. V. N. optimized conditions and carried out electrochemical measurements. J. G. built statistical models and statistically evaluated the heavy metal concentrations. I. B. prepared the samples for analysis and helped with the interpretation of results. L. N. and B. R. N. participated in preparation of the manuscript and in design of the study. D. H. coordinated experiments. J. K. provided rock samples and participated on the analysis of these samples. V.A. and R.K. designed the study and drafted manuscript.

Conflicts of Interest

The authors declare no conflict of interest.

References

1. Kleckerova, A.; Docekalova, H. Dandelion Plants as a Biomonitor of Urban Area Contamination by Heavy Metals. *Int. J. Environ. Res.* **2014**, *8*, 157–164.
2. Vega, F.A.; Weng, L.P. Speciation of heavy metals in River Rhine. *Water Res.* **2013**, *47*, 363–372.
3. Basha, S.; Jhala, J.; Thorat, R.; Goel, S.; Trivedi, R.; Shah, K.; Menon, G.; Gaur, P.; Mody, K.H.; Jha, B. Assessment of heavy metal content in suspended particulate matter of coastal industrial town, Mithapur, Gujarat, India. *Atmos. Res.* **2010**, *97*, 257–265.
4. Chen, C.; Xie, Q.J.; Wang, L.H.; Qin, C.; Xie, F.Y.; Yao, S.Z.; Chen, J.H. Experimental Platform to Study Heavy Metal Ion-Enzyme Interactions and Amperometric Inhibitive Assay of Ag^+ Based on Solution State and Immobilized Glucose Oxidase. *Anal. Chem.* **2011**, *83*, 2660–2666.
5. Witkiewicz-Kucharczyk, A.; Bal, W. Damage of zinc fingers in DNA repair proteins, a novel molecular mechanism in carcinogenesis. *Toxicol. Lett.* **2006**, *162*, 29–42.
6. Nations, U. Data on Urban and Rural Populations. In *World Urbanization Prospects*; United Nations, Department of Economic and Social Affairs: New York, NY, USA, 2011; Volume 2014.
7. Kenawy, I.M.M.; Hafez, M.A.H.; Akl, M.A.; Lashein, R.R. Determination by AAS of some trace heavy metal ions in some natural and biological samples after their preconcentration using newly chemically modified chloromethylated polystyrene-PAN ion-exchanger. *Anal. Sci.* **2000**, *16*, 493–500.
8. Karami, H.; Mousavi, M.F.; Yamini, Y.; Shamsipur, M. On-line preconcentration and simultaneous determination of heavy metal ions by inductively coupled plasma-atomic emission spectrometry. *Anal. Chim. Acta* **2004**, *509*, 89–94.
9. Faraji, M.; Yamini, Y.; Saleh, A.; Rezaee, M.; Ghambarian, M.; Hassani, R. A nanoparticle-based solid-phase extraction procedure followed by flow injection inductively coupled plasma-optical emission spectrometry to determine some heavy metal ions in water samples. *Anal. Chim. Acta* **2010**, *659*, 172–177.
10. Hynek, D.; Prasek, J.; Businova, P.; Zak, J.; Drbohlavova, J.; Chomoucka, J.; Kynicky, J.; Konecna, M.; Brtnicky, M.; Hubalek, J.; *et al.* Automated voltammetric determination of lead(II) ions using sensor array. *Int. J. Electrochem. Sci.* **2013**, *8*, 4441–4456.
11. Petrlova, J.; Potesil, D.; Zehnalek, J.; Sures, B.; Adam, V.; Trnkova, L.; Kizek, R. Cisplatin electrochemical biosensor. *Electrochim. Acta* **2006**, *51*, 5169–5173.
12. Adam, V.; Petrlova, J.; Potesil, D.; Zehnalek, J.; Sures, B.; Trnkova, L.; Jelen, F.; Kizek, R. Study of metallothionein modified electrode surface behaviour in the presence of heavy metal ions-biosensor. *Electroanalysis* **2005**, *17*, 1649–1657.
13. Nejdl, L.; Kudr, J.; Cihalova, K.; Chudobova, D.; Zurek, M.; Zalud, L.; Kopecny, L.; Burian, F.; Ruttkay-Nedecky, B.; Krizkova, S.; *et al.* Remote-controlled robotic platform Orpheus as a new tool for detection of bacteria in the environment. *Electrophoresis* **2014**, in press.
14. Nejdl, L.; Ruttkay-Nedecky, B.; Kudr, J.; Kremplova, M.; Cernei, N.; Prasek, J.; Konecna, M.; Hubalek, J.; Zitka, O.; Kynicky, J.; *et al.* Behaviour of Zinc Complexes and Zinc Sulphide Nanoparticles Revealed by Using Screen Printed Electrodes and Spectrometry. *Sensors* **2013**, *13*, 14417–14437.

15. Locatelli, C.; Melucci, D. Voltammetric method for ultra-trace determination of total mercury and toxic metals in vegetables. Comparison with spectroscopy. *Cent. Eur. J. Chem.* **2013**, *11*, 790–800.
16. Anastasiadou, Z.D.; Jannakoudakis, P.D.; Girousi, S.T. Square wave anodic stripping voltammetry determination of eco-toxic metals in samples of biological and environmental importance. *Cent. Eur. J. Chem.* **2010**, *8*, 999–1008.
17. Kensova, R.; Hynek, D.; Kynicky, J.; Konecna, M.; Eckschlager, T.; Adam, V.; Hubalek, J.; Kizek, R. Determination of Metal Ions in the Plasma of Children with Tumour Diseases by Differential Pulse Voltammetry. *Int. J. Electrochem. Sci.* **2014**, *9*, 4675–4691.
18. Fialova, D.; Kremplova, M.; Hynek, D.; Konecna, M.; Kaiser, J.; Malina, R.; Kynicky, J.; Krystofova, O.; Kizek, R.; Adam, V. Sosedka Pegmatite Metal Ions Composition Determined by Voltammetry. *Int. J. Electrochem. Sci.* **2013**, *8*, 7853–7867.
19. Bahr, J., The Chicken as a Model Organism. In *Sourcebook of Models for Biomedical Research*; Conn, P.M., Ed.; Humana Press: New York, NY, USA, 2008; pp. 161–167.
20. Shagirtha, K.; Muthumani, M.; Prabu, S.M. Melatonin abrogates cadmium induced oxidative stress related neurotoxicity in rats. *Eur. Rev. Med. Pharmacol. Sci.* **2011**, *15*, 1039–1050.
21. Xu, H.; Zeng, L.P.; Xing, S.J.; Xian, Y.Z.; Shi, G.Y. Ultrasensitive Voltammetric Detection of Trace Lead(II) and Cadmium(II) Using MWCNTs-Nafion/Bismuth Composite Electrodes. *Electroanalysis* **2008**, *20*, 2655–2662.
22. Rico, M.A. G.; Olivares-Marin, M.; Gil, E.P. Modification of carbon screen-printed electrodes by adsorption of chemically synthesized Bi nanoparticles for the voltammetric stripping detection of Zn(II), Cd(II) and Pb(II). *Talanta* **2009**, *80*, 631–635.
23. Rocha, L.S.; Pinheiro, J.P.; Carapuca, H.M. Evaluation of nanometer thick mercury film electrodes for stripping chronopotentiometry. *J. Electroanal. Chem.* **2007**, *610*, 37–45.
24. Huang, H.; Chen, T.; Liu, X.Y.; Ma, H.Y. Ultrasensitive and simultaneous detection of heavy metal ions based on three-dimensional graphene-carbon nanotubes hybrid electrode materials. *Anal. Chim. Acta* **2014**, *852*, 45–54.
25. Zhao, D.L.; Guo, X.F.; Wang, T.T.; Alvarez, N.; Shanov, V.N.; Heineman, W.R. Simultaneous Detection of Heavy Metals by Anodic Stripping Voltammetry Using Carbon Nanotube Thread. *Electroanalysis* **2014**, *26*, 488–496.
26. Pujol, L.; Evrard, D.; Groenen-Serrano, K.; Freyssinier, M.; Ruffien-Cizsak, A.; Gros, P. Electrochemical sensors and devices for heavy metals assay in water: The French groups' contribution. *Front. Chem.* **2014**, *2*, 19.
27. Pauliukaite, R.; Hocevar, S.B.; Ogorevc, B.; Wang, J. Characterization and applications of a bismuth bulk electrode. *Electroanalysis* **2004**, *16*, 719–723.
28. Suteerapataranon, S.; Jakmunee, J.; Vaneesorn, Y.; Grudpan, K. Exploiting flow injection and sequential injection anodic stripping voltammetric systems for simultaneous determination of some metals. *Talanta* **2002**, *58*, 1235–1242.
29. Ninwong, B.; Chuanuwatanakul, S.; Chailapakul, O.; Dungchai, W.; Motomizu, S. On-line preconcentration and determination of lead and cadmium by sequential injection/anodic stripping voltammetry. *Talanta* **2012**, *96*, 75–81.

30. Intarakamhang, S.; Schuhmann, W.; Schulte, A. Robotic heavy metal anodic stripping voltammetry: Ease and efficacy for trace lead and cadmium electroanalysis. *J. Solid State Electrochem.* **2013**, *17*, 1535–1542.
31. Ruhlig, D.; Schulte, A.; Schuhmann, W. An electrochemical robotic system for routine cathodic adsorptive stripping analysis of Ni^{2+} ion release from corroding NiTi shape memory alloys. *Electroanalysis* **2006**, *18*, 53–58.
32. Adam, V.; Zehnalek, J.; Petrlova, J.; Potesil, D.; Sures, B.; Trnkova, L.; Jelen, F.; Vitecek, J.; Kizek, R. Phytochelatin modified electrode surface as a sensitive heavy-metal ion biosensor. *Sensors* **2005**, *5*, 70–84.
33. Despagne, F.; Massart, D.L. Neural networks in multivariate calibration. *Analyst* **1998**, *123*, 157R–178R.
34. Wilson, D.; Gutierrez, J.M.; Alegret, S.; del Valle, M. Simultaneous Determination of Zn(II), Cu(II), Cd(II) and Pb(II) in Soil Samples Employing an Array of Potentiometric Sensors and an Artificial Neural Network Model. *Electroanalysis* **2012**, *24*, 2249–2256.
35. Wang, L.; Yang, D.; Chen, Z.L.; Lesniewski, P.J.; Naidu, R. Application of neural networks with novel independent component analysis methodologies for the simultaneous determination of cadmium, copper, and lead using an ISE array. *J. Chemom.* **2014**, *28*, 491–498.
36. Gutierrez, J.M.; Moreno-Baron, L.; Cespedes, F.; Munoz, R.; del Valle, M. Resolution of Heavy Metal Mixtures from Highly Overlapped ASV Voltammograms Employing a Wavelet Neural Network. *Electroanalysis* **2009**, *21*, 445–451.
37. Motalleb, G. Artificial Neural Network Analysis in Preclinical Breast Cancer. *Cell J.* **2014**, *15*, 324–331.
38. Khajeh, M.; Golzary, A.R. Synthesis of zinc oxide nanoparticles-chitosan for extraction of methyl orange from water samples: Cuckoo optimization algorithm-artificial neural network. *Spectrochim. Acta Part A Mol. Biomol. Spectrosc.* **2014**, *131*, 189–194.
39. Garkani-Nejad, Z.; Rashidi-Nodeh, H. Comparison of conventional artificial neural network and wavelet neural network in modeling the half-wave potential of aldehydes and ketones. *Electrochim. Acta* **2010**, *55*, 2597–2605.
40. Efendioglu, H.S.; Yildirim, T.; Fidanboylu, K. Prediction of Force Measurements of a Microbend Sensor Based on an Artificial Neural Network. *Sensors* **2009**, *9*, 7167–7176.
41. Panteli, V.S.; Kanellopoulou, D.G.; Gartaganis, S.P.; Koutsoukos, P.G. Application of Anodic Stripping Voltammetry for Zinc, Copper, and Cadmium Quantification in the Aqueous Humor: Implications of Pseudoexfoliation Syndrome. *Biol. Trace Elem. Res.* **2009**, *132*, 9–18.
42. Chan, H.; Butler, A.; Falck, D.M.; Freund, M.S. Artificial neural network processing of stripping analysis responses for identifying and quantifying heavy metals in the presence of intermetallic compound formation. *Anal. Chem.* **1997**, *69*, 2373–2378.
43. Chow, C.W. K.; Davey, D.E.; Mulcahy, D.E. A neural network approach to zinc and copper interferences in potentiometric stripping analysis. *J. Intell. Mater. Syst. Struct.* **1997**, *8*, 177–183.
44. Farias, P.A. M.; Castro, A.A.; Wagener, A.D. R.; Miguel, E.M. Adenine determination in the presence of copper in diluted alkaline electrolyte by adsorptive stripping voltammetry at the mercury film electrode. *Electroanalysis* **2008**, *20*, 1445–1453.

45. Alves, G.M.S.; Magalhaes, J.M.C.S.; Soares, H.M.V.M. Voltammetric Quantification of Zn and Cu, Together with Hg and Pb, Based on a Gold Microwire Electrode, in a Wider Spectrum of Surface Waters. *Electroanalysis* **2013**, *25*, 493–502.
46. Gallardo, J.; Alegret, S.; Munoz, R.; De-Roman, M.; Leija, L.; Hernandez, P.R.; del Valle, M. An electronic tongue using potentiometric all-solid-state PVC-membrane sensors for the simultaneous quantification of ammonium and potassium ions in water. *Anal. Bioanal. Chem.* **2003**, *377*, 248–256.
47. Laguarda-Miro, N.; Ferreira, F.W.; Garcia-Breijo, E.; Ibanez-Civera, J.; Gil-Sanchez, L.; Garrigues-Baixauli, J. Glyphosacte detection by voltammetric techniques. A comparison between statistical methods and an artificial neural network. *Sens. Actuator B Chem.* **2012**, *171*, 528–536.
48. Ariza-Avidad, M.; Cuellar, M.P.; Salinas-Castillo, A.; Pegalajar, M.C.; Vukovic, J.; Capitan-Vallvey, L.F. Feasibility of the use of disposable optical tongue based on neural networks for heavy metal identification and determination. *Anal. Chim. Acta* **2013**, *783*, 56–64.
49. Ariza-Avidad, M.; Salinas-Castillo, A.; Cuellar, M.P.; Agudo-Acemel, M.; Pegalajar, M.C.; Capitan-Vallvey, L.F. Printed Disposable Colorimetric Array for Metal Ion Discrimination. *Anal. Chem.* **2014**, *86*, 8634–8641.
50. Gutes, A.; Cespedes, F.; Cartas, R.; Alegret, S.; del Valle, M.; Gutierrez, J.M.; Munoz, R. Multivariate calibration model from overlapping voltammetric signals employing wavelet neural networks. *Chemom. Intell. Lab. Syst.* **2006**, *83*, 169–179.
51. Gutierrez, J.M.; Gutes, A.; Cespedes, F.; del Valle, M.; Munoz, R. Wavelet neural networks to resolve the overlapping signal in the voltammetric determination of phenolic compounds. *Talanta* **2008**, *76*, 373–381.
52. Dordevic, S.; Stancin, S.; Meglic, A.; Milutinovic, V.; Tomazic, S. MC Sensor—A Novel Method for Measurement of Muscle Tension. *Sensors* **2011**, *11*, 9411–9425.

5.3 Detekce nukleové kyseliny

5.3.1 Vědecký článek IV

Kudr, J.; Nejdl, L.; Skalickova, S.; Ruttkay-Nedecky, B.; Rodrigo, M. A. M.; Dostalova, S.; Jimenez, A. M. J.; Chudobova, D.; Cihalova, K.; Konecna, M.; Kopel, P.; Kynicky, J.; Adam, V.; Kizek, R. Plasmid HIV *p24* gene detection on mercury film electrode using osmium labelling. *International Journal of Electrochemical Science*, 2014, roč. 9. č. 7, s. 3409-3418. ISSN 1452-3981.

Podíl autora Kudr J.: 65 % textové části práce a 75 % experimentální práce

Patogenní bakterie mohou negativně působit na lidské zdraví *(Gorham a kol., 2016)*. Z tohoto důvodu je screening vod z hlediska bakteriální kontaminace významnou součástí environmentálního monitoringu *(Grossi a kol., 2013)*. Standardní metody identifikace a kvantifikace bakterií založené na kultivaci jsou obvykle časově náročné a i přes značný pokrok v posledních letech trvají 18 – 24 h *(Maheux a kol., 2008)*. Další jejich nevýhodou je nemožnost detekce pomalu rostoucích nebo nekultivovatelných bakterií, jež jsou ve vodním prostředí běžné *(Roszak a kol., 1987)*. Během poslední dekády bylo navrženo mnoho metod vyhýbajících se kultivaci. Tyto metody jsou založeny na imunoanalýzách, aktivitách enzymů nebo na detekci nukleové kyseliny *(Farnleitner a kol., 2001; LaGier a kol., 2005; Zhu a kol., 2011)*. Zejména metody založené na identifikaci DNA jsou atraktivní vzhledem k jejich rychlosti, citlivosti a selektivitě. Standardní metody identifikace/kvantifikace DNA jako je PCR nejsou pro environmentální analýzy vhodné – vyžadují drahou instrumentaci a reagencie, jsou náchylné k inhibici amplifikace složkami vzorku a amplifikací z odumřelých buněk mohou vést k nadhodnocení kontaminace *(Lantz a kol., 2000; Loge a kol., 2002)*. Elektrochemie naopak oplývá dostatečnou sensitivitou a nízkou cenou instrumentace. Existuje několik elektrochemických přístupů k detekci DNA. Lze využít buď samotné elektroaktivity nukleových kyselin nebo použít specifické molekuly nebo nanočástice jako redoxní značky *(Drummond a kol., 2003)*.

V uvedené publikaci je představena metoda, která umožňuje ze vzorku izolovat cílovou DNA pomocí magnetických částic a následně detekovat pomocí redoxní značky. Sonda komplementární k cílové DNA byla pomocí afinity thiolové skupiny a zlata imobilizována na magnetickou částici modifikovanou zlatými nanočásticemi. Vzorek cílové DNA byl inkubován s magnetickým konstruktem a následně proběhla

magnetická separace. Pro detekci jsme využili sondu komplementární s cílové DNA modifikovanou elektroaktivním komplexem oxidu osmičelého s bipyridinem, který je schopen se vázat na pyrimidinové báze (především tymin) jednovláknové DNA. Po hybridizaci s detekovatelnou sondou proběhla opět magnetická separace.

Ačkoliv byla tato metoda použita k detekci genu *p24* viru HIV, je možno ji aplikovat na jakoukoliv DNA, tedy i např. bakteriální, pouhou změnou sekvence imobilizační a značkou modifikované sondy.

Int. J. Electrochem. Sci., 9 **(2014)** 3409 - 3418

International Journal of ELECTROCHEMICAL SCIENCE
www.electrochemsci.org

Plasmid HIV *p24* Gene Detection on Mercury Film Electrode using Osmium Labelling

Jiri Kudr[1], *Lukas Nejdl*[1,2], *Sylvie Skalickova*[1,2], *Branislav Ruttkay-Nedecky*[1,2], *Miguel Angel Merlos Rodrigo*[1,2], *Simona Dostalova*[1,2], *Ana Maria Jimenez Jinemez*[1,2], *Dagmar Chudobova*[1,2], *Kristyna Cihalova*[1,2], *Marie Konecna*[1,2], *Pavel Kope1*[1,2], *Jindrich Kynicky*[3], *Vojtech Adam*[1,2*], *Rene Kizek*[1,2]

[1] Department of Chemistry and Biochemistry, Mendel University in Brno, Zemedelska 1, CZ-613 00 Brno, Czech Republic, European Union
[2] Central European Institute of Technology, Brno University of Technology, Technicka 3058/10, CZ-616 00 Brno, Czech Republic, European Union
[3]Karel Englis College, Sujanovo nam. 356/1, CZ-602 00, Brno, Czech Republic, European Union
[*]E-mail: ilabo@seznam.cz

Received: 18 January 2014 / *Accepted:* 17 March 2014 / *Published:* 14 April 2014

The early detection of HIV-positive individuals before infecting healthy individuals is the basic principle to fight against AIDS. Although a lot of methods has been developed to detect HIV, electrochemistry is a promising tool thanks to its high sensitivity, low cost, ease of use and mostly no antibody-based detection. The aim of our study was to perform the electrochemical detection of HIV *p24* gene for capsid protein. We utilized the ability of osmium tetroxide bipyridyl (OsO_4(bpy)) to create the complex with thymine and used it to label the oligonucleotide complementary to the *p24*. We also used the thiolated oligonucleotide probe to anchor the labelled *p24* gene to the magnetic particle, which served to isolate the construct from the solution of non-anchored molecules. The detection of *p24* gene was performed on the mercury film glassy-carbon electrode by the adsorptive transfer method using difference pulse voltammetry. The best mercury film on the surface of glassy carbon working electrode was received using KNO_3 as supporting electrolyte and by the set of potential -0.9 V for 300 s. We showed that also the femtomole amount of *p24* gene within linear plasmide can be absorbed to the electrode surface and detected.

Keywords: Electrochemistry; Glassy carbon electrode; Gel electrophoresis; *p24* gene

1. INTRODUCTION

According to the Joint United Nations Programme on HIV and AIDS, more than 35 million persons live with the human immunodeficiency virus (HIV), which causes immune deficiency disease

(AIDS). It was estimated that since the start of the epidemics about 36 million people have died of the AIDS-related illnesses. Although the number of newly infected people is decreasing and was about 2.3 million in 2012, it still remains serious issue. A lot of methods has been developed for detection of HIV including enzyme immunoassay [1], enzyme-linked immunosorbent assay (ELISA) [2] and western blot test [3]. These antibody-based methods applied on blood samples are time-consuming, have long detection "window phase" (3 weeks to 6 months) and requires highly-trained workers, however, these are still gold standard for HIV detection. Polymerase chain reaction (PCR) based techniques have been also utilised for HIV detection and exhibited high sensitivity, but these are limited in distinguishing of single base mutations [4].

Electrochemical sensing is able to resolve these limitations and offers simple, portable, sensitive, inexpensive detection and it is useful in the detection of early HIV infection because of direct molecular recognition of HIV and its components [5]. Electrochemical detection of HIV protease, an enzyme essential to the assembly and maturation of HIV, based on the enzymatic cleavage of protease substrate from the gold electrode was suggested by Esseghaier et al. [6]. HIV reverse transcriptase and HIV p24, which appears at the earlier stage of HIV infection than antibodies, became another target molecule used for HIV detection [5,7,8]. There is also interest in the detection of short DNA sequences related to the HIV [9-11].

In this study, we designed a simple method for electrochemical detection of *p24* gene. Osmium tetroxide complex with 2,2′-bipyridine (OsO_4(bpy)) has been often used as a versatile chemical DNA probe [12-14]. We utilized the ability of OsO_4(bpy) to react with pyrimidine moieties (mostly thymine) in single stranded DNA and created the electroactive oligonucleotide probe complementary to the *p24* sequence [15]. The DNA-OsO_4(bpy) adduct produces a catalytic signal (about -1.2 V) at mercury electrode and other smaller signals at less negative potentials [12]. Moreover, we used the oligonucleotide probe complementary to the 5' end of *p24* sequence bounded to a gold modified magnetic particle (AuMPs) via thiol group, which enables us to separate the anchored single stranded gene from the solution of non-targeted DNA and other molecules. The created construct was adsorbed at mercury surface of the mercury film (MFE) on glassy carbon electrode (GCE) [16]. The signal of OsO_4(bpy) reporter molecule was analysed by differential pulse voltammetry (DPV).

2. EXPERIMENTAL

2.1. Reagents and chemicals

OsO_4, 2,2´-bipyridyl, $Fe(NO_3)_3 \cdot 9H_2O$, $NaBH_4$, polyvinylpyrrolidone, $HAuCl_4$, trisodium citrate, Trizma base, HCl, Tris base, acetic acid, EDTA (Ethylenediaminetetraacetic acid), sodium acetate trihydrate, acetic acid, $Hg(NO_3)_2$, HNO_3, KNO_3, water and other chemicals were purchased from Sigma-Aldrich (USA) in ACS purity. To pipette volumes down to microlitres, pipettes used were purchased from Eppendorf Research (Eppendorf, Hamburg, Germany). Deionised water underwent demineralization by reverse osmosis using the instruments Aqua Osmotic 02 (Aqua Osmotic, Tisnov,

Czech Republic) and then it was subsequently purified using Millipore RG (Millipore Corp., USA, 18 MΩ) – MiliQ water.

2.2. Modification of oligonucleotide with OsO_4(bpy) (ODN-OsO_4(bpy))

The oligonucleotide complementary to the 3´ end of *p24* sequence (5´-TTTTTTTTATTGCTAAGCCAAAACCC-3´) was modified by OsO_4(bpy) as described in [17]. Briefly, OsO_4 (0.25 g) in water (25 ml) and 2,2´-bipyridyl (0.156 g) were shaken until both compounds were dissolved and volume was adjusted to 50 ml. Yellow solution of OsO_4(bpy) (20 mM, 8.2 mg/ml) was used for ODN labelling.

The oligonucleotide (470 µl, 100 µg/ml) was diluted with Tris-HCl buffer (200 µl, 0.1 M, pH = 7.4) and OsO_4(bpy) (4.3 µl, 20 mM) was added. The mixture was shaken and heated for 3 h at 37 °C on Thermomixer comfort (Eppendorf, Hamburg, Germany). After cooling, the sample was reduced in volume and washed five times with 200 µl portions of Tris-HCl on Amicon 3k filters (Millipore, Billerica, USA) using centrifuge (6000 rpm, 20 °C, 15 min). Final volume of sample was 470 µl.

2.3. Preparation of nanomaghemit modified with gold nanoparticles

80 ml of water was poured in a 250 ml beaker and 1.5 g of $Fe(NO_3)_3 \cdot 9H_2O$ was mixed on a magnetic rotor. 1.4 ml of 25% NH_3 (*v*/*v*) solution was mixed with 8.6 ml of water in a screw capped tube and poured in a separate beaker. 0.2 g of $NaBH_4$ was mixed with NH_3 solution. After 10 min of mixing, the solution was added to the beaker containing $Fe(NO_3)_3$. The colour of the solution became black with an initial frothing. Then it was heated at 100 °C for 2 h. The mixture was stirred overnight. The magnetic particles were separated from the solution by external magnet and washed with deionised water several times. Then, 20 ml of water was poured in the beaker and mixed with a solution of 1.5 g of polyvinylpyrrolidone (Mw 40000) dissolved in 20 ml of water. After 3 h of mixing, 25 ml of chloroauric acid ($HAuCl_4$, 1 mM) was added and mixed for 1 h. 0.75 ml of trisodium citrate (0.265 g/10 ml) was added to it and stirred overnight. Next day, the magnetic particles were separated from the solution by external magnet and washed three times with deionised water. It was collected and dried at 40 ºC. The weight of the dry sample was 0.26 g.

2.4. Cloning, sub-cloning and amplification of HIV gene p24 using polymerase chain reaction

The gene for the capsid protein p24 of human immunodeficiency virus (GenBank accession number: AJ630556.1) was synthesized and cloned into the plasmid pUC57 -Amp (GENEWIZ Gene Synthesis, Sigma-Aldrich) resulting pUC57 vector containing the HIV-cap. The chemical transformation protocol was performed following the instructions of Invitrogen using as host TOP10 chemically competent *E. coli* strain. Bacteria transformed with pUC57-HIV-cap plasmid were selected by ampicillin resistance. The positive transformants were confirmed by PCR screening. The plasmid were purified by using the Qiagen Miniprep Kit (Qiagen, Maryland, USA) and the amplification of

gene by PCR was done using a set of primers flanking the complete open reading frame (5′-ATGGTCCACCAAGCCATATC-3′ (HIV-capfw) and 5′-TTATTGCTAAGCCAAAACCC-3′ (HIV-capre)). Amplified product was analysed via agarose gel electrophoresis and the conditions were as follows: 2% agarose gel (High melt/Medium fragment, Mercury, San Diego, USA) with 1× TAE buffer, 60 V and 160 min (Bio-Rad, Hercules, USA). The 100 bp DNA ladder (New England Biolabs, Ispwich, USA) was used as a molecule size marker. Bands were visualized via UV transilluminator at 312 nm (Vilber-Lourmat, Marne-la-Vallée Cedex, France). The MiniElute PCR Purification Kit (Qiagen, Maryland, USA) was used for cleaning the PCR product.

To obtain pGEX-4T1-HIV-cap, the full-length HIV-cap was isolated from the pUC57 vector by digestion with NotI and ligated into the NotI-digested vector pGEX-4T1. Bacteria transformed with pGEX-4T1-HIV-cap were selected by ampicillin resistance. The positive transformants were confirmed by PCR screening and purified by using the Qiagen Miniprep Kit (Qiagen, Maryland, USA). Linear vector pGEX-4T1 with HIV-cap gene was obtained by digestion EcoRI following the instructions of New England Biolabs (Ispwich, USA). Linear pGEX-4T1-HIV-cap was analysed via agarose gel electrophoresis. The band corresponding to the linear vector was extracted from the agarose gel using the QIAEX II Gel Extraction kit (Qiagen, Maryland, USA).

2.5. Preparation of the construct

1 mg of magnetic particles modified by gold nanoparticles (AuMPs) was sonicated in 1 ml of deionised water for 20 min. Subsequently, it was taken 100 µl from the stock solution of the AuMPs and 2-times rinsed with ACS water. 1, 5, 10 µl of 100 µM thiolated oligonucleotide (ODN) was added to the AuMPs and shaken for 60 min. After that, the ODN-AuMPs complex was 3 times rinsed by hybridization buffer (0.1 M Na_2HPO_4; 0.1 M NaH_2PO_4; 0.6 M guanidinium thiocyanate (Amresco, USA); 0.15 M Tris-HCl (pH 7.5); NaCl (0.5 M)) to remove impurities and diluted in 100 µl of hybridization buffer. Simultaneously, 15 µl (50 $\mu g.ml^{-1}$) of the PCR product was denatured in a Thermomixer comfort (Eppendorf, Hamburg, Germany) (99 °C, 5 min) and immediately cooled. 5 µl of denatured PCR product was mixed with AuMPs in hybridization buffer and after 5 min the OsO_4(bpy)-labelled oligonucleotide (ODN-OsO_4(bpy)) was added into the mixture. After 30 min of incubation (25 °C), the complex, which consists of the ODN-OsO_4(bpy), HIV *p24* and ODN-AuMPs, was 3-times rinsed in ACS water and electrochemically analysed.

2.6. The preparation of mercury film electrode (MFE)

The glassy carbon electrode (GCE) was mechanically polished by the 0.3 µm alumina suspension (ESA Inc., Chelmford, USA) on polishing cloth to produce mirror-like surface. Then, the electrode was sonicated for 5 minutes in deionised water (25 °C) in the Sonorex digital 10 P ultrasonic bath (Bandelin, Berlin, Germany). Thin mercury film (MFE) was formed according Farias et al. with a slight modification [18]. Briefly, MFE was formed in 10 mM $Hg(NO_3)_2$ solution prepared by the dissolution of 0.4 g of mercury(II) nitrate in 100 ml of an acidified water (5 % of HNO_3, *v*/*v*). The cell

was provided with an Ag/AgCl/3M KCl reference electrode and platinum auxiliary electrode, and contained the plating solution, which composition was optimized. The plating conditions of GCE by mercury (deposition time, deposition potential and the composition of plating solution) were also optimized and are shown in results. After plating the MFE was washed and dried under nitrogen.

2.7. Voltammetric measurements (differential pulse voltammetry)

5 µl of sample was pipetted on the film and was absorbed to the surface of MFE for 3 minutes. Then, the surface was washed and transferred to the clean cell with 0.2 M acetate buffer. The differential pulse voltammetry was used to determine the OsO_4(bpy) redox signals. The signals were recorded by Autolab Pgstat101 (Metrohm, Herisau, Switzerland) and analysed using software Nova 1.8 (Metrohm, Herisau, Switzerland). The potentiostat was set to conditioning time 5 s, deposition potential -1.3 V, deposition time 120 s, interval time 0.1 s, equilibration time 5 s, modulation time 0.004 V, modulation time 0.1 s, initial potential -1.3 V, end potential -0.1 and scan rate 25 $mV.s^{-1}$. All data was obtained at ambient temperature (25 °C).

3. RESULTS AND DISCUSSION

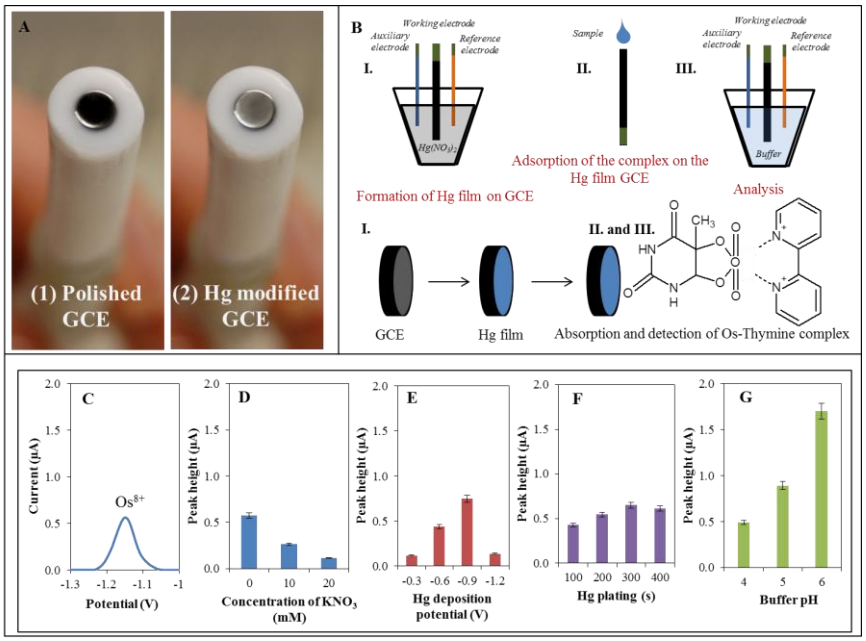

Figure 1. (**A**) The comparison of polished glassy carbon electrode (1) and mercury film modified GCE (2). (**B**) The scheme of preparing the mercury modified glassy carbon electrode and subsequent analysis of the complex. (**C**) The electrochemical signal of OsO_4(bpy) labelled ODN (100 $\mu g.ml^{-1}$). (**D**) The influence of KNO_3 on the electrochemical signal of OsO_4(bpy) labelled ODN (100 $\mu g.ml^{-1}$). (**E**) The dependence of Hg deposition potential (-0.3 – 1.2 V) on the peak height of the OsO_4(bpy) labelled ODN (100 $\mu g.ml^{-1}$). (**F**) The time dependence of Hg plating (100 – 400 s) on the peak height of the OsO_4(bpy) labelled ODN (100 $\mu g.ml^{-1}$). (**G**) The influence of acetate buffer pH (4 – 6) on the peak height of the OsO_4(bpy) labelled ODN (100 $\mu g.ml^{-1}$).

The aim of our study was to perform the electrochemical detection of HIV gene for p24 capside protein. At the first part of experiment, the molecularly-biological methods were used to obtain the *p24* gene and the linear plasmid (pGEX-4T1) with the inserted *p24*. The creation of linear plasmid with *p24* gene and *p24* gene itself was proved by gel electrophoresis and theirs concentrations were determined by UV-vis spectrophotometry. The construct, which was analysed using mercury film electrode and adsorptive transfer method with differential pulse voltammetry detection, consisted of *p24* gene, the oligonucleotide probe to anchor the construct to magnetic particles and the second probe modified by OsO_4(bpy) to enable electrochemical detection.

3.1. Optimization of voltammetric measurements

The detection optimization of OsO_4 and 2,2´-bipyridine complex bounded to oligonucleotide (ODN-OsO_4(bpy)) was performed using DPV and three-electrode cell. The working glassy carbon electrode was modified by mercury film [19,20], which is responsible for adsorption of ODN-OsO_4(bpy) on the surface of electrode [21], like in the case of hanging mercury drop electrode [22] and it is shown in Figs. 1A and B. The Os^{+8} detection included three steps (Fig. 1A). At first, GCE was immersed to the solution of $Hg(NO_3)_2$ and by the application of negative potential the thin mercury film on the surface of electrode was created (Fig. 1A I). The rate of mercury deposition is a function of the pH of the electrolyte, deposition potential and mercury(II) ion concentration [23]. To the mercury film the sample of ODN-OsO_4(bpy) (5 μl of 50 $\mu g.ml^{-1}$) was pipetted and adsorbed to the surface of electrode for 3 minutes (Fig. 1A II). The un-adsorbed sample was washed and the electrode was transferred to the three electrode cell filled with 0.2 M acetate buffer, where the measurement was performed (Fig. 1A III). The catalytic signal of ODN-OsO_4(bpy) was analysed [24] and DP voltammogram is shown in Fig. 1D. The individual (I, II and III) steps were optimized. The effect of 0, 10 and 20 mM KNO_3 dissolved in the $Hg(NO_3)_2$ plating solution on the catalytic signal of ODN-OsO_4(bpy) was observed. The increasing concentration of KNO_3 caused the decrease of analysed signal for more than 45 % (Fig. E). The effects of deposition potentials (-0.3, -0.6, -0.9 and -1.2 V) and deposition times (100, 200, 300 and 400 s) on catalytic signal were also analysed. We found out that the best properties of mercury film were obtained by the application of deposition potential -0.9 V (Fig. 1F) for 300 s (Fig. 1G). These results are in good agreement with those published by Armalis et al. [25]. The pH 4, 5 and 6 of 0.2 M acetate buffer was also optimized. The best catalytic signal of ODN-OsO_4(bpy) was obtained by performing the measurement in buffer of pH 6 (Fig. 1H).

3.2 The voltammetric detection of the p24 gene alone

The HIV capsid protein *p24* gene was amplified by polymerase chain reaction (Fig. 2A 2) from pGEX-4T1 plasmid (Fig. 2A 1). The PCR product was analysed by gel electrophoresis, which proved the presence of target gene in the PCR solution. The 677 bp long band was observed (Fig. 2A). The unwanted compounds (salts, Taq DNA polymerase) were removed from the solution by purification (Fig. 2A 3), by which we obtained the solution of target double-stranded DNA (dsDNA). The dsDNA

was subsequently denatured (95 °C, 5 minutes) and rapidly cooled to obtain the single-stranded target DNA (Fig. 2A 4).

The gold modified magnetic particles (1 mg) were treated with 1 ml of water and sonicated for 20 minutes to divide clusters. We used the rapid creation of covalent bond between thiols and gold to capture the oligonucleotide probe to the AuMPs [26]. The 100 µl of created AuMPs mixture was after rinsing treated with 1, 5 and 10 µl of thiolated 100 µM oligonucleotide, which corresponded to 0.1, 0,5 and 1.0 nM of oligonucleotide. After removing the uncaptured probes by rinsing, to 0.1 mg of AuMPs 100 µl of hybridization buffer, 10 µl of OsO_4(bpy) modified 100 µM oligonucleotide probe (1.0 nM) and 0.6 pM of target gene sequence was added (Fig. 2A 5). The complex of OsO_4(bpy) and oligonuceotide exhibits electrocatalytic activity at the surface of mercury electrode and enables highly sensitive voltammetric detection (Fig. 2A 6) [27]. The 5 µl of obtained sample was pipetted to the surface of MFE and adsorbed to the surface for 3 minutes.

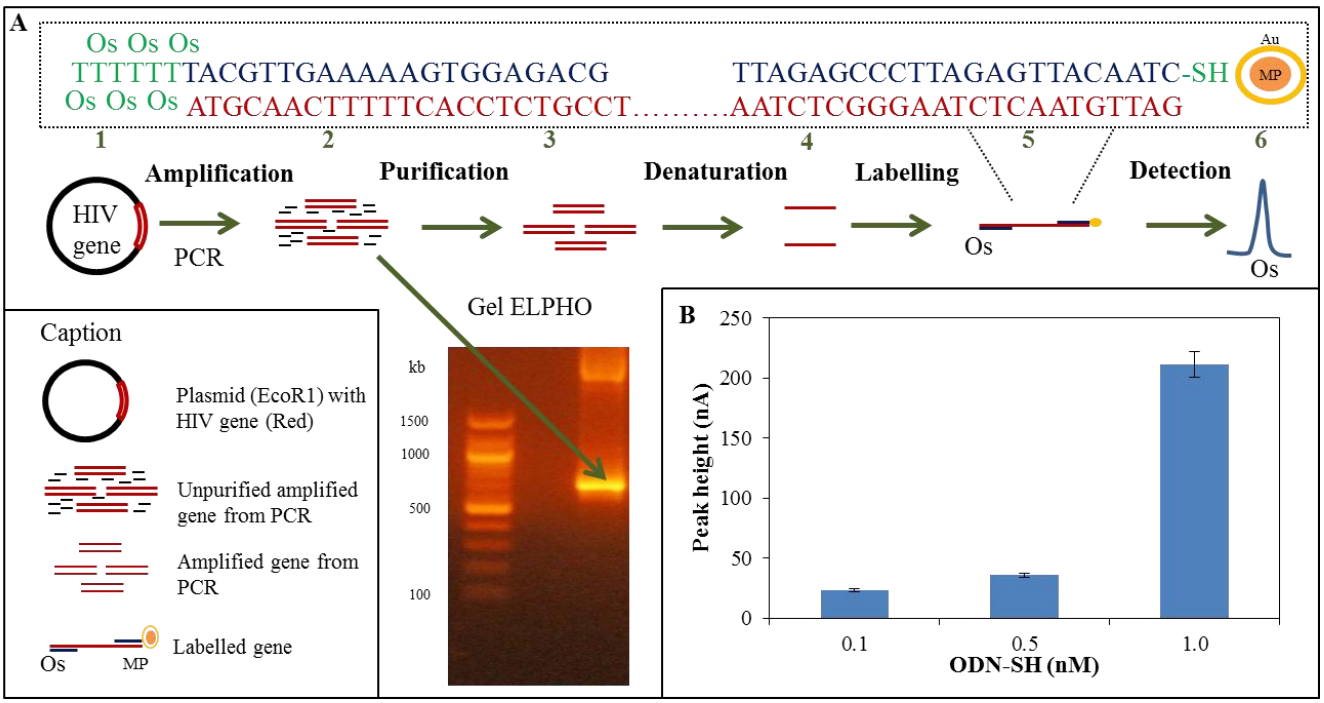

Figure 2. (**A**) Scheme of the complex preparation. Plasmid carrying the HIV gene (1) was amplified using the PCR method and analysed using the gel electrophoresis (2). Subsequently, 700 bp long amplicon was purified (3). The amplicon was denatured, afterwards labelled by thiolated oligonucleotides with bonded Au paramagnetic particle and OsO_4(bpy) modified oligonucleotide probe (5). In this way prepared complex was electrochemically analysed on MFE (6). (**B**) The dependence of the complex (I.) electrochemical signal (nA) on the concentration of thiolated ODN probe (0.1 – 1 nM).

Then, the un-adsorbed sample was washed and DPV was performed in 0.2 M acetate buffer (pH 6). We assumed that the thiolated oligonucleotide and target gene ratio (200:1, 1000:1 and 2000:1) affected the target gene detection signal (or more precisely OsO_4(bpy) oligonucleotide complex),

which was subsequently confirmed (Fig. 2B). The addition of 10-times higher amount of thiolated ODN led to the more than 9-times higher electrocatalytic signal of captured ODN-OsO_4(bpy). Based on these results we concluded 9-times higher capturing of target gene. The detection sensitivity of DNA (HIV) is comparable with the signal amplification of carbon nanotubes loaded with silver nanoparticles and placed on a gold microelectrode [28]. The alternative detection methods do not have comparable sensitivity [9,29].

3.3. The voltammetric detection of the linear plasmid with p24 gene

The detection of *p24* gene was also performed, when the gene was presented inside the linear plasmid. The pGEX-4T1 (4969 bp) plasmid with inserted target gene (Fig. 3A 1) was digested by the restriction endonuclease EcoRI (Fig. 3A 2). The presence of the linear plasmid in the sample was confirmed by the gel electrophoresis (Fig. 3A). The band was cut from the gel (Fig. 3A 3), purified and we obtained the solution of 10 $\mu g.ml^{-1}$ of dsDNA, which was subsequently denatured.

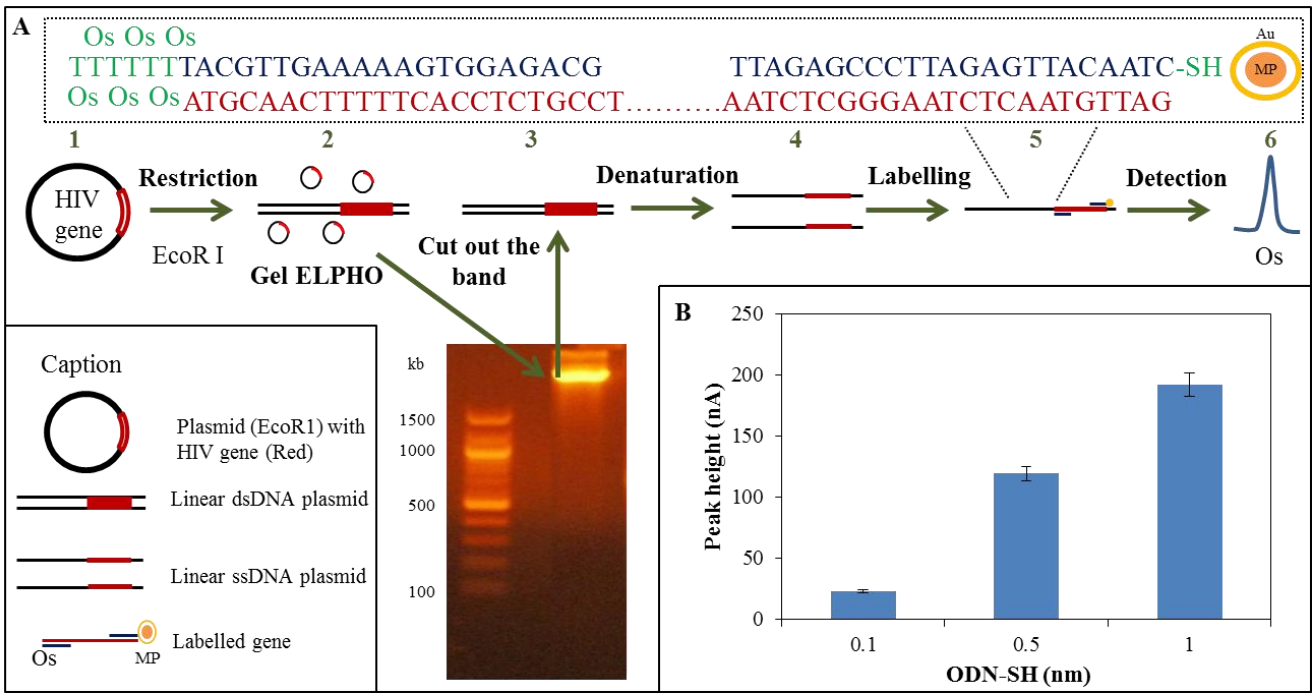

Figure 3. (**A**) Scheme of the complex II preparation. Plasmid carrying the HIV gene (1) was cleaved by restriction endonucleases (EcoRI) to linear dsDNA and analysed using gel electrophoresis (2). The band corresponding to molecular weight of linear ds DNA was cut out (3). Subsequently the sample was denatured and (4) after that the ss DNA was labelled by thiolated oligonucleotide with bounded Au paramagnetic particle and Os modified oligonucleotide probe (5). This way prepared complex was electrochemically analysed on the glassy carbon mercury film modified electrode (6). The frame shows the prepared complex. (**B**) The dependence of the complex (II.) electrochemical signal (nA) of the on the concentration of thiolated ODN probe (0.1 – 1 nM).

The samples were treated in the same manner like the sample of target gene itself and the conditions of measurement were preserved. The same volumes of samples were pipetted (5 μl) to the surface of MFE. The molar ratios of ODN-SH and target gene were 325-times higher, because no PCR was used to amplify the target gene (6500:1, 32500:1 and 65000:1). However, the detection method was able to detect the target gene in the 8 fM concentration. The increase in the amount of ODN-SH added to the MPs solution resulted in the increasing trend of detected ODN-OsO_4(bpy) (Fig. 3B).

Although the procedure of sample treating and detection were the same in the case of target gene itself and also gene within plasmid, and the gene concentrations were completely different. It must be pointed out that the analysed peak heights of detected ODN-OsO_4(bpy) are comparable (from tens to hundreds of nA). It is well known that the conformation of DNA and hybridization is influenced by temperature [30,31]. We suggest that the hybridization temperature (25 °C) did not prevent ODN-OsO_4(bpy) from nonspecific binding to the 677 bp long sequence of *p24* gene within plasmid. It is also possible that under particular conditions, the created construct is able to bind only limited amount of target gene.

4. CONCLUSIONS

In this study we succeeded in the preparation of nanoconstruct, which consisted of OsO_4(bpy) modified oligonucleotide probe hybridized to the HIV capside protein gene and its capturing to the gold modified magnetic particle. The mercury film electrode was prepared, the whole construct was adsorbed to its surface and the electrochemical signals were analysed.

ACKNOWLEDGEMENTS
The financial support from the following project CZ.1.07/2.4.00/31.0023 NanoBioMetalNet is highly acknowledged. The authors thank Martina Stankova, Lucie Dostalova, Lukas Melichar and Radek Chmela for perfect technical assistance.

CONFLICT OF INTEREST:
The authors have declared no conflict of interest.

References

1. J. Ananworanich, J. L. K. Fletcher, S. Pinyakorn, F. van Griensven, C. Vandergeeten, A. Schuetz, T. Pankam, R. Trichavaroj, S. Akapirat, N. Chomchey, P. Phanuphak, N. Chomont, N. L. Michael, J. H. Kim, M. de Souza and R. S. S. Grp, *Retrovirology*, 10 (2013) 1.
2. A. Saez-Cirion, S. Y. Shin, P. Versmisse, F. Barre-Sinoussi and G. Pancino, *Nat. Protoc.*, 5 (2010) 1033.
3. G. McAllister, S. Shepherd, J. Shepherd, L. Renwick, S. Hutchinson, D. Goldberg, R. Gunson, C. Aitken and K. Templeton, *HIV Med.*, 14 (2013) 47.
4. S. R. Jangam, A. K. Agarwal, K. Sur and D. M. Kelso, *Biosens. Bioelectron.*, 42 (2013) 69.
5. L. Zheng, L. Y. Jia, B. Li, B. Situ, Q. L. Liu, Q. Wang and N. Gan, *Molecules*, 17 (2012) 5988.
6. C. Esseghaier, A. Ng and M. Zourob, *Biosens. Bioelectron.*, 41 (2013) 335.
7. N. Gan, J. G. Hou, F. T. Hu, L. Zheng, M. J. Ni and Y. T. Cao, *Molecules*, 15 (2010) 5053.

8. S. Martic, M. Labib and H. B. Kraatz, *Talanta*, 85 (2011) 2430.
9. D. D. Zhang, Y. G. Peng, H. L. Qi, Q. Gao and C. X. Zhang, *Biosens. Bioelectron.*, 25 (2010) 1088.
10. J. Zhang, X. Y. Wu, W. J. Yang, J. H. Chen and F. F. Fu, *Chem. Commun.*, 49 (2013) 996.
11. K. J. Odenthal and J. J. Gooding, *Analyst*, 132 (2007) 603.
12. R. Kizek, L. Havran, M. Fojta and E. Palecek, *Bioelectrochemistry*, 55 (2002) 119.
13. M. Fojta, L. Havran, R. Kizek, S. Billova and E. Palecek, *Biosens. Bioelectron.*, 20 (2004) 985.
14. M. Fojta, L. Havran, R. Kizek and S. Billova, *Talanta*, 56 (2002) 867.
15. F. Jelen, P. Karlovsky, E. Makaturova, P. Pecinka and E. Palecek, *Gen. Physiol. Biophys.*, 10 (1991) 461.
16. E. Palecek, *Bioelectrochem. Bioenerg.*, 15 (1986) 275.
17. M. Fojta, L. Havran, S. Billova, P. Kostecka, M. Masarik and R. Kizek, *Electroanalysis*, 15 (2003) 431.
18. P. A. M. Farias, A. A. Castro, A. D. R. Wagener and E. M. Miguel, *Electroanalysis*, 20 (2008) 1445.
19. S. Zbeda, K. Pokpas, S. Titinchi, N. Jahed, P. G. Baker and E. I. Iwuoha, *Int. J. Electrochem. Sci.*, 8 (2013) 11125.
20. C. Serpi, A. Voulgaropoulos and S. Girousi, *Electroanalysis*, 25 (2013) 1256.
21. P. Kostecka, L. Havran, H. Pivonkova and M. Fojta, *Bioelectrochemistry*, 63 (2004) 245.
22. B. Yosypchuk, M. Fojta, L. Havran, M. Heyrovsky and E. Palecek, *Electroanalysis*, 18 (2006) 186.
23. F. N. Ertas, H. I. Gokcel and H. Tural, *Turk. J. Chem.*, 24 (2000) 261.
24. S. Billova, R. Kizek and E. Palecek, *Bioelectrochemistry*, 56 (2002) 63.
25. S. Armalis and E. Kubiliene, *Chem. Anal.*, 46 (2001) 715.
26. M. M. S. Silva, I. T. Cavalcanti, M. F. Barroso, M. G. F. Sales and R. F. Dutra, *J. Chem. Sci.*, 122 (2010) 911.
27. L. Havran, M. Fojta and E. Palecek, *Bioelectrochemistry*, 63 (2004) 239.
28. R. B. Wang, C. H. Xue, M. Gao, H. L. Qi and C. X. Zhang, *Microchim. Acta*, 172 (2011) 291.
29. S. Reisberg, B. Piro, V. Noel and M. C. Pham, *Bioelectrochemistry*, 69 (2006) 172.
30. J. Zhou, S. K. Gregurick, S. Krueger and F. P. Schwarz, *Biophys. J.*, 90 (2006) 544.
31. D. B. Ge, X. Wang, K. Williams and R. Levicky, *Langmuir*, 28 (2012) 8446.

5.4 Automatické detekce bakteriálního znečištění

5.4.1 Vědecký článek V

Nejdl, L.; **Kudr, J.**; Cihalova, K.; Chudobova, D.; Zurek, M.; Zalud, L.; Kopecny, L.; Burian, F.; Ruttkay-Nedecky, B.; Krizkova, S.; Konecna, M.; Hynek, D.; Kopel, P.; Prasek, J.; Adam, V.; Kizek R. Remote-controlled robotic platform ORPHEUS as a new tool for detection of bacteria in the environment. *Electrophoresis,* 2014, roč. 35. č. 16, s. 2333-2345. ISSN 0173-0835

Podíl autora Kudr J.: 30 % textové části práce a 35 % experimentální práce

Rozvoj v oblasti elektrotechniky a technologií neustále snižuje potřebu lidské práce v nebezpených či z jiných důvodu nepříznivých podmínkách. Nová generace robotických zařízení bohatě vybavených sensory umožňuje provádět složité úkony bez nutnosti fyzické přítomnosti obsluhy a člověka přesouvá do pozice operátora, který pouze na dálku řídí zařízení skrze efektivní komunikační technologie.

Vývoji technologií umožňující vzdálenou detekci je v současnosti věnována velká pozornost *(Noyhouzer a kol., 2013).* V případě vzdálené elektrochemické detekce bakteriální kontaminace se nabízí buď detekovat nukleové kyseliny, enzymy, anebo použít k detekci specificitu protilátek *(Mittelmann a kol., 2002; Fiksdall a kol., 2008; Paniel a kol., 2013).*

V této publikaci je popsán průtokový systém pro detekci bakterií na bázi enzymové aktivity. Elektrochemická detekce je založena na přítomnosti alkalické fosfatázy (ALP) v bakterii. Tento enzym se účastní defosforylačních procesů a je tedy přítoment ve většině živých organismů včetne extrémofilů *(Chander a kol., 2001; Nicolaus a kol., 2004).* K samotné detekci byla využita reakce, kdy ALP v alkalickém prostředí katalyzuje přeměnu neelektroaktivního naftyl fosfátu na elektroaktivní 1-naftol. Detekční zařízení se skládalo z řídící jednotky, která ovlivňovala činnost peristaltické pumpy. Nasátý vzorek byl transportován průtokem do kultivační komory, kde byly umístěny magnetické částice (experimentálně vybrány) pro zachycení bakterií. Magnetické částice umožňovaly následné odmytí kapalného vzorku. Bakterie se zde po zvolený čas kultivovaly v kultivačním médiu. Po kultivaci byl do komory přiveden alkalický roztok naftyl fosfátu, který je štěpen na 1-naftol. Roztok 1-naftolu byl následně pumpován do průtokové elektrochemické cely s tištěnou elektrodou, která diferenční pulzní voltametrií provedla detekci. Systém nabízel dva body, které

umožňovaly amplifikovat získaný signál – doba kultivace a doba inkubace naftyl fosfátu s enzymy. Byl optimalizován na bakterii *Staphylococcus aureus*, nicméně může sloužit pro detekci jakékoliv bakterie vylučující ALP. Tento průtokový senzor byl následně implementován na mobilní robotickou platformu ORPHEUS-HOPE, která umožňuje aplikaci systému v nepřístupných podmínkách.

Lukas Nejdl[1]
Jiri Kudr[1]
Kristyna Cihalova[1]
Dagmar Chudobova[1]
Michal Zurek[1]
Ludek Zalud[2]
Lukas Kopecny[2]
Frantisek Burian[2]
Branislav Ruttkay–Nedecky[1,2]
Sona Krizkova[1,2]
Marie Konecna[1,2]
David Hynek[1,2]
Pavel Kopel[1,2]
Jan Prasek[2]
Vojtech Adam[1,2]
Rene Kizek[1,2]

[1]Department of Chemistry and Biochemistry, Faculty of Agronomy, Mendel University in Brno, Czech Republic
[2]Central European Institute of Technology, Brno University of Technology, Czech Republic

Received November 19, 2013
Revised March 3, 2014
Accepted March 10, 2014

Research Article

Remote-controlled robotic platform ORPHEUS as a new tool for detection of bacteria in the environment

Remote-controlled robotic systems are being used for analysis of various types of analytes in hostile environment including those called extraterrestrial. The aim of our study was to develop a remote-controlled robotic platform (ORPHEUS-HOPE) for bacterial detection. For the platform ORPHEUS-HOPE a 3D printed flow chip was designed and created with a culture chamber with volume 600 μL. The flow rate was optimized to 500 μL/min. The chip was tested primarily for detection of 1-naphthol by differential pulse voltammetry with detection limit (S/N = 3) as 20 nM. Further, the way how to capture bacteria was optimized. To capture bacterial cells (*Staphylococcus aureus*), maghemite nanoparticles (1 mg/mL) were prepared and modified with collagen, glucose, graphene, gold, hyaluronic acid, and graphene with gold or graphene with glucose (20 mg/mL). The most up to 50% of the bacteria were captured by graphene nanoparticles modified with glucose. The detection limit of the whole assay, which included capturing of bacteria and their detection under remote control operation, was estimated as 30 bacteria per μL.

Keywords:
Alkaline phosphatase / Bacteria / Electrochemical detection / Magnetic particles / 1-Naphthyl phosphate / Planetary science / Remote sensing
DOI 10.1002/elps.201300576

Additional supporting information may be found in the online version of this article at the publisher's web-site

1 Introduction

Remote sensing is a rapidly developing branch [1]. Progress in the field of electronics and technology constantly restricts the requirement of manpower to carry out dangerous work. The current third generation of ''smart'' robots richly equipped with sensors can be used in extreme environments (sea depths, space, volcanos). The emphasis is placed mainly on the effective communication and remote control, which gives to the operator a perfect control of the robot and the real-time transmission of an image to the operator's station. Space rovers need a considerable amount of electricity to move and power their equipment, so energy-efficient scientific devices are important for remote sensing [2]. Extraterrestrial environment shows the extremes of temperature, salinity, dryness, radiation [3, 4] and amorphous land components are similar to the composition of the soil resulting from volcanic igneous rocks [5–7]. The electrochemical applications are suitable for the analysis of such hostile environment and, moreover, for miniaturization to be a part of remote sensing devices [8]. Currently an automated technique is being developed to detect the presence of microorganisms, which should facilitate the collection and detection of samples in the environment for humans hardly accessible. Like terrestrial extremophile organisms, Mars also may have some analogous niches such as sulfur-rich subsurface areas for chemoautotrophic organisms, rocky areas for endolithic communities, cold environment, and the permafrost regions [9]. Therefore, it is necessary to have a robust instrument capable to detect the presence of bacteria based on selected biomarker(s) as some unspecific enzymes.

Alkaline phosphatase (ALP) belonging to above mentioned enzymes is a metalloenzyme involved in the dephosphorylation process. It is a catalyst of the hydrolysis of phosphoric acid monoester to phosphoric acid and alcohol in the alkaline environment [10, 11]. Phosphoric acid

Correspondence: Dr. Rene Kizek, Brno University of Technology, Zemedelska 1, CZ-613 00 Brno, Czech Republic
E-mail: kizek@sci.muni.cz
Fax: +420-5-4521-2044

Abbreviations: **ALP**, alkaline phosphatase; **CFU**, colony forming unit; **DOF**, degrees of freedom; **LBM**, Luria Bertani medium; **MP**, magnetic particle; **SECM**, scanning electrochemical microscope; **SPE**, screen-printed electrode

Colour Online: See the article online to view Figs. 1–7 in colour.

is represented in most living organisms [10], including extremophilic microorganisms [12, 13], where it affects the metabolism of macroergic phosphate bonds. Thus, it is not surprising that the ALP is produced during the growth and sporulation of various bacterial strains (*Staphylococcus aureus* [14], *Bacillus cereus*, and *Bacillus amyloliquefaciens* [15–17], *Escherichia coli* [18], thermophilic bacteria [19] such as *Thermotoga neapolitana*, *Thermus caldophilus*, *Thermus thermophilus*, *Bacillus stearothermophilus*, *Pyrococcus abyssi*, and *Deinococcus radiodurans*, which is able to live in a radioactive environment [20–22]).

For detection of enzymatic activity, electrochemical detectors (ECD) can provide competitive advantages with respect to other detection systems such as portability, low cost, and low power requirements [23–25]. Additionally, ECD can analyze turbid samples, can be easily miniaturized [26], and requires electrodes that can be fabricated using low cost instrumentation [27]. Recently it can be observed that the interest in 3D printing technology for manufacturing of flow chip and equipment has been growing [28–31]. Described technology (lab-on-a-chip) can be extended to the mobile platform (lab-on-a-robot) [26, 32, 33]. More recently, the first integrated system capable of performing remote analysis of air samples using microchip-CE was presented [33]. The screen-printed electrodes (SPEs) can be used as a suitable detectors in CE microchips [34]. Thus, the technology becomes more accessible in new robotic controls and applications are developed [32, 35–41].

The aim of our study was to create a remote-controlled robotic platform (ORPHEUS-HOPE) capable of carrying different types of detectors for remote-controlled exploration of extreme environments. Combination of the robotic platform ORPHEUS-HOPE and a 3D printed flow chip can perform remote detection of *S. aureus* based on ALP activity, which could be applied also for other bacterial strains. The electrochemical detection was based on enzymatic cleaving of electrochemically inactive 1-naphthyl phosphate to electrochemically active 1-naphthol. Modified magnetic particles (MPs) within the chip were used to attach bacteria from a solution.

2 Materials and methods

2.1 Chemicals and pH measurement

Chemicals used in this study were purchased from Sigma-Aldrich® (St. Louis, Missouri, USA) in ACS purity (chemicals meet the specifications of the American Chemical Society), unless noted otherwise. Washing solutions were prepared in ultrapure water obtained using reverse osmosis equipment Aqual 25 (Aqual, Brno, Czech Republic). The deionized water was further purified by using apparatus Direct-Q 3 UV Water Purification System equipped with the UV lamp from Millipore (Billerica, Massachusetts, USA). The resistance was established to 18 MΩ/cm. The pH was measured using pH meter WTW (inoLab, Weilheim, Germany).

2.2 Fabrication of 3D microfluidic chip

The microfluidic chip was 3D processed in Blender 2.65 (Blender foundation, Amsterdam, the Netherlands) and further edited in NetFabb (Netfabb, Parsberg, Germany). The model was opened in the program G3D maker (DO-IT, Straznice Czech Republic) and printed by Easy 3D maker (DO-IT). Chip was printed with an accuracy of [x, y, z] 0.1/0.1/0.08 mm under the following conditions: the size of the chip was [x, y, z] 40/40/35 mm. Acrylonitrile butadiene styrene was used as a material (DO-IT), and every printed chip was fitted with five input tubes with a diameter of 0.5 mm, one output tube with diameter 0.5 mm, two electromagnets and thermostatic system.

2.3 SPE design and fabrication

Electrode system was designed and fabricated as a disposable planar three-electrode sensor in LabSensNano laboratories (Brno University of Technology, Czech Republic). The properties of design and optimization can be found in the following papers [42, 43]. The working electrode was fabricated using a special carbon paste for electrodes of electrochemical sensors BQ221 (DuPont, Wilmington, USA), reference and auxiliary electrodes were printed using the Ag/AgCl (65:35) paste 5874 (DuPont) and Pt-based paste 5545 (Electroscience, King of Prussia, USA), respectively.

2.4 Microfluidic analysis with differential pulse voltammetric detection

The flow cell for SPE was designed in the shape of a cuboid with sides of 1 cm (width) × 1.5 cm (height) × 3 cm (length). The reaction zone was dimensioned for 20 μL of analyte with 0.7 mm wide inlet and outlet channel. The sample was injected using a peristaltic pump (Amersham Biosciences, Uppsala, Sweden). After optimization of the automated flow system additionally a peristaltic pump Minipuls®3 (Gilson, Middleton, USA) and a stirred water bath WB-4MS (Biosan, Riga, Latvia) were used. Changes of reduction signals were measured with a potentiostat PGSTAT 101 (Metrohm, Herisau, Switzerland) and the results were evaluated by the Software NOVA 1.8 (Metrohm). Settings of the potentiostat were as follows: initial potential −0.2 V, end potential +0.5 V, step potential 0.005 V, modulation amplitude 0.1 V, modulation time 0.004 s, interval time 0.1 s, deposition time 60 s, and equilibration time 5 s. For ALP detection 50 mM carbonate buffer (32 mM Na_2CO_3 and 68 mM $NaHCO_3$) pH 9.9 with 1 mM 1-naphthyl phosphate was used [44].

2.5 Preparation of modified MPs

Maghemite nanoparticles (MPs) were prepared according to the following approach [45, 46]. Shortly, 10 g of $FeCl_3.6H_2O$ was dissolved in 800 mL of MilliQ grade water under vigorous stirring at room temperature. 2 g of

$NaBH_4$ solution in ammonia (3.5% v/v, 100 mL) was then quickly added to the mixture. In a short time after the reduction reaction occurrence, the temperature of the system was increased to 100°C and kept constant for 2 h. After 12 h at room temperature, this magnetic product was separated by application of an external magnet and washed several times with water. The step of solution heating to boiling is very important, because it leads to stabilization of particles and oxidizing of Fe^{2+} to Fe^{3+}. Graphite oxide (GPO) was prepared from graphite flakes (Sigma-Aldrich) by the Hummers method [47]. Graphene (GR) was prepared by reduction of GPO by hydrazine [48]. MPs were modified with the following chemicals: graphene (GR), hyaluronic acid (HA), gold (GO), glucose (GL), collagen (CO), graphene (GR) and glucose (GL), graphene (GR), and gold (GO). The experimental details can be found in Supporting Information 1.

2.6 Cultivation of *S. aureus*

S. aureus (NCTC 8511) was obtained from the Czech Collection of Microorganisms, Faculty of Science, Masaryk University, Brno, Czech Republic. Strains were stored in the form of a spore suspension in 20% v/v glycerol at −20°C. Prior to use, the strains were thawed and the glycerol was removed by washing with distilled water in this study. More details about their cultivation are shown in Supporting Information 4.

2.7 Preparation of *S. aureus* samples with modified MPs and microbiological determination of growth curves

A 2.5 mg of each type of modified MPs was weighted and these particles were diluted in 0.5 mL of water in ACS purity. These solutions were resuspended in ultrasonic bath Sonorex digital 10p (Bandelin, Berlin, Germany) for 5 min at 25°C and then added to 0.5 mL of the *S. aureus* bacterial culture (3.7×10^7 CFU/mL) and incubated in the thermomixer Comfort (Eppendorf, Hamburg, Germany) at 37°C, 600 rpm for 1 h. After incubation, MPs were separated and washed three times with 1000 μL of phosphate buffer (pH 7) tempered at 37°C. To the washed particles, 1000 μL of cultivation LBM (Himedia, Mumbai, India) containing tryptone 10 g/L, yeast extract 5 g/L, and NaCl 5 g/L was added at 37°C. Particles with LBM were incubated in the thermomixer Comfort (Eppendorf) for 1 h at 37°C and 600 rpm. After cultivation the solution was pipetted off and the MPs with adhered bacteria were three times washed with phosphate buffer (pH 7). To the washed particles 1 mL of the LBM was added and the solution was incubated at the same conditions as mentioned above. The inoculum with released bacteria was then pipetted to the microplate and the absorbance using Multiskan EX (Thermo Fisher Scientific, Bremen, Germany) was measured, and the analysis of the growth curves was used to assess the amount and growth ability of the isolated bacteria. Then the growth curves were measured. Measurements were carried out at time 0, and then in 30 min intervals for 10 h at 37°C, at the wavelength 600 nm. The obtained data were analyzed in graphical form of growth curves for each modification of the MPs.

2.8 UV/Vis spectrophotometry

Absorption spectra were recorded using a SPECORD 210 spectrophotometer (Analytik Jena, Jena, Germany) in $\lambda =$ 405 nm and $\lambda = 600$ nm. Automated spectrophotometric measurements were carried out using chemical analyzer BS-400 (Mindray, Schenzen, China). Alkaline phosphatase was determined in the suspensions of bacteria with culture medium of appropriate cell density ($OD_{600\,nm} = 1.5$ AU). In a reaction catalyzed by ALP the substrate *p*-nitrophenyl phosphate is split to *p*-nitrophenol and inorganic phosphate. ALP activity is determined kinetically and is based on the rate of *p*-nitrophenol concentration increase during reaction. Experimental details are in Supporting Information 5.

2.9 Mathematical treatment of data and estimation of detection limits

Mathematical analysis of the data and their graphical interpretation was realized by software Matlab (version 7.11., MathWorks, USA). Results are expressed as mean ± SD unless noted otherwise (EXCEL®, Microsoft, USA). Limits of detection S/N = 3, were calculated, whereas N was expressed as SD of noise determined in the signal domain unless stated otherwise [49].

3 Results

3.1 Bacterial activity of ALP

The whole concept of electrochemical detection is based on the capturing of bacteria producing ALP on modified MPs [50] and the subsequent multiplication of bacteria in a culture chamber (Fig. 1A). ALP produced by bacteria cleaves the 1-naphthyl phosphate (electrochemically inactive) to the electrochemically active product 1-naphthol (Fig. 1B), which can be easily detected by voltammetry (Fig. 1C). ALP activity was measured in two bacterial species; Gram-positive *S. aureus* and Gram-negative *E. coli*, with cell count of (2×10^7 cells per mL). *S. aureus* showed 2.3 times higher ALP activity in comparison with *E. coli* (Fig. 1D). Due to this fact, the further experiments were performed with *S. aureus* as a model microorganism. It was found that *S. aureus* ALP activity was linear within the range from 1×10^5 to 420×10^5 per mL with $R^2 = 0.9989$ (Fig. 1E). Reaction kinetics of the ALP was also studied (Fig. 1F). Michaelis Menten constant of bacterial ALP was determined as 2.3 mM. Finally, the dependence of the *S. aureus* (2×10^7 cells per mL) growth was monitored photometrically ($\lambda = 600$ nm) in the time interval 0–140 min simultaneously with the formation of the *p*-nitrophenol

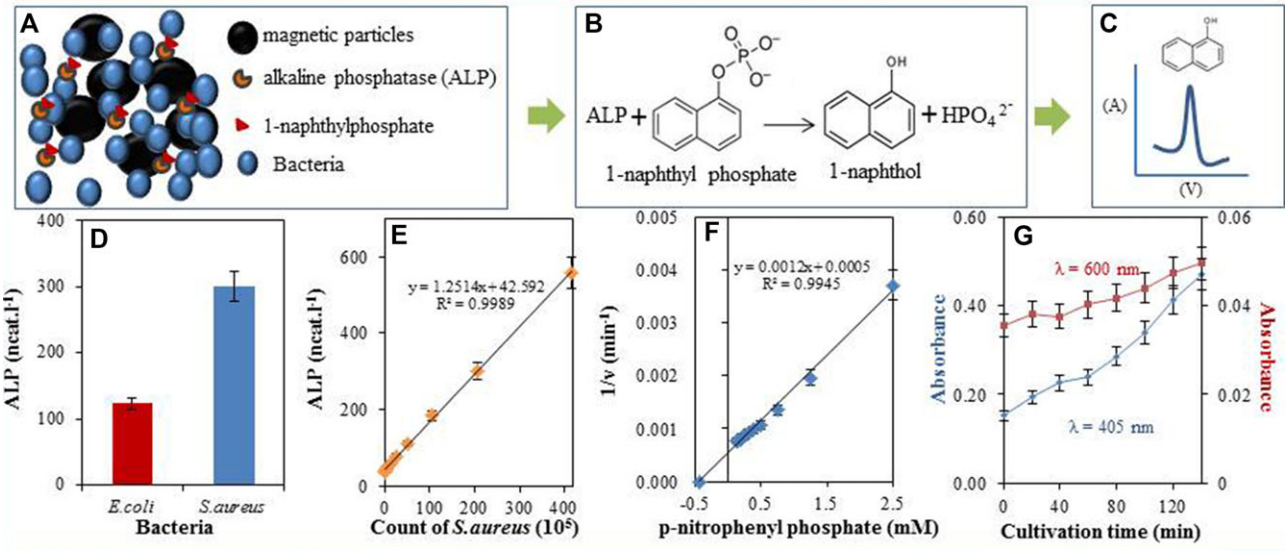

Figure 1. (A) The mechanism, which enables electrochemical detection of *S. aureus*. Alkaline phosphatase (ALP) released by *S. aureus*, which has been captured by magnetic particles (MPs), cleaves 1-naphthyl phosphate in naphthol and phosphate. (B) Chemical reaction, which is the principle of *S. aureus* electrochemical detection. (C) The electrochemical signal of 1-naphthol. (D) Spectrophotometrically measured activity of ALP released by *E. coli* compared with *S. aureus*. (E) The dependence of ALP activity on count of *S. aureus*. (F) Reaction kinetics of ALP. (G) The dependence of *p*-nitrophenol ($\lambda = 405$ nm) and *S. aureus* ($\lambda = 600$ nm) absorbance on mixture of alkaline phosphatase photometric substrate and *S. aureus* (2×10^7 cells) cultivation time.

($\lambda = 405$ nm), a product of the ALP reaction with the photometric ALP substrate (*p*-nitrophenyl phosphate) (Fig. 1G).

3.2 Optimization of 1-naphthol detection

Screen printed electrodes were characterized by cyclic voltammetry (CV) in 50 mM carbonate buffer (pH 9.9). Primarily, the dependence of the CV signals of 10 mM 1-naphthol on the changes of scan rate (5–500 mV/s) was investigated (Fig. 2A-a1). The growing trend of electrochemical signal and peak potentials (Ep) was observed as the scan rate (ν) was increased (Fig. 2A-a2). There is no peak in reverse scan, which means that electrode reaction is totally irreversible, which is consistent with Ep shift. A graph of cathodic peak currents (Ip, c) versus square root of scan rate ($\nu^{1/2}$) was plotted (Fig. 2A-a3). This relationship indicates that diffusion mechanisms are involved in the electrochemical reaction. The same characterization of SPE was done by flow analysis under 500 μL/min (Fig. 2B-b1). When the scan rate (ν) was increased, the electrochemical signal of naphthol was increasing in the same way as without flow (Fig. 2B-b3). Peak currents exhibit logarithmic dependence on $\nu^{1/2}$, which suggests that flow of analyte affects diffusion mechanism of its reduction and partly some adsorption-controlled mechanism can run. This was confirmed by the slope of logIp dependence on logν (not shown). The substrate temperature was optimized by DPV of 2 μM naphthol. From the range of 5–40°C, the optimal temperature of 35 ± 2°C for 1-naphthol detection was selected (Fig. 2C-c1). Accumulation time was the next parameter, which we were interested in. The difference between the peak height with accumulation time 60 and 120 s was lower than SPE RSD, so accumulation time 60 s was chosen as the best. The calibration curve of 1-naphthol with regression coefficient $R^2 = 0.999$ was measured (Fig. 2C-c3) and the LOD and LOQ were calculated (Table 1).

3.3 Characterization of MPs

Between various magnetic metal oxides, the cubic spinel structured maghemite is technologically important and is widely used for the production of permanent magnetic materials [51, 52]. In this experiment variously modified maghemite MPs were characterized. MPs without surface modification are shown in the first SEM photo (Fig. 3A). The different structures of MPs with modified surface can be recognized in other SEM micrographs (Figs. 3C, E, G, I, K, M, and O). It can be seen that maghemite nanoparticles form clusters unequally deployed on each carrier surface and thus provide perfect paramagnetic properties. The average current of unmodified MPs is 70 nA. The presence of Fe in MPs with typical Skα a Skβ signals corresponding to positions of Fe was proved by X-ray fluorescence (XRF) analysis (Fig. 3B). Taking into account that all MPs have γ-Fe_2O_3 core, all X-ray spectra are nearly the same. The peak positions are always the same and only their intensity is changing (Figs. 3D, F, H, J, L, N, and P). MPs modified by tetrachlorauric acid are the only exception, because gold nanoparticles are presented after reduction (trisodium citrate dihydrate) on the surface (zoomed part of Fig. 3P).

For scanned current level of collagen modified MPs there are typical transitions between recorded current levels of 40 nA. It means that distribution and the amount of

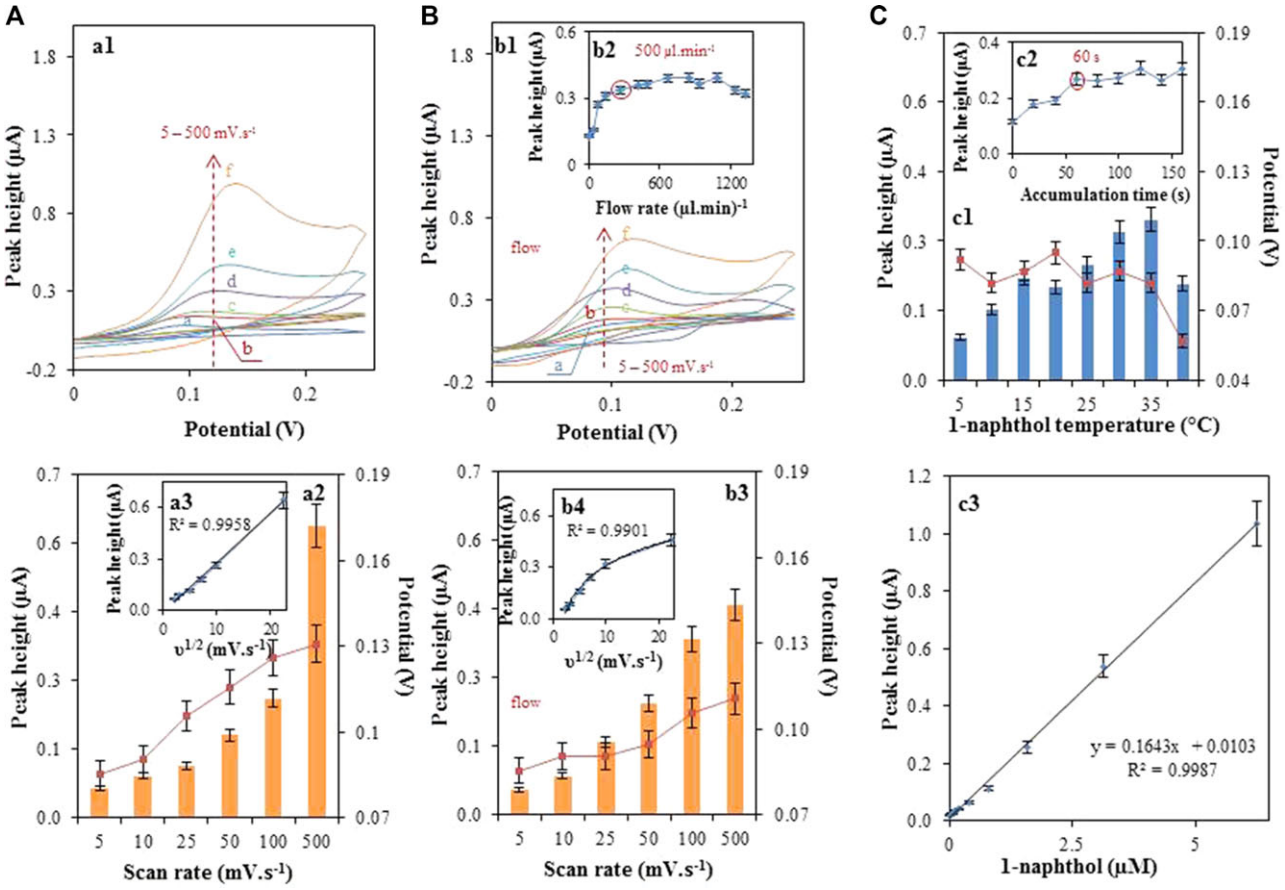

Figure 2. (A) Characterization of 1-naphthol analysis using SPEs. (a1) Cyclic voltammograms measured at different scan rates (mV/s), a = 5, b = 10, c = 25, d = 50, e = 100, and f = 500. (a2) The dependence of the peak height on applied scan rate (5–500 mV/s). (a3) The dependence of the peak height on square root of scan rate. (B) Characterization of 1-naphthol analysis in flow using SPEs. (b1) Cyclic voltammograms measured at different scan rates same as a1. (b2) The dependence of peak height on applied flow rate (0–1300 µL/min). (b3) The dependence peak height on square root of scan rate the flow 500 µL/min. (C) Optimization of measurement by DPV. (c1) The dependence of peak height on temperature (5, 10, 15, 20, 25, 30, 35, and 40°C). (c2) The dependence of peak height on accumulation time (0–120 s). (c3) Calibration curve of 1-naphthol obtained by DPV under the optimized conditions (measurement temperature 35°C, flow rate 500 µL/min, accumulation time 60 s). In all cases the electrochemical response of 10 mM 1-naphthol was studied.

Table 1. Analytical parameters of electrochemical determination of 1-naphthol

Substance	Regression equation	Linear dynamic range (µM)	R^2 a)	LOD b) (nM)	LOQ c) (nM)	RSD (%)
1-naphthol	$y = 0.1643x + 0.0103$	0.079–6.25	0.999	20	79	6.5

a) Regression coefficients.
b) LOD of detector (S/N = 3).
c) LOQ of detector (S/N = 10).

electrochemical charge are completely different from the values of unmodified MPs (Fig. 3D). The significant changes of electrochemical current levels (30 nA) are shown in Fig. 3E, and the charge is spreading out of larger area. SECM record of hyaluronic acid modified MPs shows little units of MP in current level of 80 nA (Fig. 3H). SECM scan of gold-modified MPs is depicting unequal precipitation of gold on the surface of MPs. The higher current level recorded in this case was 70 nA (Fig. 3J). The graphene-modified MPs create greater units with current level of about 70 nA (Fig. 3L). The MPs modified by graphene and glucose create similar aggregates as in the previous case. In addition, the electrochemical charges are overlaying themselves, thus, particular parts of MPs cannot be recognized (Fig. 3M). The SECM record of MPs modified by graphene and gold nanoparticles differs from other records. These MPs bind specifically to macroelectrode and the difference between gold macroelectrode and immobilized MPs is 10 nA.

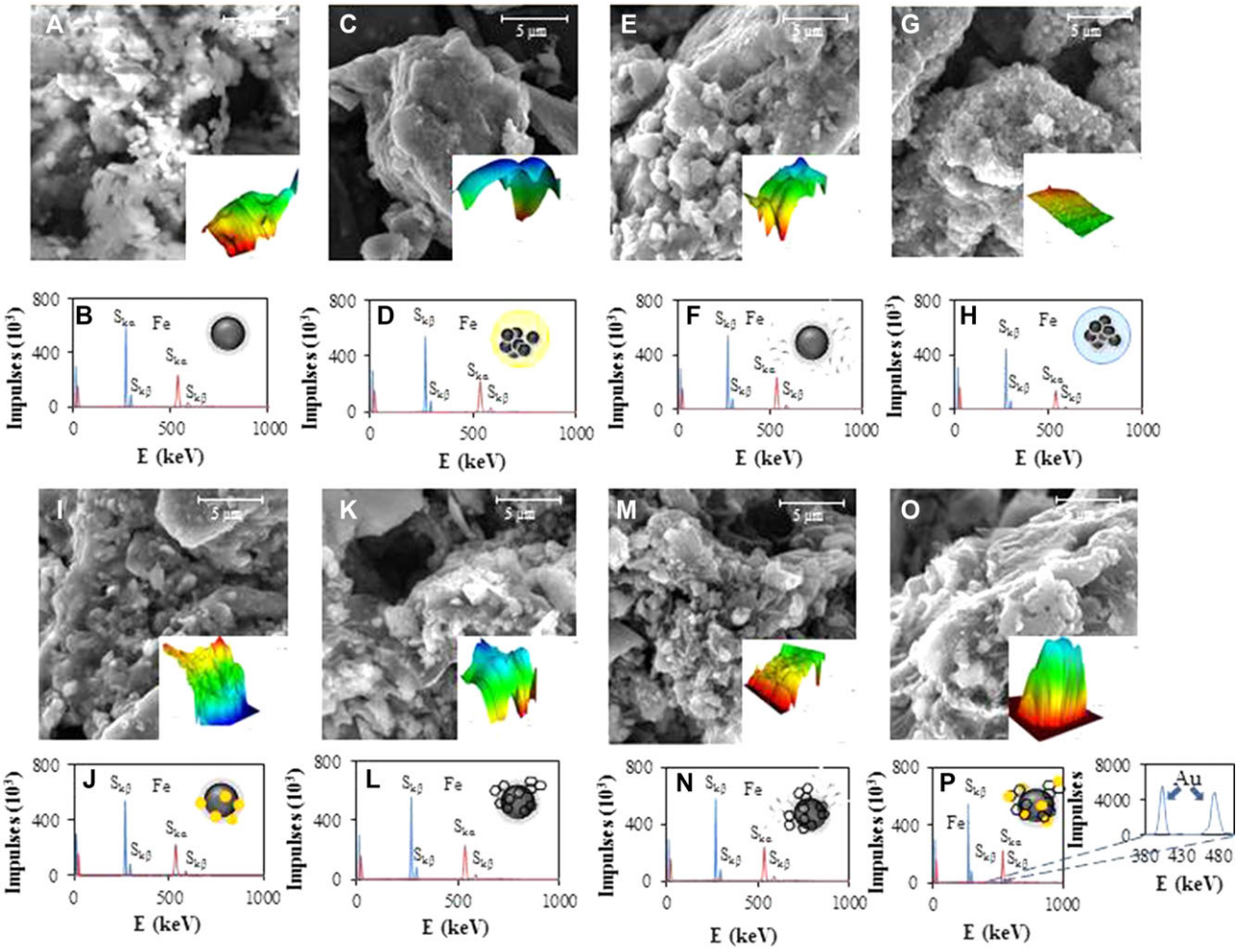

Figure 3. Characterization of different modifications of MPs. (A, B) Maghemite electron microscope image, 3D SECM image (range of current levels 10–80 nA) and XRF spectrum (with typical signals Skα and Skβ) of magnetic particles (MPs) without modification or modified with (C, D) 1% collagen, (E, F) 12.5 mg/mL glucose, (G, H) 12.5 mg/mL glucose and 1.25 mg/mL graphene, (I, J) gold nanoparticles (1 mM $HAuCl_4$), (K, L) 1.25 mg/mL graphene, (M, N) 20 mg/mL hyaluronic acid, and/or (O, P) 1.25 mg/mL graphene with gold nanoparticles (1 mM $HAuCl_4$).

3.4 Optimization of *S. aureus* isolation using modified MPs

The scheme of the sample preparation used for the analysis of growth curves is shown in Fig. 4A. Bacterial culture was isolated using magnetic separation. After separation of MPs from inoculated medium, incurred inoculum was measured under optimal conditions for 10 h (see Section 2.7). The absorbance values for *S. aureus* growth (volume 300 μL, amount of bacteria 3.7×10^7 CFU/mL) after application of 2.5 mg of MPs (1:1) modified in eight different ways were recorded (Fig. 4B-i). Stacked bar chart (Fig. 4J) shows the quantitative growth (CFU/mL) of *S. aureus* bacteria after cultivation on MPs, which differ by its modification. Recording of the CFU was conducted in the tenth hour of bacterial growth after cultivation with MPs according to scheme in Fig. 4A. Cultivation with MPs was run on a thermomixer at 20°C or at 37°C for 1 or 2 h at 600 rpm. The last suitable option for all modifications of MPs has proved application of the temperature of 20°C with the duration of the 1 h, when the number of bacteria in all MPs except MPs modified by graphene with glucose (1.3×10^8 CFU/mL) ranged from 6.7×10^7 to 8.6×10^7 CFU/mL. Another possibility was to apply temperature of 37°C, again with a shaking period of 1 h with the number of bacteria in the range of 7.5×10^7 to 12.3×10^7 CFU/mL. Increasing CFU at the temperature of 20°C with a shaking period of 2 h confirmed us the fact that for capturing the bacteria on MPs the duration of shaking period plays more important role than temperature. In the case of MPs modified by graphene and gold, number of bacteria is significantly lower (6.3×10^7 CFU/mL^{-1}), but in other modifications of MPs bacterial counts ranged from 8.7×10^7 to 12.6×10^7 CFU/mL. However, the highest number of bacteria was captured by the MPs at application of the temperature of 37°C with a shaking period of 2 h. MPs modified by graphene and gold again showed the lowest value (4.3×10^7 CFU/mL), but for other

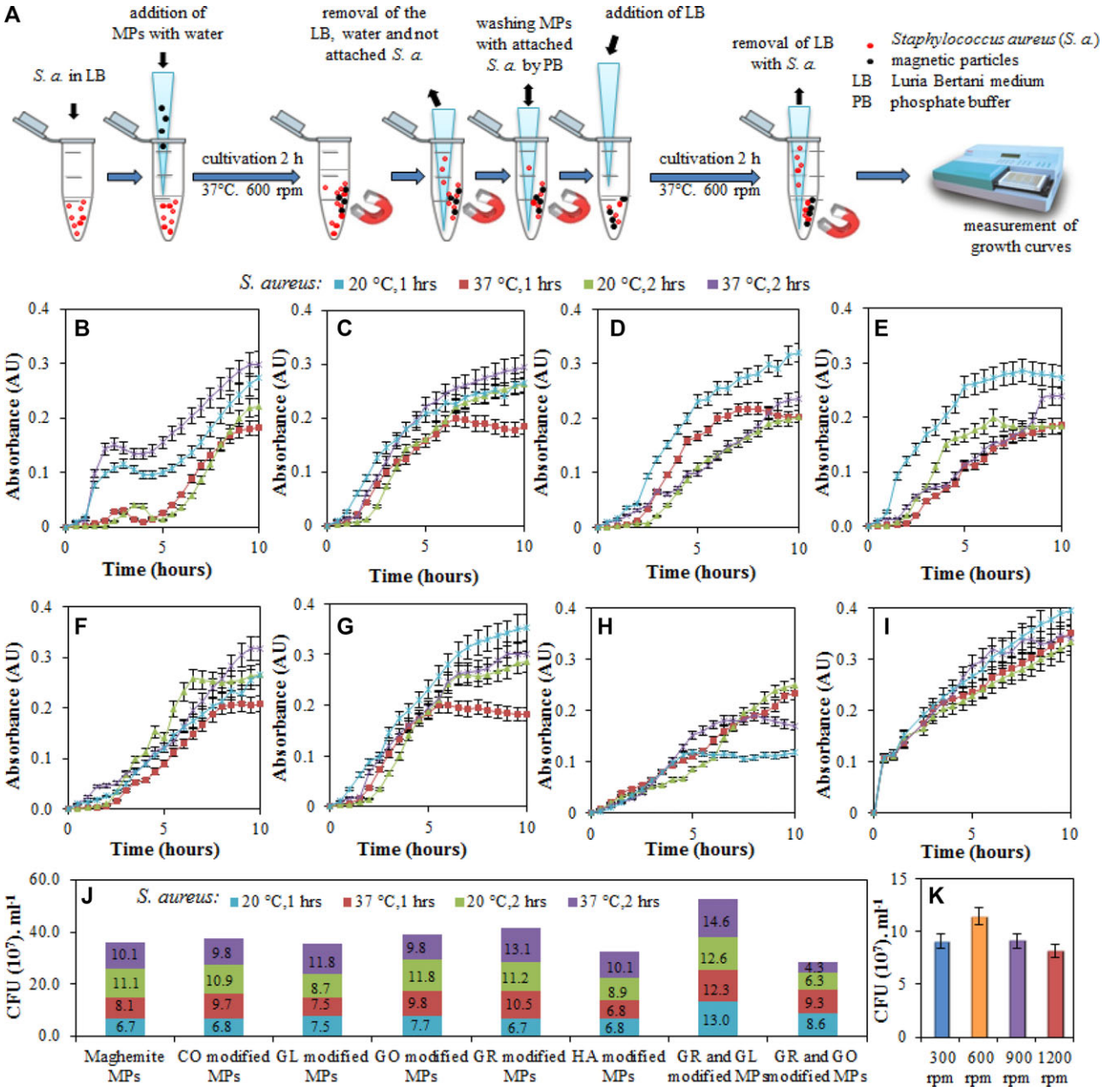

Figure 4. (A) The treatment of *S. aureus* with magnetic particles (MPs) before measurement of growth curves. (B) Dependence of washing buffer temperature and incubation time on *S. aureus* attached to MPs without modification, (C) collagen, (D) glucose, (E) graphene with gold nanoparticles, (F) gold nanoparticles, (G) graphene, (H) hyaluronic acid, (I) graphene with glucose. (J) Spectrophotometric determination of CFU 10^7 per microliter of *S. aureus* obtained by condition changes for different modified MPs (CO – collagen, GL – glucose, GO – gold nanoparticles, GR – graphene, HA – hyaluronic acid). (K) Spectrophotometric determination of CFU 10^7 per microliter of *S. aureus* affected by MPs modified with graphene and glucose after action of different intensity of rotation (300, 600, 900, and 1200 rpm).

modifications, the bacterial count was within the range from 9.8×10^7 to 14.6×10^7 CFU/mL. Best particles were determined as MPs modified by graphene with glucose, when the number of bacteria was determined as 1.46×10^8 CFU/mL after cultivation at 37°C for 2 h. By such modified MPs the bacterial count values were higher for all applied temperatures and time conditions. This variant was then used for the next steps of the study and was further tested for determination of the optimal number of rotation to achieve the highest yield in terms of the growth of *S. aureus* (Fig. 4K).

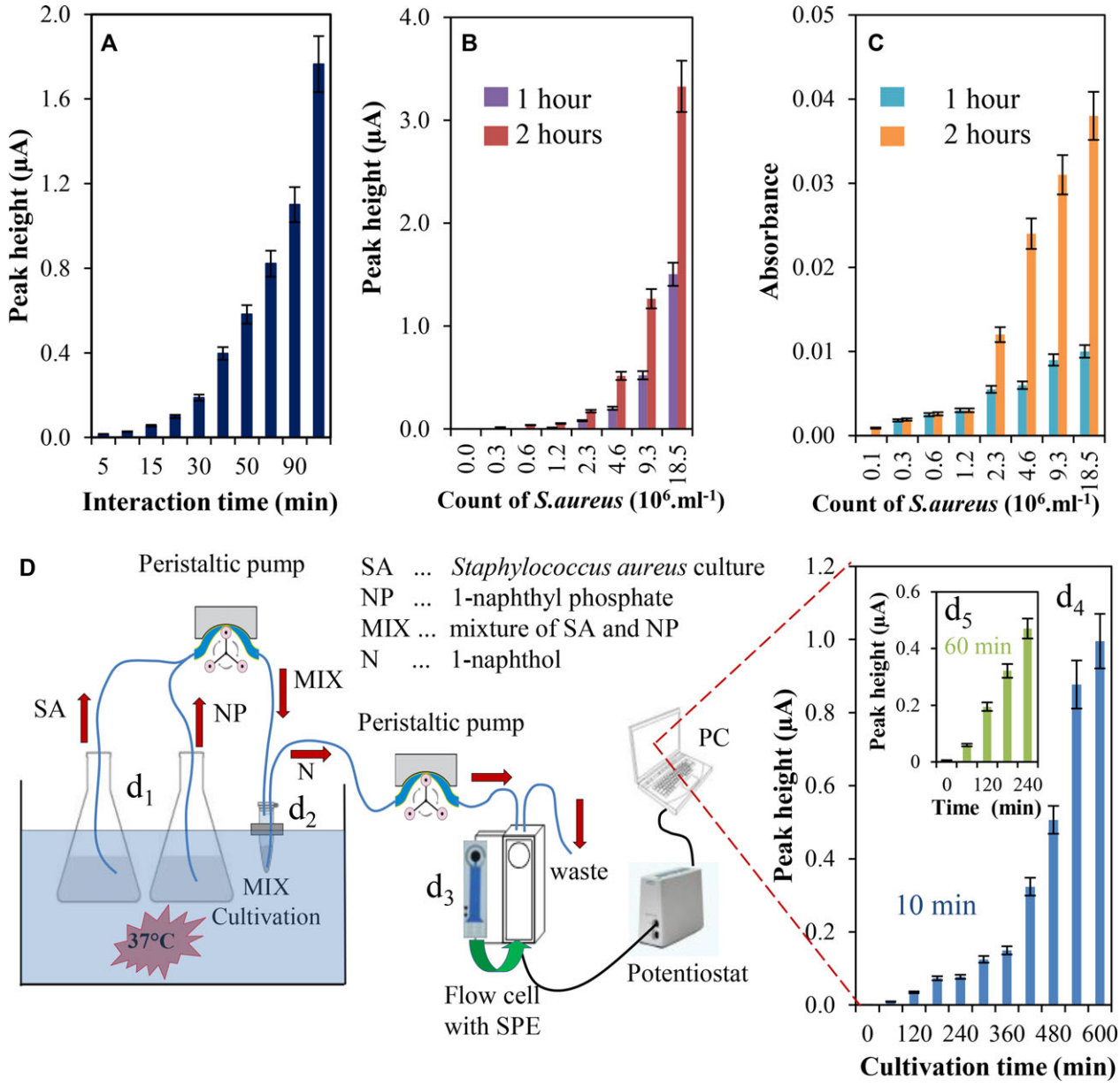

Figure 5. (A) The dependence of 1-naphthol peak height on time (5–120 min) of interaction between 1 mM 1-naphthyl phosphate and culture with same count of *S. aureus*. (B) Mixture of 1 mM 1-naphthyl phosphate and particular *S. aureus* culture was incubated for 1 h (violet line) and 2 h (red line). (C) The counts of *S. aureus* measured spectrometrically (λ = 600 nm) after 1 (blue line) and 2 h (orange line) of particular bacterial cell culture cultivation. (D) Scheme of the measuring system at laboratory conditions, d1 = stock solutions of *S. aureus* and 1 mM 1-naphthyl phosphate, d2 = mixing chamber, d3 = flow cell with screen printed electrode, d4 = in particular time part of growing *S. aureus* culture was mixed with 1-naphthyl phosphate and incubated for 10 and 60 min (d5).

3.5 Flow analysis of *S. aureus* using an automatic system

At first, the interaction time (5–120 min, 37°C) of 1 mM 1-naphthyl phosphate in 50 mM carbonate buffer (the substrate) and constant *S. aureus* concentration (18.5 × 10^6 per mL) was studied by electrochemistry. The electrochemical signal of 1-naphthol was increasing with the interaction time (Fig. 5A). One and/or 2 h long interaction (37°C) of different bacterial concentration (0–18.5 × 10^6 mL) with the substrate was investigated. More than 100% increase in electrochemical signal after 2 h of interaction was revealed (Fig. 5B), which corresponds to the reproducing *S. aureus* cells (Fig. 5C).

The optimization of the automatic flow system for *S. aureus* detection was performed. The scheme of this system is shown in Fig. 5D. *S. aureus* bacteria were attached to MPs modified with graphene and glucose according to previous optimization and were mixed with 19 mL of LBM (Fig. 5D-d1). LBM heated at 37°C in water bath and stirred by magnetic stirrer to aerate the medium. MPs were also attached by the

Table 2. Analytical parameters of electrochemical determination of bacteria

Substance	Regression equation	Linear dynamic range (bacteria)	R^2 a)	LOD b) (bacteria/μL)	LOQ c) (bacteria/μL)	RSD (%)
Bacteria – ALP	$y = 0.1788x - 0.1481$	120–18.5 × 106	0.9828	30	120	8.5

a) Regression coefficients.
b) LOD of detector (S/N = 3).
c) LOQ of detector (S/N = 10).

stirrer so that MPs could not affect the electroanalysis. The substrate (37°C) together with bacterial culture was pumped to the reaction chamber (Fig. 5D-d2) by peristaltic pump. The multichannel peristaltic pump was used and tubes of the same length and diameter were dosing the substrate and analyte precisely (1:1). The mixture of uncleaved substrate, *S. aureus*, LBM, and finally 1-naphthol was pumped to flow detection cell by another peristaltic pump at flow rate of 500 μL/min (Fig. 5D-d3). After 10 (Fig. 5D-d4) and 60 min long interaction (Fig. 5D-d5) the signal of 1-naphthol was analyzed. The LOD and LOQ was estimated as 3 S/N (Table 2).

3.6. ORPHEUS-HOPE

ORPHEUS-HOPE is a rugged robotic system designed to measure bacterial contamination in field conditions and can be easily equipped with additional devices, such as radiation and biological sensors. The robot is able to go across obstacles up to 20 cm high and work well during night or in bad visibility conditions, because it has sensitive full user control. The maximum ascension angle is 31° and is limited only by adhesion. Robot performs well in mud and snow, but it is also fully capable of indoor operation. Even the control of the robot is ready for narrow space operations, the operator can reverse the control of the robot, thus it can switch the meaning of forward and backward. The robot itself is made to be easy-to-decontaminate. The whole robot is waterproof, with three-layers resistive paintings and the whole mechanical construction is made to repel or at least not keep liquids. Only few parts of the robot are marked as nondecontaminable and have to be replaced (tires, antennas, and two cables). The robot may be operated wirelessly or by wire. Designed for compliance with various MIL-STD-810F environmental and MIL-STD-461E EMI/EMC standards, the ORPHEUS-HOPE robotic system offers exceptional low-temperature operation and resistance to shock and vibration profiles experienced by jet and terrestrial transport. The robot is equipped with two cameras: the first pan/tilt color camera with both manual and automatic parameter settings, and the second rigid high resolution color camera for precise analyte placement and measurement. The robot has one degree of freedom (DOF) manipulator with suction device, while other sensors can be either rigidly connected to the robot body or also placed on the manipulator. The maximum payload on the end of the manipulator is 0.85 kg.

The robot may be controlled with the help of so-called visual telepresence. The operator wears head mounted display (HMD) with inertial measurement unit (IMU) as shown in Fig. 6A. The head-movement data from the IMU are mathematically transformed and sent to the robot. The robot has a camera manipulator with two DOFs (left-to-right and up-to-down). The camera manipulator basically copies movements of the operator's head, while the image from the camera is transmitted to the operator's station and displayed to the operator. Therefore, the operator should feel to be in the robot's place and can intuitively control the main camera movements.

One of the key issues of ORPHEUS-HOPE project is precise "manipulation" with the suction device (Fig. 6B). Positioning of the suction device is performed in four DOFs. In general we are able to move on the Earth's surface and control the "deepness" of the suction device penetration to the liquid. All of these movements have to be precise to be able to achieve precise detection in various conditions. The necessary precision is in the order of millimetres. The control of the robot is currently provided by an operator. Thus, the feedback control loop consists of mechanical parts (motors, gearboxes, and wheels), and electronics, but also human-to-robot user interface and the operator itself.

Rugged operator's station (Fig. 6A-d) was made to control the robot in tactical conditions. The operator's station is battery operated, but may work also continuously when connected to DC power. It is made to allow easy and intuitive operation control of the robot. The movements of robot body are controlled by a joystick, and the other functions are controlled by a series of buttons.

The electronics system of ORPEHUS-HOPE is distributed, and all communication is done via Ethernet or RS-485. Freescale Coldfire microcontroller is responsible for motor control and accelerometer data acquisition, Rabbit microcontroller communicates to the chemical analysis sensors. The cameras and microphone are connected to axis framegrabber. All the main processors, as well as the wireless module are connected to the 5-port miniature Ethernet switch.

3.7 Remote controlled detection of *S. aureus*

Automated analysis of sample containing *S. aureus* bacteria is performed by ORPHEUS-HOPE robotic platform, which is equipped with a flow detection device (Fig. 7A) including the MPs within a chip. The detection flow device consists of a movable robotic arm (Fig. 7A-a), which enables to dip a suction tube (Fig. 7A-b) into the liquid. The resistance detector is responsible for a precise suction tube immersion to analyte. The depth of suction tube immersion can also

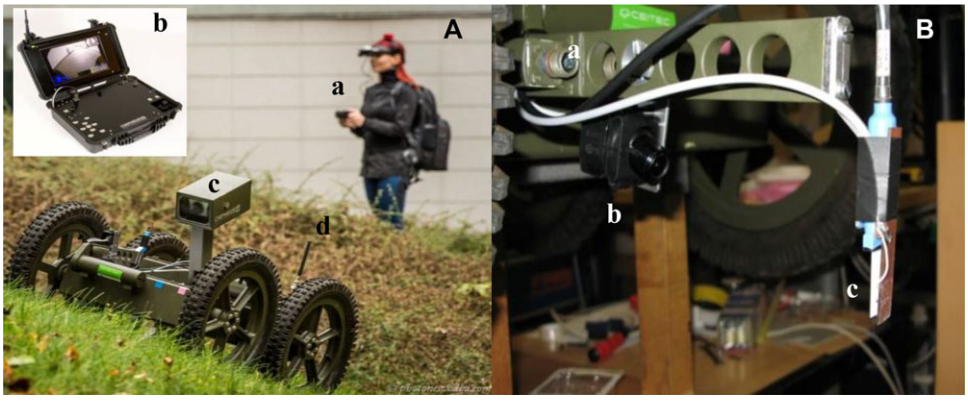

Figure 6. (A) Remote control of ORPHEUS-HOPE (robot dimensions: 881 × 590 × 426 mm, wheel diameter: 426 mm, weight: 42 kg, battery operation: 90 min to 4 h, operating temperatures: −32 to 78°C, charging voltage: 18–32 V, max. charging current: 5 A, max. speed: 3.6 km/h, max. obstacle height: 20 cm, climb ability: 31°, max. reach of cable: 100 m, wireless max. reach: 1 km). Person (a) with joystick and HMD with IMU, which receives signal from camera (b) with two degrees of freedom via wireless transmitter (c). Rugged operator's station (b), which enables to control the robot in tactical conditions. (B) Sensor arm (a) with video camera (b), suction device and submerge detector (c).

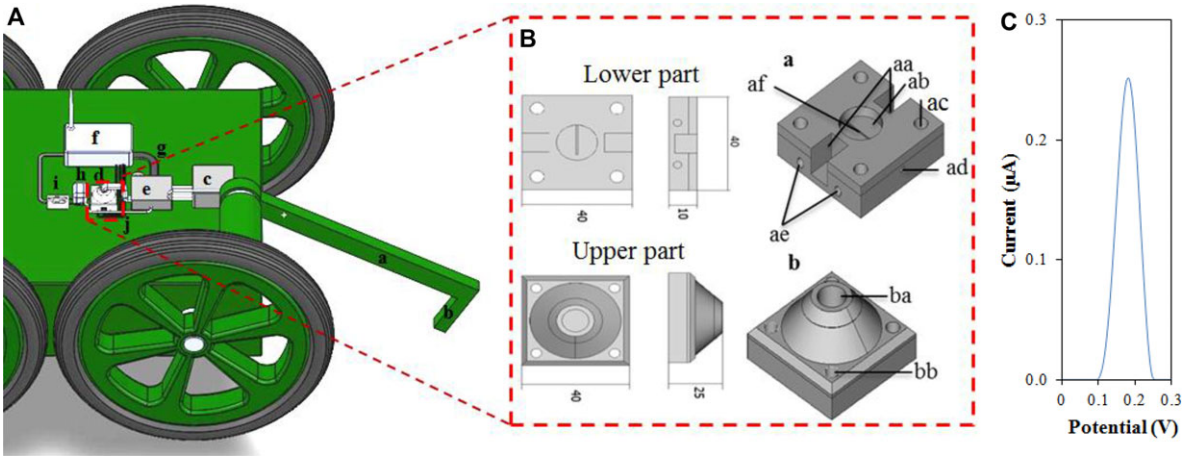

Figure 7. (A) Manipulator (a) with suction device (b) collects the samples of potentially contaminated water with *S. aureus*. It goes through peristaltic pump (c) in tube to cultivation chamber (d) with magnetic particles (MPs) inside, where *S. aureus* is attached to particles. Excess of water is pumped from cultivation chamber to the waste collector (e) by peristaltic pump, which receives instructions from control unit with integrated potentiostat (f) via communication wires (g). Then, LBM is pumped to cultivation chamber (d) from waste collector (e), which serves also as a reagent stock. After several hours of *S. aureus* reproducing, culture is mixed with 1-naphthyl phosphate in a mixing chamber (h). After particular time of alkaline phosphatase (ALP) cleaving of 1-naphthyl phosphate to 1-naphthol, mixture is pumped to flow cell (i), where 1-naphthol can be detected by potentiostat (f). The waste goes through tube (j) to the waste collector (e). The control unit with an integrated potentiostat (Fig. 7AB/a-f) controls actions of peristaltic pump, heating of the chip and magnetic stirring within the chip. The control unit is thus responsible for the alternate turning off and the turning on of the electromagnets. (B) Scheme of the cultivation chip: (a) Lower part of the chip. Places for electromagnets (aa), cultivation chamber (ab), holes for attaching with the cover (ac), the hole for temperature symbol (ad), holes for heating elements (ae) and the outflow canal (af). (b) Upper part of the chip. Hole for injection needles (ba) and holes for attaching to lower part of the chip (bb). (C) DPV signal of 1-naphthol, confirming the presence of bacteria in the sample.

be controlled visually by robotic arm camera. The peristaltic pump (Fig. 7A-c) doses stock solution of the substrate (1-naphthyl phosphate in 50 mM carbonate buffer, pH 9.9) to a cultivation chip (Fig. 7A-d). The control unit with an integrated potentiostat (Fig. 7A-f) controls actions of peristaltic pump, heating of the chip, and magnetic stirring within the chip. All electronic devices are connected via communication cables (Fig. 7A-g). The analyzed sample is mixed with substrate (1:1) in the reaction chamber (Fig. 7A-h) and the mixture is cultivated there for 1 h, then it is pumped with a speed of 500 µL/min to a flow electrode cell (Fig. 7A-i), where electrochemical detection takes place at accumulation time of 60 s.

Cultivation chip consists of two parts (Fig. 7B-a and B-b). Lower part of the chip includes two opposite holes, where two electromagnets are placed (Fig. 7B-aa) next to cultivation chamber of 500 µL volume (Fig. 7B-ab). Every corner has hole to merge upper and lower part of the chip

(Fig. 7B-ac). A thermistor is placed under the cultivation chamber to control the temperature of the chip, which was set to 37°C (Fig. 7B-ad), and the heating elements on the sides of chip (Fig. 7B-ae). The outflow canal is placed in the lower part of the chip (Fig. 7B-af). The upper part of the chip has hole for inflow tube (Fig. 7B-ba) and also holes for the lower part attachment (Fig. 7B-bb).

Robotic remote controlled analysis of *S. aureus* sample (30 cells/μL) was performed automatically. The sample (500 μL) was pumped via suction device to the cultivation chamber, where *S. aureus* was attached to MPs. After attaching period, the excess of solution was pumped to waste collector and LBM (600 μL) was pumped there. During cultivation time (2 h) the sample was stirred. Then, the sample was mixed with substrate for 1 h in mixing chamber. Finally, the sample was pumped (500 μL/min) to flow cell with electrode and electrochemical signal, which detected the presence of bacteria, was recorded at accumulation time of 60 s (Fig. 7C).

4 Discussion

In this study, the remote detection of the bacterial contamination using a microfluidic chip is showed. Automatic detection of microorganisms on the mobile unit allows sampling and determination of the presence of microorganisms in the hardly accessible environment. Mobile unit with a detection device controlled remotely by human is demanding on simple and reliable samples processing and detection itself [53, 54]. Detection of bacterial contamination by classic methods is generally time-consuming and hardly automated, as well as immuno- and PCR-based techniques. Alkaline phosphatase is a thermostable enzyme, which is active in extreme temperatures, even at 308°C [19]. It is produced by wide range of bacteria and archaebacteria [55] and it has been shown that the phosphatases can be used as a marker of life in extreme conditions [55]. Electrochemical detection of ALP using a 1-naphthyl-phosphate is a commonly used and elaborated detection step in electrochemical sensors and immunoassays [44, 56].

The detection limit of 30 bacterial cells per microliter was obtained, which is approximately 50 times higher than beads-based immunoextraction technique for *S. aureus* detection, but the detection limit in this work was obtained after 2 h of cultivation, while in work from Krizkova et al. the enrichment cultivation was performed for 5 h [14]. Whole protocol was possible to realize by remote-controlled robot, which makes it usable for monitoring of distant areas without contamination. Moreover, the process can be easily modified by addition of a specific substrate or an inhibition agent. There are two possibilities how to improve our system for handling several samples. The first possibility is to use a rinsing mechanism with ethanol. The second possibility is to involve several chambers (ca. 10) and each chamber would be used only once.

Wagstaffe et al. developed determination of *S. aureus* in a liquid medium by method based on fluorescence immunoassay, which allows the detection of thermonuclease enzyme produced by *S. aureus* and thus provides confirmation of the presence of *S. aureus* in vitro [57]. The work of Valeriani et al. dealt with methods for the rapid control of the aquatic environment intended for recreational purposes. Their goal was to find a rapid and reliable method for identification of low concentrations of the bacteria *S. aureus*. Using traditional culture microbiological methods is time consuming and therefore molecular techniques are a better choice. Approach of these authors is based on the specific amplification of genomic DNA using the universal primers (23S rDNA), and specific real-time PCR amplification. This procedure refers to the high sensitivity and specificity, which is typical for nucleic acids. The method is suitable for monitoring hygiene and detection of indicators of bacterial pollution [58].

Sensitive method based on fluorescence of carboxymethyl chitosan with cadmium nanoparticles (CMC-CD QDS) was developed by Wang et al. for the specific detection of *S. aureus* in foods and the environment. After a certain period of cultivation of CMC-Cd QDs with *S. aureus* and after removal of the free fluorescent QDs, the bacteria were observed by fluorescence microscopy. The cells of *S. aureus* were recognized as being applicable bioprobes. Using this method, the authors also managed to identify *E. coli* and *Bacillus subtilis* [59].

LaGier et al. aimed at studying the purity and water quality. They decided to develop a biosensor to achieve rapid identification of on-site sampling. The sensor device can simultaneously detect harmful algae, indicators of faecal pollution, and human pathogens in water. The sensor is capable of electrochemical detection of the presence of nucleic acids for matching parameters such as the size, low cost, and low power requirements [60].

In the above mentioned methods, tedious sample preparation procedures are used and a lot of expensive chemicals are required, whereas the capture of bacteria on the MPs and their subsequent proliferation in culture medium and electrochemical detection represents another way, which is unique in its simplicity, versatility, and feasibility.

In summary, due to the availability of technologies, and even more sophisticated detection techniques (lab-on-a-chip) that are compatible with different types of robotic platforms (lab-on-a-robot), it can be expected that the development of remote-controlled robotic systems will be of interest for more and more research teams. In this study, we develop a robotic platform ORPHEUS-HOPE, which can carry different types of detectors. The robot is manufactured as a highly reliable device and meets the requirements of military standards. For this reason robotic platform was designed and printed by a 3D printer. A flow chip was used for electrochemical detection of bacteria. The low chip was completed with the modified MPs that allow capturing and cultivating bacteria inside the chip. In addition, we automated detection system for remote detection of bacteria.

Financial support from the project CEITEC CZ.1.05/1.1.00/02.0068 is highly acknowledged. The authors wish to express their

thanks also to Jan Zitka, Lukas Zima, Martina Stankova, Lukas Melichar, and Radek Chmela for perfect technical assistance.

The authors have declared no conflict of interest.

5 References

[1] Noyhouzer, T., Mandler, D., *Electroanalysis* 2013, *25*, 109–115.

[2] Kimura, R., Yoshida, T., *J. Nucl. Sci. Technol.* 2013, *50*, 998–1010.

[3] Crisler, J. D., Newville, T. M., Chen, F., Clark, B. C., Schneegurt, M. A., *Astrobiology* 2012, *12*, 98–106.

[4] Kounaves, S. P., Hecht, M. H., West, S. J., Morookian, J. M., Young, S. M. M., Quinn, R., Grunthaner, P., Wen, X. W., Weilert, M., Cable, C. A., Fisher, A., Gospodinova, K., Kapit, J., Stroble, S., Hsu, P. C., Clark, B. C., Ming, D. W., Smith, P. H., *J. Geophys. Res.-Planets* 2009, *114*, 1–12.

[5] Bish, D. L., Blake, D. F., Vaniman, D. T., Chipera, S. J., Morris, R. V., Ming, D. W., Treiman, A. H., Sarrazin, P., Morrison, S. M., Downs, R. T., Achilles, C. N., Yen, A. S., Bristow, T. F., Crisp, J. A., Morookian, J. M., Farmer, J. D., Rampe, E. B., Stolper, E. M., Spanovich, N., *Science* 2013, *341*, 1–5.

[6] Meslin, P. Y., Gasnault, O., Forni, O., Schroder, S., Cousin, A., Berger, G., Clegg, S. M., Lasue, J., Maurice, S., Sautter, V., Le Mouelic, S., Wiens, R. C., Fabre, C., Goetz, W., Bish, D., Mangold, N., Ehlmann, B., Lanza, N., Harri, A. M., Anderson, R., Rampe, E., McConnochie, T. H., Pinet, P., Blaney, D., Leveille, R., Archer, D., Barraclough, B., Bender, S., Blake, D., Blank, J. G., Bridges, N., Clark, B. C., DeFlores, L., Delapp, D., Dromart, G., Dyar, M. D., Fisk, M., Gondet, B., Grotzinger, J., Herkenhoff, K., Johnson, J., Lacour, J. L., Langevin, Y., Leshin, L., Lewin, E., Madsen, M. B., Melikechi, N., Mezzacappa, A., Mischna, M. A., Moores, J. E., Newsom, H., Ollila, A., Perez, R., Renno, N., Sirven, J. B., Tokar, R., de la Torre, M., d'Uston, L., Vaniman, D., Yingst, A., *Science* 2013, *341*, 1–6.

[7] Stolper, E. M., Baker, M. B., Newcombe, M. E., Schmidt, M. E., Treiman, A. H., Cousin, A., Dyar, M. D., Fisk, M. R., Gellert, R., King, P. L., Leshin, L., Maurice, S., McLennan, S. M., Minitti, M. E., Perrett, G., Rowland, S., Sautter, V., Wiens, R. C., *Science* 2013, *341*, 1–4.

[8] Lukow, S. R., Kounaves, S. R., *Electroanalysis* 2005, *17*, 1441–1449.

[9] Onstott, T. C., McGown, D. J., Bakermans, C., Ruskeeniemi, T., Ahonen, L., Telling, J., Soffientino, B., Pfiffner, S. M., Sherwood-Lollar, B., Frape, S., Stotler, R., Johnson, E. J., Vishnivetskaya, T. A., Rothmel, R., Pratt, L. M., *Microb. Ecol.* 2009, *58*, 786–807.

[10] Chander, R., Thomas, P., *J. Food Biochem.* 2001, *25*, 91–103.

[11] Santos, I. C., Mesquita, R. B. R., Bordalo, A. A., Rangel, A., *Talanta* 2012, *98*, 203–210.

[12] Nicolaus, B., Moriello, V. S., Lama, L., Poli, A., Gambacorta, A., *Orig. Life Evol. Biosph.* 2004, *34*, 159–169.

[13] Seckbach, J., Oren, A., in: Hoover, R. B. (Ed.), *Instruments, Methods, and Missions for Astrobiology III*, Spie-Int Soc Optical Engineering, Bellingham 2000, pp. 89–95.

[14] Krizkova, S., Jilkova, E., Krejcova, L., Cernei, N., Hynek, D., Ruttkay-Nedecky, B., Sochor, J., Kynicky, J., Adam, V., Kizek, R., *Electrophoresis* 2013, *34*, 224–234.

[15] Panosian, T. D., Nannemann, D. P., Watkins, G. R., Phelan, V. V., McDonald, W. H., Wadzinski, B. E., Bachmann, B. O., Iverson, T. M., *J. Biol. Chem.* 2011, *286*, 8043–8054.

[16] Iverson, T. M., Panosian, T. D., Birmingham, W. R., Nannemann, D. P., Bachmann, B. O., *Biochemistry* 2012, *51*, 1964–1975.

[17] Ramesh, A., Sharma, S. K., Joshi, O. P., Khan, I. R., *Indian J. Microbiol.* 2011, *51*, 94–99.

[18] Koksharov, M., Lv, C. Q., Zhai, X. H., Ugarova, N., Huang, E., *Protein Expr. Purif.* 2013, *90*, 186–194.

[19] Takano, Y., Edazawa, Y., Kobayashi, K., Urabe, T., Marumo, K., *Earth Planet. Sci. Lett.* 2005, *229*, 193–203.

[20] Nitzan, Y., Ashkenazi, H., *Photochem. Photobiol.* 1999, *69*, 505–510.

[21] Brim, H., McFarlan, S. C., Fredrickson, J. K., Minton, K. W., Zhai, M., Wackett, L. P., Daly, M. J., *Nat. Biotechnol.* 2000, *18*, 85–90.

[22] Sghaier, H., Bouchami, O., Desler, C., Lazim, H., Saidi, M., Rasmussen, L. J., Ben Hassen, A., *Ann. Microbiol.* 2012, *62*, 493–500.

[23] Wang, J., *Electroanalysis* 2005, *17*, 1133–1140.

[24] Vandaveer, W. R., Pasas-Farmer, S. A., Fischer, D. J., Frankenfeld, C. N., Lunte, S. M., *Electrophoresis* 2004, *25*, 3528–3549.

[25] Nugen, S. R., Asiello, P. J., Connelly, J. T., Baeumner, A. J., *Biosens. Bioelectron.* 2009, *24*, 2428–2433.

[26] Garcia, C. D., Henry, C. S., *Electroanalysis* 2005, *17*, 1125–1131.

[27] Garcia, C. D., Henry, C. S., *Electroanalysis* 2005, *17*, 223–230.

[28] Zhao, L. L., Lee, V. K., Yoo, S. S., Dai, G. H., Intes, X., *Biomaterials* 2012, *33*, 5325–5332.

[29] Dragone, V., Sans, V., Rosnes, M. H., Kitson, P. J., Cronin, L., *Beilstein J. Org. Chem.* 2013, *9*, 951–959.

[30] Mathieson, J. S., Rosnes, M. H., Sans, V., Kitson, P. J., Cronin, L., *Beilstein J. Nanotechnol.* 2013, *4*, 285–291.

[31] Kitson, P. J., Rosnes, M. H., Sans, V., Dragone, V., Cronin, L., *Lab. Chip.* 2012, *12*, 3267–3271.

[32] Lamberti, F., Sanna, A., Paravati, G., Montuschi, P., Gatteschi, V., Demartini, C., *Int. J. Adv. Robot. Syst.* 2013, *10*, 1–11.

[33] Berg, C., Valdez, D. C., Bergeron, P., Mora, M. F., Garcia, C. D., Ayon, A., *Electrophoresis* 2008, *29*, 4914–4921.

[34] Wang, J., Pumera, M., Chatrathia, M. P., Rodriguez, A., Spillman, S., Martin, R. S., Lunte, S. M., *Electroanalysis* 2002, *14*, 1251–1255.

[35] Tao, W. J., Ou, Y., Feng, H. T., *Int. J. Adv. Robot. Syst.* 2012, *9*, 1–9.

[36] Dobie, G., Pierce, S. G., Hayward, G., *NDT E Int.* 2013, *58*, 10–17.

[37] Kulich, M., Chudoba, J., Kosnar, K., Krajnik, T., Faigl, J., Preucil, L., *IEEE Trans. Educ.* 2013, *56*, 18–23.

[38] Li, D. R., Liu, Y., Yuan, X. X., *Sci. China-Inf. Sci.* 2013, *56*, 1–14.

[39] Susperregi, L., Martinez-Otzeta, J. M., Ansuategui, A., Ibarguren, A., Sierra, B., *Int. J. Adv. Robot. Syst.* 2013, *10*, 1–9.

[40] da Costa, E. T., Neves, C. A., Hotta, G. M., Vidal, D. T. R., Barros, M. F., Ayon, A. A., Garcia, C. D., do Lago, C. L., *Electrophoresis* 2012, *33*, 2650–2659.

[41] Valdez, D. C., Garcia, C. D., Ayon, A. A., *Analog Integr. Circuits Process* 2012, *71*, 29–38.

[42] Prasek, J., Trnkova, L., Gablech, I., Businova, P., Drbohlavova, J., Chomoucka, J., Adam, V., Kizek, R., Hubalek, J., *Int. J. Electrochem. Sci.* 2012, *7*, 1785–1801.

[43] Nejdl, L., Merlos, M. A. R., Kudr, J., Ruttkay-Nedecky, B., Konecna, M., Kopel, P., Zitka, O., Hubalek, J., Kizek, R., Adam, V., *Electrophoresis* 2014, *35*, 393–404.

[44] Zitka, O., Krizkova, S., Krejcova, L., Hynek, D., Gumulec, J., Masarik, M., Sochor, J., Adam, V., Hubalek, J., Trnkova, L., Kizek, R., *Electrophoresis* 2011, *32*, 3207–3220.

[45] Magro, M., Sinigaglia, G., Nodari, L., Tucek, J., Polakova, K., Marusak, Z., Cardillo, S., Salviulo, G., Russo, U., Stevanato, R., Zboril, R., Vianello, F., *Acta Biomater.* 2012, *8*, 2068–2076.

[46] Prucek, R., Tucek, J., Kilianova, M., Panacek, A., Kvitek, L., Filip, J., Kolar, M., Tomankova, K., Zboril, R., *Biomaterials* 2011, *32*, 4704–4713.

[47] Hummers, W. S., Offeman, R. E., *J. Am. Chem. Soc.* 1958, *80*, 1339–1339.

[48] Stankovich, S., Dikin, D. A., Piner, R. D., Kohlhaas, K. A., Kleinhammes, A., Jia, Y., Wu, Y., Nguyen, S. T., Ruoff, R. S., *Carbon* 2007, *45*, 1558–1565.

[49] Long, G. L., Winefordner, J. D., *Anal. Chem.* 1983, *55*, A712–A724.

[50] Paleček, E., Kizek, R., Havran, L., Billova, S., Fojta, M., *Anal. Chim. Acta* 2002, *469*, 73–83.

[51] Laurent, S., Forge, D., Port, M., Roch, A., Robic, C., Elst, L. V., Muller, R. N., *Chem. Rev.* 2008, *108*, 2064–2110.

[52] Gupta, A. K., Naregalkar, R. R., Vaidya, V. D., Gupta, M., *Nanomedicine* 2007, *2*, 23–39.

[53] Karl, D. M., *Nat. Rev. Microbiol.* 2007, *5*, 759–769.

[54] Foing, B. H., Stoker, C., Zavaleta, J., Ehrenfreund, P., Thiel, C., Sarrazin, P., Blake, D., Page, J., Pletser, V., Hendrikse, J., Direito, S., Kotler, J. M., Martins, Z., Orzechowska, G., Gross, C., Wendt, L., Clarke, J., Borst, A. M., Peters, S. T. M., Wilhelm, M. B., Davies, G. R., Team, I. E., *Int. J. Astrobiol.* 2011, *10*, 141–160.

[55] Baltar, F., Aristegui, J., Gasol, J. M., Yokokawa, T., Herndl, G. J., *Microb. Ecol.* 2013, *65*, 277–288.

[56] Hayat, A., Andreescu, S., *Anal. Chem.* 2013, *85*, 10028–10032.

[57] Wagstaffe, S. J., Hill, K. E., Williams, D. W., Randle, B. J., Thomas, D. W., Stephens, P., Riley, D. J., *Anal. Chem.* 2012, *84*, 5876–5884.

[58] Valeriani, F., Giampaoli, S., Buggiotti, L., Gianfranceschi, G., Spica, V. R., *Water Sci. Technol.* 2012, *66*, 2305–2310.

[59] Wang, X. H., Du, Y. M., Li, Y., Li, D., Sun, R. C., *J. Biomater. Sci.Polym. Ed.* 2011, *22*, 1881–1893.

[60] LaGier, M. J., Jack, W. F. B., Goodwin, K. D., *Mar. Pollut. Bull.* 2007, *54*, 757–770.

6 ZÁVĚR

Znečištění životního prostředí se stalo během 21. století závažným problémem. Odpovědný přístup k otázkám ochrany životního prostředí je zárukou zachování trvale udržitelného rozvoje a zachování zdrojů pro následující generace. Kontinuální monitorování stavu životního prostředí z hlediska přítomnosti polutantů a jejich koncentrací je prvním krokem v řadě s cílem snížit zatěžování prostředí chemickými látkami.

Elektroanalytické metody jsou vhodným nástrojem pro environmentální analýzy. Jejich dostatečná selektivita umožňuje měřit i v složitých matricích, typických pro reálné vzorky. V minulosti bylo mnohokrát prokázáno, že elektroanalytické metody jsou z hlediska dosahovaných detekčních limitů vhodným nástrojem pro analýzu těžkých kovů. Na druhou stranu, koncentrace těžkých kovů v běžných reálných vzorcích jsou nízké. Jak bylo v předložené práci prokázáno, použití redukovaného grafen oxidu jako modifikátoru pracovní elektrody je vhodným nástrojem ke zlepšení analytických vlastností elektrody k iontům těžkých kovů.

Elektrochemická instrumentace je poměrně levná a jednoduchá, což se odráží v tendencích vyvíjet automatizované elektrochemické analytické systémy a systémy schopné provádět *in situ* analýzy. V rámci publikací přiložených k disertační práci byly představeny automatizované metody pro analýzu iontů těžkých kovů a bakteriální kontaminace (*Staphylococcus aureus).* V prvním případě se jednalo o softwarem řízený polohovací systém, který umožňoval tříelektrodovému elektrochemickému detektoru pohyb mezi vzorky umístěnými v mikrotitrační destičce. Ionty Cd(II), Cu(II), Zn(II) a Pb(II) byly detekovány pomocí rtuťovým filmem modifikované uhlíkové elektrody. K detekci bakterií *S. aureus* byl sestaven automatizovaný průtokový systém, který využíval přeměnu elektrochemicky neaktivního naftyl fosfátu na elektrochemicky aktivní 1-naftol bakteriálním enzymem – alkalickou fosfatázou. Tento systém byl schopen stanovit 30 bakterií *S. aureus* v 1 μl. Alternativní způsob detekce bakteriální kontaminace (tj. na bázi detekce DNA) byl založen na separaci cílové sekvence pomocí magnetických mikročástic a jejím označení oligonukleotidovou sondou s navázaným komplexem osmia jako elektrochemicky aktivní značkou.

7 LITERATURA

ADAM, V., PETRLOVA, J., POTESIL, D., ZEHNALEK, J., SURES, B., TRNKOVA, L., JELEN, F. a KIZEK, R. Study of metallothionein modified electrode surface behavior in the presence of heavy metal ions-biosensor. *Electroanalysis*, 2005, roč. 17. č. 18, s. 1649-1657.

AIBAIDULA, A., ZHAO, W., WU, J. S., CHEN, H., SHI, Z. F., ZHENG, L. L., MAO, Y., ZHOU, L. F. a SUI, G. D. Microfluidics for rapid detection of isocitrate dehydrogenase 1 mutation for intraoperative application. *Journal of Neurosurgery*, 2016, roč. 124. č. 6, s. 1611-1618.

BELTAGI, A. M. a GHONEIM, M. M. Simultaneous determination of trace aluminum (III), copper (II) and cadmium (II) in water samples by square-wave adsorptive cathodic stripping voltammetry in the presence of oxine. *Journal of Applied Electrochemistry*, 2009, roč. 39. č. 5, s. 627-636.

CARUGO, D., BOTTARO, E., OWEN, J., STRIDE, E. a NASTRUZZI, C. Liposome production by microfluidics: potential and limiting factors. *Scientific Reports*, 2016, roč. 6.

CUI, N. W., ZHANG, H. D., SCHNEIDER, N., TAO, Y., ASAHARA, H., SUN, Z. Y., CAI, Y. M., KOEHLER, S. A., DE GREEF, T. F. A., ABBASPOURRAD, A., WEITZ, D. A. a CHONG, S. R. A mix-and-read drop-based in vitro two-hybrid method for screening high-affinity peptide binders. *Scientific Reports*, 2016, roč. 6.

DAFNER, E. V. Segmented continuous-flow analyses of nutrient in seawater: intralaboratory comparison of Technicon AutoAnalyzer II and Bran plus Luebbe Continuous Flow AutoAnalyzer III. *Limnology and Oceanography-Methods*, 2015, roč. 13. č. 10, s. 511-520.

DRUMMOND, T. G., HILL, M. G. a BARTON, J. K. Electrochemical DNA sensors. *Nature Biotechnology*, 2003, roč. 21. č. 10, s. 1192-1199.

ESASHI, M., SHOJI, S. a NAKANO, A. Normally closed microvalve and micropump fabricated on a silicon-wafer. *Sensors and Actuators*, 1989, roč. 20. č. 1-2, s. 163-169.

FARNLEITNER, A. H., HOCKE, L., BEIWL, C., KAVKA, G. G., ZECHMEISTER, T., KIRSCHNER, A. K. T. a MACH, R. L. Rapid enzymatic detection of Escherichia coli contamination in polluted river water. *Letters in Applied Microbiology*, 2001, roč. 33. č. 3, s. 246-250.

FIKSDALL, L. a TRYLAND, I. Application of rapid enzyme assay techniques for monitoring of microbial water quality. *Current Opinion in Biotechnology*, 2008, roč. 19. č. 3, s. 289-294.

GAO, B. B., LIU, H. a GU, Z. Z. Patterned Photonic Nitrocellulose for Pseudo-Paper Microfluidics. *Analytical Chemistry*, 2016, roč. 88. č. 10, s. 5424-5429.

GORHAM, T. J. a LEE, J. Pathogen Loading From Canada Geese Faeces in Freshwater: Potential Risks to Human Health Through Recreational Water Exposure. *Zoonoses and Public Health*, 2016, roč. 63. č. 3, s. 177-190.

GROSSI, M., LAZZARINI, R., LANZONI, M., POMPEI, A., MATTEUZZI, D. a RICCO, B. A Portable Sensor With Disposable Electrodes for Water Bacterial Quality Assessment. *Ieee Sensors Journal*, 2013, roč. 13. č. 5, s. 1775-1782.

HABILA, M. A., ALOTHMAN, Z. A., EL-TONI, A. M., LABIS, J. P. a SOYLAK, M. Synthesis and application of Fe3O4@SiO2@TiO2 for photocatalytic decomposition of organic matrix simultaneously with magnetic solid phase extraction of heavy metals prior to ICP-MS analysis. *Talanta*, 2016, roč. 154, s. 539-547.

HOLLAARM, K. a NEELE, B. Industrial and environmental applications of continuous flow analysis. In: M. Trojanowicz, ed. *Advances in flow analysis* [online]. Wiley-VCH, 2008, s. 639-661. ISBN: 978-3-527-31830-8 [vid. 16.9. 2008]. Dostupné z: http://onlinelibrary.wiley.com/book/10.1002/9783527623259

HUANG, H. Y., NIE, R., SONG, Y. Y., JI, Y. S., GUO, R. a LIU, Z. H. Highly sensitive electrochemical sensor for tulobuterol detection based on facile graphene/Au nanowires modified glassy carbon electrode. *Sensors and Actuators B-Chemical*, 2016, roč. 230, s. 422-426.

CHAIYO, S., APILUK, A., SIANGPROH, W. a CHAILAPAKUL, O. High sensitivity and specificity simultaneous determination of lead, cadmium and copper using mu PAD with dual electrochemical and colorimetric detection. *Sensors and Actuators B-Chemical*, 2016, roč. 233, s. 540-549.

CHANDER, R. a THOMAS, P. Alkaline phosphatase from Jawala shrimp (Acetes indicus). *Journal of Food Biochemistry*, 2001, roč. 25. č. 2, s. 91-103.

CHUANG, C. H., DU, Y. C., WU, T. F., CHEN, C. H., LEE, D. H., CHEN, S. M., HUANG, T. C., WU, H. P. a SHAIKH, M. O. Immunosensor for the ultrasensitive and quantitative detection of bladder cancer in point of care testing. *Biosensors & Bioelectronics*, 2016, roč. 84, s. 126-132.

INTARAKAMHANG, S., SCHUHMANN, W. a SCHULTE, A. Robotic heavy metal anodic stripping voltammetry: ease and efficacy for trace lead and cadmium electroanalysis. *Journal of Solid State Electrochemistry*, 2013, roč. 17. č. 6, s. 1535-1542.

KANG, W. J., PEI, X., YUE, W., BANGE, A., HEINEMAN, W. R. a PAPAUTSKY, I. Lab-on-a-Chip Sensor with Evaporated Bismuth Film Electrode for Anodic Stripping Voltammetry of Zinc. *Electroanalysis*, 2013, roč. 25. č. 12, s. 2586-2594.

KHALILZADEH, B., CHAROUDEH, H. N., SHADJOU, N., MOHAMMAD-REZAEI, R., OMIDI, Y., VELAEI, K., ALIYARI, Z. a RASHIDI, M. R. Ultrasensitive caspase-3 activity detection using an electrochemical biosensor engineered by gold nanoparticle functionalized MCM-41: Its application during stem cell differentiation. *Sensors and Actuators B-Chemical*, 2016, roč. 231, s. 561-575.

KOJTA, A. K. a FALANDYSZ, J. Metallic elements (Ca, Hg, Fe, K, Mg, Mn, Na, Zn) in the fruiting bodies of Boletus badius. *Food Chemistry*, 2016, roč. 200, s. 206-214.

KOKKINOS, C. a ECONOMOU, A. Microfabricated chip integrating a bismuth microelectrode array for the determination of trace cobalt(II) by adsorptive cathodic stripping voltammetry. *Sensors and Actuators B-Chemical*, 2016, roč. 229, s. 362-369.

LAGIER, M. J., SCHOLIN, C. A., FELL, J. W., WANG, J. a GOODWIN, K. D. An electrochemical RNA hybridization assay for detection of the fecal indicator bacterium Escherichia coli. *Marine Pollution Bulletin*, 2005, roč. 50. č. 11, s. 1251-1261.

LANGE, B. a SCHOLZ, F. Cathodic stripping voltammetric determination of selenium(IV) at a thin-film mercury electrode in a thiocyanate-containing electrolyte. *Fresenius Journal of Analytical Chemistry*, 1997, roč. 358. č. 6, s. 736-740.

LANTZ, P. G., ABU AL-SOUD, W., KNUTSSON, R., HAHN-HAGERDAL, B. a RADSTROM, P. Biotechnical use of polymerase chain reaction for microbiological analysis of biological samples. *Biotechnology annual review*, 2000, roč. 5, s. 87-130.

LICHTENBERG, J., DE ROOIJ, N. F. a VERPOORTE, E. Sample pretreatment on microfabricated devices. *Talanta*, 2002, roč. 56. č. 2, s. 233-266.

LIN, D., ZHAO, Q. a YAN, M. M. Surface modification of polydimethylsiloxane microfluidic chips by polyamidoamine dendrimers for amino acid separation. *Journal of Applied Polymer Science*, 2016, roč. 133. č. 25.

LIN, X. X., LEUNG, K. H., LIN, L., LIN, L. Y., LIN, S., LEUNG, C. H., MA, D. L. a LIN, J. M. Determination of cell metabolite VEGF(165) and dynamic analysis of protein-DNA interactions by combination of microfluidic technique and luminescent switch-on probe. *Biosensors & Bioelectronics*, 2016, roč. 79, s. 41-47.

LOGE, F. N., THOMPSON, D. E. a CALL, D. R. PCR detection of specific pathogens in water: A risk-based analysis. *Environmental Science & Technology*, 2002, roč. 36. č. 12, s. 2754-2759.

LUOMA, S. N. a RAINBOW, P. S. Why is metal bioaccumulation so variable? Biodynamics as a unifying concept. *Environmental Science & Technology*, 2005, roč. 39. č. 7, s. 1921-1931.

MAHEUX, A. F., HUPPE, V., BOISSINOT, M., PICARD, F. J., BISSONNETTE, L., BERNIER, J. L. T. a BERGERON, M. G. Analytical limits of four beta-glucuronidase and beta-galactosidase-based commercial culture methods used to detect Escherichia coli and total coliforms. *Journal of Microbiological Methods*, 2008, roč. 75. č. 3, s. 506-514.

MANZ, A., GRABER, N. a WIDMER, H. M. Miniaturized total chemical-analysis system - A novel concept for chemical sensing. *Sensors and Actuators B-Chemical*, 1990, roč. 1. č. 1-6, s. 244-248.

MASON, R. P., REINFELDER, J. R. a MOREL, F. M. M. Uptake, toxicity, and trophic transfer of mercury in a coastal diatom. *Environmental Science & Technology*, 1996, roč. 30. č. 6, s. 1835-1845.

MITTELMANN, A. S., RON, E. Z. a RISHPON, J. Amperometric quantification of total coliforms and specific detection of Escherichia coli. *Analytical Chemistry*, 2002, roč. 74. č. 4, s. 903-907.

NEFF, J. M. Ecotoxicology of arsenic in the marine environment. *Environmental Toxicology and Chemistry*, 1997, roč. 16. č. 5, s. 917-927.

NICOLAUS, B., MORIELLO, V. S., LAMA, L., POLI, A. a GAMBACORTA, A. Polysaccharides from extremophilic microorganisms. *Origins of Life and Evolution of the Biosphere*, 2004, roč. 34. č. 1-2, s. 159-169.

NOYHOUZER, T. a MANDLER, D. A New Electrochemical Flow Cell for the Remote Sensing of Heavy Metals. *Electroanalysis*, 2013, roč. 25. č. 1, s. 109-115.

PANIEL, N. a BAUDART, J. Colorimetric and electrochemical genosensors for the detection of Escherichia coli DNA without amplification in seawater. *Talanta*, 2013, roč. 115, s. 133-142.

PANTELI, V. S., KANELLOPOULOU, D. G., GARTAGANIS, S. P. a KOUTSOUKOS, P. G. Application of Anodic Stripping Voltammetry for Zinc, Copper, and Cadmium Quantification in the Aqueous Humor: Implications of Pseudoexfoliation Syndrome. *Biological Trace Element Research*, 2009, roč. 132. č. 1-3, s. 9-18.

PRASEK, J., TRNKOVA, L., GABLECH, I., BUSINOVA, P., DRBOHLAVOVA, J., CHOMOUCKA, J., ADAM, V., KIZEK, R. a HUBALEK, J. Optimization of Planar Three-Electrode Systems for Redox System Detection. *International Journal of Electrochemical Science*, 2012, roč. 7. č. 3, s. 1785-1801.

ROSZAK, D. B. a COLWELL, R. R. Metabolic-activity of bacterial-cells enumerated by direct viable count. *Applied and Environmental Microbiology*, 1987, roč. 53. č. 12, s. 2889-2983.

RUHLIG, D., SCHULTE, A. a SCHUHMANN, W. An electrochemical robotic system for routine cathodic adsorptive stripping analysis of Ni2+ ion release from corroding NiTi shape memory alloys. *Electroanalysis*, 2006, roč. 18. č. 1, s. 53-58.

RUZICKA, J. Discovering flow-injection - Journey from sample to a live cell and from solution to suspension. *Analyst*, 1994, roč. 119. č. 9, s. 1925-1934.

RUZICKA, J. a HANSEN, E. H. Flow injection analyses. 1. New concept of fast continuous-flow analysis. *Analytica Chimica Acta*, 1975, roč. 78. č. 1, s. 145-157.

RUZICKA, J. a HANSEN, E. H. Integrated microconduits for flow-injection analysis. *Analytica Chimica Acta*, 1984, roč. 161, s. 1-25.

RUZICKA, J. a MARSHALL, G. D. Sequential injection - A new concept for chemical sensors, process analysis and laboratory assays. *Analytica Chimica Acta*, 1990, roč. 237. č. 2, s. 329-343.

RUZICKA, J., POLLEMA, C. H. a SCUDDER, K. M. Jet ring cell - A tool for flow-injection spectroscopy and microscopy on a renewable solid support. *Analytical Chemistry*, 1993, roč. 65. č. 24, s. 3566-3570.

SARDANS, J., MONTES, F. a PENUELAS, J. Determination of As, Cd, Cu, Hg and Pb in biological samples by modern electrothermal atomic absorption spectrometry. *Spectrochimica Acta Part B-Atomic Spectroscopy*, 2010, roč. 65. č. 2, s. 97-112.

SINGH, N. K., RAGHUBANSHI, A. S., UPADHYAY, A. K. a RAI, U. N. Arsenic and other heavy metal accumulation in plants and algae growing naturally in contaminated area of West Bengal, India. *Ecotoxicology and environmental safety*, 2016, roč. 130. č., s. 224-233.

SIVASAMY, J., CHIM, Y. C., WONG, T. N., NGUYEN, N. T. a YOBAS, L. Reliable addition of reagents into microfluidic droplets. *Microfluidics and Nanofluidics*, 2010, roč. 8. č. 3, s. 409-416.

SKEGGS, L. T. An automatic method for colorimetric analysis. *American Journal of Clinical Pathology*, 1957, roč. 28. č. 3, s. 311-322.

SUREN, E., YILMAZ, S., TURKOGLU, M. a KAYA, S. Concentrations of cadmium and lead heavy metals in Dardanelles seawater. *Environmental Monitoring and Assessment*, 2007, roč. 125. č. 1-3, s. 91-98.

TAO, Y., ROTEM, A., ZHANG, H. D., COCKRELL, S. K., KOEHLER, S. A., CHANG, C. B., UNG, L. W., CANTALUPO, P. G., REN, Y. K., LIN, J. S., FELDMAN, A. B., WOBUS, C. E., PIPAS, J. M. a WEITZ, D. A. Artifact-Free Quantification and Sequencing of Rare Recombinant Viruses by Using Drop-Based Microfluidics. *Chembiochem*, 2015, roč. 16. č. 15, s. 2167-2171.

TERRY, S. C., JERMAN, J. H. a ANGELL, J. B. Gas-chromatographic air analyzer fabricated on a silicon-wafer. *Ieee Transactions on Electron Devices*, 1979, roč. 26. č. 12, s. 1880-1886.

VALCÁRCEL, M. a LUQUE DE CASTRO, M. D. *Automatic methods of analysis*. 1st ed. Amsterdam: Elsevier Science, 1988. ISBN 9780444430052

VANDEPOL, F. C. M., VANLINTEL, H. T. G., ELWENSPOEK, M. a FLUITMAN, J. H. J. A thermopneumatic micropump based on micro-engineering techniques. *Sensors and Actuators a-Physical*, 1990, roč. 21. č. 1-3, s. 198-202.

VANLINTEL, H. T. G., VANDEPOL, F. C. M. a BOUWSTRA, S. A piezoelectric micropump based on micromachining of silicon. *Sensors and Actuators*, 1988, roč. 15. č. 2, s. 153-167.

VOLESKY, B. Biosorption and me. *Water Research*, 2007, roč. 41. č. 18, s. 4017-4029.

WANG, L., YANG, D., CHEN, Z. L., LESNIEWSKI, P. J. a NAIDU, R. Application of neural networks with novel independent component analysis methodologies for the

simultaneous determination of cadmium, copper, and lead using an ISE array. *Journal of Chemometrics*, 2014, roč. 28. č. 6, s. 491-498.

WANG, W. T., FAN, X. J., XU, S. H., DAVIS, J. J. a LUO, X. L. Low fouling label-free DNA sensor based on polyethylene glycols decorated with gold nanoparticles for the detection of breast cancer biomarkers. *Biosensors & Bioelectronics*, 2015, roč. 71, s. 51-56.

WHITESIDES, G. M. The origins and the future of microfluidics. *Nature*, 2006, roč. 442. č. 7101, s. 368-373.

Exposure to lead: A major public health concern [online]. WHO [vid. 2010]. Dostupné z: http://www.who.int/ipcs/features/lead..pdf?ua=1.

Public health and environment [online]. WHO [vid. 2012] Dostupné z: http://www.who.int/gho/phe/en/.

WILSON, D., GUTIERREZ, J. M., ALEGRET, S. a DEL VALLE, M. Simultaneous Determination of Zn(II), Cu(II), Cd(II) and Pb(II) in Soil Samples Employing an Array of Potentiometric Sensors and an Artificial Neural Network Model. *Electroanalysis*, 2012, roč. 24. č. 12, s. 2249-2256.

YAN, J. L. Determinationation of Kanamycin by Square-Wave Cathodic Adsorptive Stripping Voltammetry. *Russian Journal of Electrochemistry*, 2008, roč. 44. č. 12, s. 1334-1338.

YEHEZKEL, B. T., RIVAL, A., RAZ, O., COHEN, R., MARX, Z., CAMARA, M., DUBERN, J. F., KOCH, B., HEEB, S., KRASNOGOR, N., DELATTRE, C. a SHAPIRO, E. Synthesis and cell-free cloning of DNA libraries using programmable microfluidics. *Nucleic Acids Research*, 2016, roč. 44. č. 4.

ZHANG, W., ZHANG, H., WILLIAMS, S. E. a ZHOU, A. H. Microfabricated three-electrode on-chip PDMS device with a vibration motor for stripping voltammetric detection of heavy metal ions. *Talanta*, 2015, roč. 132, s. 321-326.

ZHENG, W. F., HUANG, R., JIANG, B., ZHAO, Y. Y., ZHANG, W. a JIANG, X. Y. An Early-Stage Atherosclerosis Research Model Based on Microfluidics. *Small*, 2016, roč. 12. č. 15, s. 2022-2034.

ZHU, P. X., SHELTON, D. R., LI, S. H., ADAMS, D. L., KARNS, J. S., AMSTUTZ, P. a TANG, C. M. Detection of E. coli O157:H7 by immunomagnetic separation coupled with fluorescence immunoassay. *Biosensors & Bioelectronics*, 2011, roč. 30. č. 1, s. 337-341.

8 SEZNAM OBRÁZKŮ A TABULEK

9 SEZNAM ZKRATEK

AAS	Atomová absorpční spektroskopie
AFM	Mikroskopie atomárních sil
BIA	Částicová injekční analýza
DNA	Deoxyribonukleová kyselina
FIA	Průtoková injekční analýza
GCE	Elektroda ze skelného uhlíku
IDE	Prolínající se elektroda
MFE	Rtuťová filmová elektroda
ICP-MS	Hmotnostní spektroskopie s indukčně vázaným plazmatem
ICP-AES	Emisní spektroskopie s indukčně vázaným plazmatem
PCR	Polymerázová řetězová reakce
SEM	Skenovací (rastrovací) elektronová mikroskopie
SPE	Tištěná elektroda
SFA	Segmentová průtoková analýza
SIA	Sekvenční injekční analýza
WHO	World health organisation